SOLAR RADIATION AND DISSOLVED ORGANIC MATTER IN AQUATIC ENVIRONMENTS

by

KUN MA

(Under the Direction of Jay A. Brandes)

ABSTRACT

At 662 ± 32 Pg C, dissolved organic matter (DOM) is the second largest bioreactive reservoir of C in the ocean, and comparable in size to the atmospheric CO_2 pool. Photodegradation can be an important DOM sink but remains a poorly understood mechanism. Dissolved inorganic carbon (DIC) is a major product of DOM photodegradation in riverine and coastal waters. However, the *in situ* rates and magnitude of DIC photoproduction in the global oceans are poorly constrained due to analytical difficulties. The goal of my thesis was to fill some of the knowledge gaps in DOM photodegradation and DIC photoproduction. To assess the effect of increasing terrestrial DOM input to the coastal Baltic Sea, we conducted photoirradiation experiments during a mesocosm amendment experiment. We determined that humic substances added to the ecosystem can be photodegraded rapidly. Added humic substances reduced the CDOM fading rates but did not affect DIC photoproduction significantly. Photodegradation was likely not the dominant process for CDOM degradation *in situ*, and the importance of photodegradation needs to be further assessed. We also conducted experiments extracting DOM and enriching seawater with the extracted DOM. We determined that there was no difference in CDOM fading but difference in DIC photoproduction among the amended and

unamended samples. It is likely that both solid phase extraction and electrodialysis reverse osmosis extracts had lower CDOM:DOC ratios than the original seawater. When extrapolating to rates in the original water sample from the amended samples, either method is likely to provide useful answers if one is interested in CDOM fading in coastal waters, but color extrapolation likely provides a better approximate to DIC photoproduction rate of the original sample, especially when using solid phase extraction-amended samples. In addition, we determined that photodegradation of microplastic fibers (microfibers) may be a source of DOM and CDOM, although the produced DOM may be highly photolabile. My research suggested that color change, or CDOM fading, may not be a good predictor of DOM photodegradation, particularly for DIC photoproduction. Photodegradation can be a sink of marine DOM, however, teasing out its relative importance remains difficult.

INDEX WORDS: Dissolved organic matter, dissolved organic carbon, chromophoric dissolved organic matter, photochemistry, photodegradation, dissolved inorganic carbon, carbon dioxide, solid phase extraction, electrodialysis reverse osmosis, microplastic, microfiber

SOLAR RADIATION AND DISSOLVED ORGANIC MATTER IN AQUATIC ENVIRONMENTS

by

KUN MA

BS, State University of New York at Geneseo, 2010

MS, Shippensburg University of Pennsylvania, 2017

A Dissertation Submitted to the Graduate Faculty of The University of Georgia in Partial Fulfillment of the Requirements for the Degree

DOCTOR OF PHILOSOPHY

ATHENS, GEORGIA

2022

SOLAR RADIATION AND DISSOLVED ORGANIC MATTER IN AQUATIC ENVIRONMENTS

by

KUN MA

Major Professor:	Jay A. Brandes
Committee:	William L. Miller
	Aron Stubbins
	Elizabeth Harvey
	Adrian B. Burd

Electronic Version Approved:

Ron Walcott
Vice Provost for Graduate Education and Dean of the Graduate School
The University of Georgia
December 2022

DEDICATION

This work is dedicated to my husband Todd, who shares my love for nature and science.

ACKNOWLEDGEMENTS

There is no way I can adequately thank everyone who helped me along the way. First, I would like to thank my advisor Jay Brandes, who encourages me to stay curious and search for answers through scientific enquiries. I would also like to thank Jay and my committee Bill Miller, Aron Stubbins, Liz Harvey, and Adrian Burd for their constructive criticism and unique insights to help me become a better scientist, and for their guidance through the thesis writing process. I especially like to thank Leanne Powers and Bill Miller, for teaching me so much about photochemistry, and for the countless cruises we went on together to collect samples and conduct experiments. I would like to thank Sasha Wagner and Aron Stubbins for teaching me about DOM, Kevin Ryan for teaching me how to run MoDIE, Dodie Sanders for teaching me about microplastics and education, Tina Walters for always have an answer for any question I have, and Caitlin Amos for being the best writing buddy. I would also like to thank Catherine Edwards for her great advice on handling stress and being a productive scientist. I'm grateful to everyone at Skidaway Institute of Oceanography and the UGA Marine Sciences department for all the support I received. Finally, I'd like to thank my husband, my parents, my extended family, and my friends for their continued support and encouragement.

TABLE OF CONTENTS

Page

LIST OF TABLES

Page

LIST OF FIGURES

Page

CHAPTER 1

INTRODUCTION AND LITERATURE REVIEW

Dissolved organic matter (DOM) and chromophoric dissolved organic matter (CDOM)

Dissolved organic matter (DOM) is operationally defined as organic matter that can pass through filters of certain pore size (Repeta, 2015). Many studies utilize glass fiber filters of 0.7 μm nominal pore size because of the ease to clean, especially where large volume samples are required (Repeta, 2015). Smaller pore sizes (0.1-0.2 μm) are frequently used to exclude bacteria from water samples, whereas 10-15 nm pore size filters are needed to exclude viruses (Repeta, 2015). Therefore, DOM may include viruses, bacteria, colloidal organic matter, and truly dissolved species (Repeta, 2015).

Chemically, DOM is a complex mixture of likely millions of organic compounds and not well characterized (Hertkorn et al., 2013; Stubbins and Dittmar, 2015; Stubbins et al., 2010b). DOM can include amino acids, simple sugars, vitamins, fatty acids, pigments, proteins, polysaccharides, lignins, phenols, humic substances, and black carbon (Repeta, 2015).
Since DOM is about 50 % carbon by weight, DOM is also frequently reported as and used interchangeably with dissolved organic carbon (DOC) (Krogh, 1934; Moody and Worrall, 2017). At 662 ± 32 Pg C, DOM is the second largest bioreactive reservoir of carbon in the ocean, and comparable in size to the atmospheric CO_2 pool (Carlson and Hansell, 2015; Hansell and Carlson, 1998; Hansell et al., 2009b; Williams and Druffel, 1987).

DOM can support microbial growth and the microbial food web (Amon and Benner, 1996; Kroer, 1993). DOM also offers organisms protection from reactive oxygen radicals (Del

Vecchio and Blough, 2002). Because of the large size of the reservoir, even 1 % of marine DOM mineralized to CO_2 can exceed the annual production of atmospheric CO_2 by fossil fuel combustion (Hansell, 2002; Hedges, 2002).

Chromophoric dissolved organic matter (CDOM), the light absorbing portion of DOM , is the principal chromophore in marine waters (Mopper et al., 2007). CDOM is highly photoreactive, and can influence light availability to photosynthesis and penetration of ultraviolet (UV) radiation in the water column (Arrigo and Brown, 1996; Coble, 2007; Mopper et al., 2015; Repeta, 2015; Siegel et al., 2005; Siegel et al., 2002; Stedmon and Nelson, 2015). CDOM can also serve as photosensitizer, trigger secondary reactions, and lead to degradation of other DOM components (Coble, 2007).

Oceanic DOM derives mainly from biological production and is rapidly recycled through microbial consumption (Carlson and Hansell, 2015; Wagner et al., 2020). Studies suggest that CDOM and DOC can leach from microplastics (Galgani and Loiselle, 2019; Romera-Castillo et al., 2018). The presence of microplastic can stimulate bacterial activity and either enhance the microbial release of CDOM (Galgani et al., 2018), or increase CDOM processing and thus decrease CDOM (Boldrini et al., 2021).

DOM photodegradation and dissolved inorganic carbon (DIC) photoproduction

Photochemistry is one of the most significant abiotic reaction mechanisms in the surface ocean and an important sink for DOM (Gonsior et al., 2014; Mopper et al., 1991; Wagner et al., 2020; Zafiriou et al., 2003). DOM photodegradation can lead to loss of absorbance (color) through CDOM fading and thus affect light availability to photosynthesis and penetration of UV radiation in the water column (Del Vecchio and Blough, 2002; Mopper and Kieber, 2002a).

DOM photochemistry impacts the cycling of important elements such as carbon, nitrogen, sulfur, phosphorus, iron, manganese, and copper in the photic zone (Mopper and Kieber, 2002b and references within; Zepp et al., 2011 and references within). Photochemical reactions of DOM produce reactive species such as superoxide anion and hydroxyl radical, which could influence biological and chemical processes in sunlit surface waters (Blough and Zepp, 1995; O'Sullivan et al., 2005; Qian et al., 2001). In addition, atmospherically important gases, such as CO and CO_2, can be produced from photochemical degradation of DOM (Clark et al., 2004; Johannessen and Miller, 2001; Miller and Zepp, 1995; Powers et al., 2017a; Powers et al., 2017b; Powers and Miller, 2015b; Reader and Miller, 2012; White et al., 2010; Ziolkowski and Miller, 2007). Finally, biolabile photoproducts (compounds that could be consumed by marine microorganisms) could be produced from photochemistry of refractory DOM (Miller and Moran, 1997; Miller et al., 2002), although photochemistry could also decrease the bioavailability of DOM (Bittar et al., 2015).

Despite the importance of DOM photochemistry in the ocean, DOM photodegradation remains a poorly understood mechanism (Wagner et al., 2020), and the rates of oceanic DOC photochemical reactions remain poorly constrained. The photochemical efficiencies of each of these processes need to be determined for a diverse range of marine waters before global rates of DOC photoreactions can be calculated. The photochemical efficiency, or quantum yield, is defined as the number of moles of product formed or reactant lost per mole of photons absorbed by a specific photoreactant. In natural waters, CDOM is the dominant UV light absorber and thus presumably the dominant photoreactant (Coble, 2007; Nelson and Siegel, 2013). However, CDOM is an optical term that contains the sum of ALL specific light-absorbing compounds and processes, making observed photoreactions and mechanisms difficulty to define and understand.

Consequently, “apparent” quantum yield (AQY) is most often used to describe photochemical efficiency of DOM in natural waters. For AQY, the total absorbed radiation by CDOM is used to determine the photon dose absorbed relative to photochemical products (Hu et al., 2002a; Mopper et al., 2015).

Dissolved inorganic carbon (DIC) is the Earth’s largest active pool of carbon at the surface, and a major product of DOC photooxidation in riverine and coastal waters (Miller and Zepp, 1995; Reader and Miller, 2012). However, quantification of DIC photoproduction rate poses analytical challenges due to the high background concentrations of DIC in seawater (~2 mM). Typical DIC photoproduction rates in sunlight are on the order of nM h^{-1} to μM h^{-1} in the ocean, so that previous efforts to determine DIC photochemical production rates and efficiencies (AQY) used data from DIC-stripped samples (Bélanger et al., 2006; Powers and Miller, 2015b; Reader and Miller, 2012; White et al., 2010) or indirect proxies such as CO (Powers and Miller, 2015b; Reader and Miller, 2012; Stubbins et al., 2006; White et al., 2010; Zafiriou et al., 2003) and H_2O_2 (Powers and Miller, 2015a). Therefore, there’s a lack of direct efficiency measurements of DIC photoproduction in blue waters, i.e. ocean water with very low DOM and CDOM so that CDOM Napierian absorption coefficients at 325 nm ($a_g(325)$) is less than 0.25 m^{-1} (Siegel et al., 2002; Stedmon and Nelson, 2015). Since the subtropical gyres receive more than half of the global solar UV irradiance (290-400 nm; System for Transfer of Atmospheric Radiation model, Ruggaber et al., 1994), the lack of blue water DIC AQY spectra leads to a significant deficiency in modeling the importance of photochemistry in oceanic carbon cycling. Previous studies using DIC-stripped samples have shown that open ocean waters have higher DIC AQYs than coastal waters (Johannessen and Miller, 2001), but the acidification, sparging and pH readjustment required to remove DIC could lead to changes in the integrity and

photoreactivity of the DOC pool (White et al., 2008). Furthermore, currently measured ratios of CO_2:CO, obtained in CDOM-rich fresh and coastal waters, vary from 2 to greater than 60 (Miller and Zepp, 1995; Powers and Miller, 2015b; White et al., 2010), and may not represent the true relationships in blue water. Powers and Miller (2015a) reported an average CO_2:H_2O_2 ratio of about 9 for South Atlantic Bight offshore water samples, but the samples were DIC-striped before irradiation.

The Moderate DI^{13}C Isotope Enrichment (MoDIE) method was developed to directly measure sub-micromolar changes in DIC concentrations, so that DIC photoproduction rates and efficiency can be obtained with minimal sample manipulation and high sensitivity (Powers et al., 2017b). A small amount (< 10 % total DIC concentration) of ^{13}C is added to the sample seawater to achieve about 5000 - 9000 ‰ enrichment, so that photoproduced DIC leads to significant shifts of δ^{13}C values. The photoproduced DIC likely has δ^{13}C in the range of −25 to −45 ‰ (Franke et al., 2012; Lalonde et al., 2014; Opsahl and Zepp, 2001; Powers et al., 2017a; Vähätalo and Wetzel, 2008), however, the δ^{13}C values of photoproduced DIC (δ^{13}C-DIC$_{photo}$) cannot be determined directly for marine samples. Powers et al. (2017b) determined that the MoDIE calculation has a very low sensitivity to variations in δ^{13}C-DIC$_{photo}$, so that a δ^{13}C-DIC$_{photo}$ value of −33.3 ‰ were frequently used for DIC photoproduction determinations in the work presented in this dissertation.

The initial DIC photoproduction rate of Gulf Stream sample with $a_g(325)$ of 0.299 m^{-1} was determined to be 0.043 ± 0.009 μM h^{-1} using the MoDIE method, and the sample detection limit for this sample was 505 nM (Powers et al., 2017b). Only one other study reported DIC photoproduction rate for low CDOM seawater (S > 35; $a_g(325)$ < 0.25 m^{-1}), but the production rate was significantly lower.

General methodology

I used an Atlas Suntest™ CPS or an Atlas Suntest™ CPS+ solar simulator with 1.5 kW xenon lamp to conduct photochemical experiments (Powers and Miller, 2015b). Sample waters were irradiated in Spectrocell spectrophotometric quartz cuvettes (cells), which were housed in a water-cooled black aluminum block. Once placed inside the solar simulator, the optical windows of the cells were perpendicular to the incident irradiance. This design provides a reproducible and quantifiable irradiance field, known irradiation pathlengths for all cells, and eliminates off-axis photons and light transfer between cells.

For DIC photoproduction rate (time series) experiments, a daylight filter (cuts off light below ~300 nm) was used with the solar simulator. For AQY experiments, a polychromatic irradiation system with a range of Schott long-pass optical filters (280, 295, 305, 320, 380, 400, 435, and 480 nm cut-on wavelengths) was used to provide statistical power (Johannessen and Miller, 2001; Powers et al., 2017a; Powers et al., 2017b; Reader and Miller, 2012). The primary goals of the time series experiments were to determine the DIC photoproduction rates, the minimum photon doses (irradiation time) required to produce measurable CDOM bleaching, DOC loss or δ^{13}C-DIC shift (DIC photoproduction), and the maximum photon doses before CDOM bleaching, DOC loss or δ^{13}C-DIC shift become nonlinear. Integrated AQY (AQY(int)) was calculated from the production rates by multiplying the production rates by the sample volume (~ 30 mL, determined precisely for each cell). The durations of AQY experiments were determined based on the minimum irradiation times required to obtain measurable DIC photoproduction, which were determined with time series experiments.

The spectral downwelling irradiance ($E_0(\lambda)$) from the solar simulator entering each cell was quantified using a spectroradiometer, and the CDOM absorbance spectra for each sample

were measured using a spectrophotometer. Absorbance was converted to Napierian absorption coefficient ($a_g(\lambda)$) after correcting for offsets due to scattering and instrument drift (Powers et al., 2017a; Powers et al., 2017b; Stubbins et al., 2011).

The photon dose absorbed ($Q_a(\lambda)$) by CDOM in each cell over the course of the experiment was calculated using the following equation (Hu et al., 2002a):

$$Q_a(\lambda) = E_0(\lambda)\left(1 - e^{-a_g(\lambda)L}\right)S$$

where L is the pathlength, and S is the area of the irradiated surface of the cells. The integrated photon dose Q_a(int) was then determined by integrating $Q_a(\lambda)$ from 280 nm to 600 nm.

The DIC photoproduction rate (dP/dt, M h^{-1}) was determined using linear regression of photoproduced DIC concentration ($[DIC]_{photo}$) versus photon dose Q_a(int). The AQY ($\phi(\lambda)$, mol DIC (mol photons absorbed)$^{-1}$) spectrum was determined using a nonlinear weighted least squares regression model (nls in R, RCoreTeam, 2021) using the following equations (Powers et al., 2017a):

$$\phi(\lambda) = e^{-(m_1 + m_2(\lambda - 290))}$$

$$\frac{dP}{dt} = \int_{280}^{600} [\phi(\lambda) \times Q_a(\lambda)] d\lambda$$

where λ is the wavelength (nm), and m_1 and m_2 are fitting parameters for *nls*.

Dissolved organic carbon concentrations ([*DOC*]) were measured using a high temperature catalytic oxidation method with a Shimadzu TOC analyzer equipped with an autosampler (Stubbins et al., 2012).

The MoDIE method uses a liquid chromatography-isotope ratio mass spectrometry (LC-IRMS) system to measure the initial DIC concentrations and δ^{13}C-DIC of ^{13}C-enriched seawater samples (Powers et al., 2017b). The DIC photoproduction rate (M (mol photons)$^{-1}$ or mol (mol

photons)$^{-1}$) was calculated from linear regression of the concentration or amount of DIC produced in each cell over integrated photon dose.

Dissolved inorganic carbon photoproduction rates from blue water samples remained difficult to measure even using MoDIE. System exchange with atmosphere CO_2 could cause the $^{13}C/^{12}C$ isotope ratio to drift even in dark controls, despite efforts to increase airtightness of the system and reduce this exchange. We explored options to extract DOM and enrich whole water samples with the extracted DOM, to achieve a more measurable level of DIC photoproduction using the MoDIE method. Two extraction methods, solid phase extraction (SPE) using Agilent Bond Elut™ PPL cartridges and electrodialysis reverse osmosis (EDRO) were used to extract DOM. The photodegradation rates and efficiencies of samples after amended with extracted DOM were compared. To my knowledge this kind of comparison was not done previously. The use of PPL for SPE is efficient and rapid, the extraction can be performed at sea, and the method extracts a more representative proportion of DOM than other sorbents such as C18 (Dittmar et al., 2008). EDRO efficiently removes the majority of the salt in a sample, reduces the sample volume, and provides good compositional representation of the DOM present in the original samples (Chambers et al., 2016). However, SPE and EDRO may have different recovery and selectivity towards different molecular classes (Chambers et al., 2016). Therefore, SPE- and EDRO-DOM may have different photoreactivity. It is assumed that when CDOM and/or DOM of blue water was concentrated to levels comparable to coastal waters, the DIC photoproduction rates should be also comparable, but our results have shown that DIC photoproduction rate of North Atlantic Subtropical Gyre (NASG) water, extrapolated from CDOM absorption coefficients and DIC photoproduction rates in SPE-DOM-amended NASG water, was much

lower than expected based on extrapolation from CDOM absorption coefficients and DIC photoproduction rates of South Atlantic Bight offshore water.

Dissertation overview

The goal of my thesis was to fill some of the knowledge gaps in DOM photodegradation and DIC photoproduction. First, the effects of added humic substances and nutrients to the photodegradation rates of CDOM and DOM were examined for an estuarine Baltic Sea system. The results shed some light on the potential of photochemistry to alleviate the browning effects at this coastal system. Secondly, enriching seawater samples with extracted DOM to increase DIC photoproduction was investigated for its effectiveness to estimate DIC photoproduction in marine waters. The photochemistry of the amended samples was compared to that of the original seawater, to provide insights on how well the extract-amended samples can represent the original seawater in CDOM fading and DIC photoproduction for coastal samples. Lastly, the photodegradation of microplastic fibers (microfiber) was studied in the context of CDOM and DOM production.

REFERENCES

Amon, R.M.W. and Benner, R., 1996. Bacterial utilization of different size classes of dissolved organic matter. Limnology and Oceanography, 41(1): 41-51.

Arrigo, K.R. and Brown, C.W., 1996. Impact of chromophoric dissolved organic matter on UV inhibition of primary productivity in the sea. Marine Ecology Progress Series, 140(1-3): 207-216.

Bélanger, S. et al., 2006. Photomineralization of terrigenous dissolved organic matter in Arctic coastal waters from 1979 to 2003: Interannual variability and implications of climate change. Global Biogeochemical Cycles, 20(4): 13.

Bittar, T.B., Vieira, A.A.H., Stubbins, A. and Mopper, K., 2015. Competition between photochemical and biological degradation of dissolved organic matter from the cyanobacteria Microcystis aeruginosa. Limnology and Oceanography, 60(4): 1172-1194.

Blough, N.V. and Zepp, R.G., 1995. Reactive Oxygen Species in Natural Waters. In: C.S. Foote, J.S. Valentine, A. Greenberg and J.F. Liebman (Editors), Active Oxygen in Chemistry. Springer Netherlands, Dordrecht, pp. 280-333.

Boldrini, A., Galgani, L., Consumi, M. and Loiselle, S.A., 2021. Microplastics Contamination versus Inorganic Particles: Effects on the Dynamics of Marine Dissolved Organic Matter. Environments, 8(3): 14.

Carlson, C.A. and Hansell, D.A., 2015. Chapter 3 - DOM Sources, Sinks, Reactivity, and Budgets. Biogeochemistry of Marine Dissolved Organic Matter: 65-126.

Chambers, L.R. et al., 2016. Enhanced Dissolved Organic Matter Recovery from Saltwater Samples with Electrodialysis. Aquatic Geochemistry, 22(5-6): 555-572.

Clark, C.D. et al., 2004. CDOM distribution and CO(2) production on the southwest Florida shelf. Marine Chemistry, 89(1-4): 145-167.

Coble, P.G., 2007. Marine optical biogeochemistry: The chemistry of ocean color. Chemical Reviews, 107(2): 402-418.

Del Vecchio, R. and Blough, N.V., 2002. Photobleaching of chromophoric dissolved organic matter in natural waters: kinetics and modeling. Marine Chemistry, 78(4): 231-253.

Dittmar, T., Koch, B., Hertkorn, N. and Kattner, G., 2008. A simple and efficient method for the solid-phase extraction of dissolved organic matter (SPE-DOM) from seawater. Limnology and Oceanography-Methods, 6: 230-235.

Franke, D., Hamilton, M.W. and Ziegler, S.E., 2012. Variation in the photochemical lability of dissolved organic matter in a large boreal watershed. Aquatic Sciences, 74(4): 751-768.

Galgani, L., Engel, A., Rossi, C., Donati, A. and Loiselle, S.A., 2018. Polystyrene microplastics increase microbial release of marine Chromophoric Dissolved Organic Matter in microcosm experiments. Scientific Reports, 8(1): 14635.

Galgani, L. and Loiselle, S.A., 2019. Plastic Accumulation in the Sea Surface Microlayer: An Experiment-Based Perspective for Future Studies. Geosciences, 9(2).

Gonsior, M. et al., 2014. Photochemical production of polyols arising from significant photo-transformation of dissolved organic matter in the oligotrophic surface ocean. Marine Chemistry, 163: 10-18.

Hansell, D.A., 2002. DOC in the global ocean carbon cycle. In: D.A. Hansell and C.A. Carlson (Editors), Biogeochemistry of marine dissolved organic matter. Academic Press, pp. 685-716.

Hansell, D.A. and Carlson, C.A., 1998. Deep-ocean gradients in the concentration of dissolved organic carbon. Nature, 395(6699): 263-266.

Hansell, D.A., Carlson, C.A., Repeta, D.J. and Schlitzer, R., 2009. Dissolved organic matter in the ocean: a controversy stimulates new insights. Oceanography, 22(4): 202-211.

Hedges, J.I., 2002. Why dissolved organics matter? . In: D.A. Hansell and C.A. Carlson (Editors), Biogeochemistry of marine dissolved organic matter. Academic Press, pp. 1-34.

Hertkorn, N., Harir, M., Koch, B.P., Michalke, B. and Schmitt-Kopplin, P., 2013. High-field NMR spectroscopy and FTICR mass spectrometry: powerful discovery tools for the molecular level characterization of marine dissolved organic matter. Biogeosciences, 10(3): 1583-1624.

Hu, C., Muller-Karger, F.E. and Zepp, R.G., 2002. Absorbance, absorption coefficient, and apparent quantum yield: A comment on common ambiguity in the use of these optical concepts. Limnology and Oceanography, 47(4): 1261-1267.

Johannessen, S.C. and Miller, W.L., 2001. Quantum yield for the photochemical production of dissolved inorganic carbon in seawater. Marine Chemistry, 76(4): 271-283.

Kroer, N., 1993. Bacterial-growth efficiency on natural dissolved organic matter. Limnology and Oceanography, 38(6): 1282-1290.

Krogh, A., 1934. Conditions of Life in the Ocean. Ecological Monographs, 4(4): 421-429.

Lalonde, K., Vähätalo, A.V. and Gelinas, Y., 2014. Revisiting the disappearance of terrestrial dissolved organic matter in the ocean: a delta C-13 study. Biogeosciences, 11(13): 3707-3719.

Miller, W.L. and Moran, M.A., 1997. Interaction of photochemical and microbial processes in the degradation of refractory dissolved organic matter from a coastal marine environment. Limnology and Oceanography, 42(6): 1317-1324.

Miller, W.L., Moran, M.A., Sheldon, W.M., Zepp, R.G. and Opsahl, S., 2002. Determination of apparent quantum yield spectra for the formation of biologically labile photoproducts. Limnology and Oceanography, 47(2): 343-352.

Miller, W.L. and Zepp, R.G., 1995. Photochemical production of dissolved inorganic carbon from terrestrial organic matter: significance to the oceanic organic carbon cycle Geophysical Research Letters, 22(4): 417-420.

Moody, C.S. and Worrall, F., 2017. Modeling rates of DOC degradation using DOM composition and hydroclimatic variables. Journal of Geophysical Research: Biogeosciences, 122(5): 1175-1191.

Mopper, K. and Kieber, D.J., 2002a. Chapter 9 - Photochemistry and the Cycling of Carbon, Sulfur, Nitrogen and Phosphorus. In: D.A. Hansell and C.A. Carlson (Editors), Biogeochemistry of Marine Dissolved Organic Matter. Academic Press, San Diego, pp. 455-507.

Mopper, K. and Kieber, D.J., 2002b. Chapter 9 - Photochemistry and the Cycling of Carbon, Sulfur, Nitrogen and Phosphorus. Biogeochemistry of Marine Dissolved Organic Matter: 455-507.

Mopper, K., Kieber, D.J. and Stubbins, A., 2015. Marine Photochemistry of Organic Matter: Processes and Impacts. In: D.A. Hansell and C.A. Carlson (Editors), Biogeochemistry of Marine Dissolved Organic Matter, 2nd Edition. Academic Press Ltd-Elsevier Science Ltd, London, pp. 389-450.

Mopper, K., Stubbins, A., Ritchie, J.D., Bialk, H.M. and Hatcher, P.G., 2007. Advanced instrumental approaches for characterization of marine dissolved organic matter: Extraction techniques, mass spectrometry, and nuclear magnetic resonance spectroscopy. Chemical Reviews, 107(2): 419-442.

Mopper, K. et al., 1991. Photochemical degradation of dissolved organic carbon and its impact on the oceanic carbon cycle. Nature, 353(6339): 60-62.

Nelson, N.B. and Siegel, D.A., 2013. The Global Distribution and Dynamics of Chromophoric Dissolved Organic Matter. In: C.A. Carlson and S.J. Giovannoni (Editors), Annual Review of Marine Science, Vol 5. Annual Review of Marine Science. Annual Reviews, Palo Alto, pp. 447-476.

O'Sullivan, D.W., Neale, P.J., Coffin, R.B., Boyd, T.J. and Osburn, S.L., 2005. Photochemical production of hydrogen peroxide and methylhydroperoxide in coastal waters. Marine Chemistry, 97(1-2): 14-33.

Opsahl, S.P. and Zepp, R.G., 2001. Photochemically-induced alteration of stable carbon isotope ratios (delta C-13) in terrigenous dissolved organic carbon. Geophysical Research Letters, 28(12): 2417-2420.

Powers, L.C., Brandes, J.A., Miller, W.L. and Stubbins, A., 2017a. Using liquid chromatography-isotope ratio mass spectrometry to measure the delta C-13 of dissolved inorganic carbon photochemically produced from dissolved organic carbon. Limnology and Oceanography-Methods, 15(1): 103-115.

Powers, L.C., Brandes, J.A., Stubbins, A. and Miller, W.L., 2017b. MoDIE: Moderate dissolved inorganic carbon ((DIC)-C-13) isotope enrichment for improved evaluation of DIC photochemical production in natural waters. Marine Chemistry, 194: 1-9.

Powers, L.C. and Miller, W.L., 2015a. Hydrogen peroxide and superoxide photoproduction in diverse marine waters: A simple proxy for estimating direct CO2 photochemical fluxes. Geophysical Research Letters, 42(18): 7696-7704.

Powers, L.C. and Miller, W.L., 2015b. Photochemical production of CO and CO2 in the Northern Gulf of Mexico: Estimates and challenges for quantifying the impact of photochemistry on carbon cycles. Marine Chemistry, 171: 21-35.

Qian, J.G., Mopper, K. and Kieber, D.J., 2001. Photochemical production of the hydroxyl radical in Antarctic waters. Deep-Sea Research Part I-Oceanographic Research Papers, 48(3): 741-759.

RCoreTeam, 2021. R: A language and environment for statistical computing. The R Foundation for Statistical Computing, Vienna, Austria.

Reader, H.E. and Miller, W.L., 2012. Variability of carbon monoxide and carbon dioxide apparent quantum yield spectra in three coastal estuaries of the South Atlantic Bight. Biogeosciences, 9(11): 4279-4294.

Repeta, D.J., 2015. Chemical characterization and cycling of dissolved organic matter. In: D.A. Hansell and C.A. Carlson (Editors), Biogeochemistry of marine dissolved organic matter. Academic Press.

Romera-Castillo, C., Pinto, M., Langer, T.M., Alvarez-Salgado, X.A. and Herndl, G.J., 2018. Dissolved organic carbon leaching from plastics stimulates microbial activity in the ocean. Nature Communications, 9: 7.

Ruggaber, A., Dlugi, R. and Nakajima, T., 1994. MODELING RADIATION QUANTITIES AND PHOTOLYSIS FREQUENCIES IN THE TROPOSPHERE. Journal of Atmospheric Chemistry, 18(2): 171-210.

Siegel, D.A., Maritorena, S., Nelson, N.B., Behrenfeld, M.J. and McClain, C.R., 2005. Colored dissolved organic matter and its influence on the satellite-based characterization of the ocean biosphere. Geophysical Research Letters, 32(20): 4.

Siegel, D.A., Maritorena, S., Nelson, N.B., Hansell, D.A. and Lorenzi-Kayser, M., 2002. Global distribution and dynamics of colored dissolved and detrital organic materials. Journal of Geophysical Research-Oceans, 107(C12).

Stedmon, C.A. and Nelson, N.B., 2015. Chapter 10: The Optical Properties of DOM in the Ocean. Biogeochemistry of Marine Dissolved Organic Matter: 481-508.

Stubbins, A. and Dittmar, T., 2015. Illuminating the deep: Molecular signatures of photochemical alteration of dissolved organic matter from North Atlantic Deep Water. Marine Chemistry, 177: 318-324.

Stubbins, A., Law, C.S., Uher, G. and Upstill-Goddard, R.C., 2011. Carbon monoxide apparent quantum yields and photoproduction in the Tyne estuary. Biogeosciences, 8(3): 703-713.

Stubbins, A. et al., 2010. Illuminated darkness: Molecular signatures of Congo River dissolved organic matter and its photochemical alteration as revealed by ultrahigh precision mass spectrometry. Limnology and Oceanography, 55(4): 1467-1477.

Stubbins, A. et al., 2006. Open-ocean carbon monoxide photoproduction. Deep-Sea Research Part Ii-Topical Studies in Oceanography, 53(14-16): 1695-1705.

Vähätalo, A.V. and Wetzel, R.G., 2008. Long-term photochemical and microbial decomposition of wetland-derived dissolved organic matter with alteration of C-13 : C-12 mass ratio. Limnology and Oceanography, 53(4): 1387-1392.

Wagner, S. et al., 2020. Soothsaying DOM: A Current Perspective on the Future of Oceanic Dissolved Organic Carbon. Frontiers in Marine Science, 7: 17.

White, E.M., Kieber, D.J. and Mopper, K., 2008. Determination of photochemically produced carbon dioxide in seawater. Limnology and Oceanography-Methods, 6: 441-453.

White, E.M., Kieber, D.J., Sherrard, J., Miller, W.L. and Mopper, K., 2010. Carbon dioxide and carbon monoxide photoproduction quantum yields in the Delaware Estuary. Marine Chemistry, 118(1-2): 11-21.

Williams, P.M. and Druffel, E.R.M., 1987. Radiocarbon in dissolved organic matter in the central North Pacific Ocean. Nature, 330(6145): 246-248.

Zafiriou, O.C., Andrews, S.S. and Wang, W., 2003. Concordant estimates of oceanic carbon monoxide source and sink processes in the Pacific yield a balanced global "blue-water" CO budget. Global Biogeochemical Cycles, 17(1).

Zepp, R.G., Erickson, D.J., Paul, N.D. and Sulzberger, B., 2011. Effects of solar UV radiation and climate change on biogeochemical cycling: interactions and feedbacks. Photochemical & Photobiological Sciences, 10(2): 261-279.

Ziolkowski, L.A. and Miller, W.L., 2007. Variability of the apparent quantum efficiency of CO photoproduction in the Gulf of Maine and Northwest Atlantic. Marine Chemistry, 105(3-4): 258-270.

CHAPTER 2

EFFECTS OF ADDED HUMIC SUBSTANCES AND NUTRIENTS ON PHOTOCHEMICAL DEGRADATION OF DISSOLVED ORGANIC MATTER IN A MESOCOSM AMENDMENT EXPERIMENT IN THE GULF OF FINLAND, BALTIC SEA[1]

[1]Ma, K., L.C. Powers, J. Seppälä, J. Norkko, J.A. Brandes (2022). Effects of added humic substances and nutrients on photochemical degradation of dissolved organic matter in a mesocosm amendment experiment in the Gulf of Finland, Baltic Sea. *Photochemistry and Photobiology*, 98(5): 1025-1042. https://doi.org/10.1111/php.13597. Reprinted here with permission of publisher.

Abstract

Humic substances, a component of terrestrial dissolved organic matter (tDOM), contribute to dissolved organic matter (DOM) and chromophoric DOM (CDOM) in coastal waters, and have significant impacts on biogeochemistry. There are concerns in recent years over browning effects in surface waters due to increasing tDOM inputs, and their negative impacts on aquatic ecosystems, but relatively little work has been published on estuaries and coastal waters. Photodegradation could be a significant sink for tDOM in coastal environments, but the rates and efficiencies are poorly constrained. We conducted large-scale DOM photodegradation experiments in mesocosms amended with humic substances and nutrients in the Gulf of Finland to investigate the potential of photochemistry to remove added tDOM and the interactions of DOM photochemistry with eutrophication. The added tDOM was photodegraded rapidly, as CDOM absorption decreased, and spectral slopes increased with increasing photons absorbed in laboratory experiments. The *in situ* DOM optical properties became similar among the control, humic- and humic+nutrients-amended mesocosm samples toward the end of the amendment experiment, indicating degradation of the excess CDOM/DOM through processes including photodegradation. Nutrient additions did not significantly influence the effects of added humic substances on CDOM optical property changes, but induced changes in DOM removal.

Introduction

Dissolved organic matter (DOM) is the second largest bioreactive reservoir of carbon in the ocean after dissolved inorganic carbon (Hansell and Carlson, 1998; Hansell et al., 2009b; Hedges, 1992; Williams and Druffel, 1987), and plays an important role in many oceanographic processes such as supporting microbial growth (Amon and Benner, 1996; Cherrier and Bauer, 2004; Kroer, 1993). Marine DOM can be autochthonous or allochthonous, and one of the main allochthonous DOM sources is rivers (Carlson and Hansell, 2015), which supply from 0.17 Pg C y^{-1} (Mayorga et al., 2010) to 0.36 Pg C y^{-1} (Aitkenhead and McDowell, 2000) of terrestrial DOM (tDOM) to the ocean. Humic substances, such as lignin polyphenols, are a component of tDOM (Coble, 2007) and can have significant impacts on the biogeochemistry of coastal waters (Blough and Del Vecchio, 2002). In coastal areas, soil humic substances can make a large contribution to the colored portion of the DOM pool (chromophoric dissolved organic matter, or CDOM), which has been attributed to their relatively high aromatic content (Coble, 2007). The ultimate fate of this material is still poorly understood and highly debated however, and we need a better understanding of how tDOM degrades in coastal systems.

In recent years, there are increasing concerns that climate change and anthropogenic activities can lead to increased terrestrial input of humic substances to surface waters and browning of surface waters, or browning effects (de Wit et al., 2016; Monteith et al., 2007). Such effects, in turn, can affect carbon cycling and climate (Tranvik et al., 2009) and significantly impact aquatic ecosystems (Brothers et al., 2014; Feuchtmayr et al., 2019; Karlsson et al., 2009; Kritzberg et al., 2014; Santonja et al., 2017; Urrutia-Cordero et al., 2017; Vasconcelos et al., 2018). Most studies on browning effects are on rivers and lakes, with relatively less work published on estuaries and coastal water environments at the receiving end of river supplied

tDOM (Andersson et al., 2013; Deininger and Frigstad, 2019). In addition, increased tDOM could have complex effects on coastal eutrophication processes depending on initial nutrients and tDOM conditions of the system (Andersson et al., 2013; Deininger and Frigstad, 2019). For example, Andersson et al. (2013) conducted a mesocosm experiment using northern Baltic Sea water amended with humic carbon and inorganic nutrients to investigate the biological effects of browning from allochthonous DOM and the interaction of added humic carbon with nutrients, and found that the addition of humic carbon may counteract the effect of eutrophication (Andersson et al., 2013).

Lauerwald et al. (2012) estimated that at least 25 % of tDOM is removed before reaching the coast. The remaining tDOM fractions could be transformed in estuaries or coastal oceans (Coble, 2007; Deininger and Frigstad, 2019; Massicotte et al., 2017; Osburn and Bianchi, 2016), through biotic (Asmala et al., 2014a; Farjalla et al., 2009; Moran et al., 1999; Moran et al., 2000; Santos et al., 2014) and abiotic processes such as flocculation (Asmala et al., 2014b; Sholkovitz, 1976), sorption (Pinsonneault et al., 2020) and photodegradation (Bélanger et al., 2006; Chupakova et al., 2018; Dalzell et al., 2009; Minor et al., 2007; Moran et al., 2000; Osburn et al., 2009; Santos et al., 2014).

Photodegradation can lead to loss of color due to degradation of CDOM and subsequent decrease in CDOM absorbance (Coble, 2007; Mopper and Kieber, 2000b; Mopper et al., 2015). CDOM can also act as a photosensitizer, passing absorbed solar energy along and triggering a suite of secondary reactions that lead to the degradation of other DOM components (Coble, 2007). In coastal oceans and estuaries, especially for water with high tDOM input, color bleaching of water samples can often be a good indicator of DOM photolability (Mopper et al., 2015). Photodegradation of CDOM can have multiple effects on the local ecosystems, by

changing the light availability, for example, the penetration of photosynthetically active radiation and potentially harmful ultraviolet (UV) radiation (Anderson et al., 2001; Coble, 2007). Photodegradation of DOM can also lead to changes in biolability of DOM, for example, transformation of biologically recalcitrant DOM into biolabile substrates that support bacterial growth (Aarnos et al., 2012). In addition, DOM photodegradation could influence the ocean-atmosphere fluxes of important atmospheric gases such as CO_2 through dissolved inorganic carbon (DIC) photoproduction (Mopper et al., 2015). However, rates of CDOM and DOM photodegradation in coastal zones span a large range and the role of photochemistry in tDOM cycling is still poorly understood (Fichot and Benner, 2014; Miller and Moran, 1997; Miller et al., 2002). Therefore, due to the presumed role of photochemistry in tDOM cycling/removal and considering potential future coastal water browning, more quantitative information on CDOM photobleaching and DOM photodegradation in coastal waters is sorely needed.

In the Baltic Sea, allochthonous tDOM contributes to a large portion (~ 43 - 83 %) of the high molecular weight DOM pool in the surface water (Deutsch et al., 2012), and photochemistry is thought to be a major sink for DOM, with the total photochemical transformation of dissolved organic carbon (DOC) (2.71 - 3.94 Tg C y^{-1}) exceeding the annual riverine input of allochthonous photoreactive DOC to the Baltic Sea (< 2.45 Tg C y^{-1}) (Aarnos et al., 2012). As large numbers of Finland lakes and streams are currently experiencing DOM concentration increases, or browning (Monteith et al., 2007), it is conceivable that the Baltic Sea - at the receiving end of these freshwater systems - may in the future experience similar browning effects. In addition, coastal eutrophication is a prevailing problem in large portions of the Baltic Sea (Carstensen et al., 2020; Thomas et al., 2010). However, the potential of photochemistry to remove additional inputs of tDOM in the Gulf of Finland, as well as the

interactions of DOM photochemistry with eutrophication, is not well constrained. It is expected that bacterial consumption and photodegradation of the added DOM could lead to a decrease in DOM and CDOM contents, but primary production may also add autochthonous DOM and/or CDOM to the system. A previous browning experiment at the IGB LakeLab in Germany indicated an interesting and complex pattern of DOM composition change over the course of the experiment, suggesting that there are both losses and inputs of DOM to the mesocosms after amendments (Stella Berger, personal communication). To that end, we conducted large-scale DOM photodegradation experiments in mesocosms with and without added humic substances (to simulate coastal browning). Mesocosm experiments bridge small-scale laboratory experiments and large-scale environmental sampling, and are frequently conducted to assess the response of a system to changing conditions, such as added carbon or nutrients (Andersson et al., 2013; Deininger and Frigstad, 2019). The LightCycle experiment was conducted to continue the investigation to constrain the photochemical sink of added humic substances to an estuarine system. We took mesocosm samples to monitor the changes that occurred *in situ* after the addition of humic substances and nutrients, and conducted laboratory photoirradiation experiments using sterile-filtered mesocosm samples to examine only the effects of photodegradation. More specifically, the following hypotheses were tested in this study: (1) added humic substances can be photochemically degraded rapidly in this coastal Baltic Sea system, (2) comparing *in situ* and laboratory rates will reveal the importance of photodegradation in removing added humic substances, and (3) added nutrients will affect photochemical degradation of added humic substances.

Materials and Methods

The AQUACOSM JOMEX experiments were mesocosm experiments covering a range of aquatic systems, and the JOMEX: Systems Responses to A Pulse of Dissolved Organic Carbon project was one such experiment conducted at the Tvärminne Mesocosm Facility (TMF, Tvärminne Zoological Station (TZS), University of Helsinki, https://www.aquacosm.eu/mesocosm/tvarminne-mesocosm-facility-tmf/) in the Western Gulf of Finland. This Baltic Sea site is a brackish water estuarine environment (Kullenberg, 1981; Rolff and Elmgren, 2000) and the experiment investigated the biological and physicochemical system responses of this site to added humic substances and/or nutrients. The LightCycle experiment was a component of the JOMEX project, testing the photodegradation rates and trends of the added humic substances and native CDOM/DOM as well as the interactions of DOM photochemistry with added inorganic nutrients (phosphate and ammonium).

Sampling

The JOMEX experiment ran from 26 June to 10 July 2019. The experimental setup consisted of 9 2000 L capacity (0.9 m diameter × 3 m depth) mesocosms at the TMF at 59.843144 N, 23.260337 E. Humic substances (Humintech GmbH HuminFeed® WSG) and nutrients (NH_4Cl and KH_2PO_4) were added to mesocosms on 26 June 2019 (day 1). The mesocosms were divided into three treatment groups: three control mesocosms with no humic substances or nutrients added, three humic-amended mesocosms with only humic substances added to a final concentration of 2 mg L^{-1} in each mesocosm and three humic+nutrients-amended mesocosms with humic substances (2 mg L^{-1} final concentration) and NH_4Cl and KH_2PO_4 (80 µg

L^{-1} N and 20 μg L^{-1} P final concentrations) added. All mesocosms were covered with transparent acrylic covers (cut off wavelength below ~380 nm) during the experiment.

The surface salinity at the mesocosm site was relatively low (5.6 - 6.1 for the 13-day sampling period of the LightCycle experiments) with little variation (5.8 ± 0.2). The surface water temperature was 15 °C at the beginning of the amendment experiment, but decreased to 11 °C on day 8 and stayed low, until it was 1 degree higher on day 13 at 12 °C.

Surface (1 m) water samples for our LightCycle experiments were collected using precleaned 10 L HDPE canisters (Plastex®, Finland) from one each of control, humic-amended and humic+nutrients amended mesocosms, immediately after the amendment (day 1) and 2, 5, 7, 9 and 12 days after the amendment (days 3, 6, 8, 10 and 13). Water samples were filtered through 0.2 μm Whatman Polycap 36 AS nylon membrane cartridge filters to remove particulate matter, plankton and bacteria, using a Masterflex L/S Digital Standard Drive peristaltic pump with Easy Load II and Masterflex L/S 17 silicone tubing at 100 mL min^{-1}, directly into precleaned 10 L polyethylene Hedwin Cubitainers™. Filtered sample waters were stored in the dark in an environmental chamber set at temperatures matching the *in situ* temperatures of the JOMEX site before use. Sample waters were used in photoirradiation experiments at the TZS within 2 days of collection. CDOM absorbance and DOC concentrations were measured for these experiments. Aliquots of remaining water samples were shipped on ice to the Skidaway Institute of Oceanography (SkIO), Savannah GA, USA, and were stored in the dark at 4 °C before use; two more photoirradiation experiments were run on these shipped samples on 18 September and 24 September 2019. CDOM absorbance and photoproduced dissolved inorganic carbon concentrations were measured during these two additional experiments.

All plastic containers, filters, tubing and other labware for sampling and photoirradiation experiments were acid cleaned; first, rinsed with copious amount of MilliporeSigma 18.2-MΩ.cm Milli-Q® Type 1 ultrapure water (Milli-Q water), and then soaked overnight in 0.1 % HCl solution (pH 2). After rinsing again with an excess of Milli-Q water, these were stored with a small amount of fresh pH-2 HCl solution to prevent bacterial growth. Before use, plasticware were again rinsed with copious amounts of Milli-Q water. All glassware was acid washed following the same procedure, then dried and baked at 450 °C for at least 5 h. All labware was rinsed three times with a small volume of sample water prior to use. All acid solutions were made using Fisher Chemical Certified ACS Plus grade HCl and Milli-Q water.

Photoirradiation experiment

Photoirradiation experiments were carried out following the protocols described in Powers et al. (2017) (Powers et al., 2017b). Samples from the control, humic-amended and humic+nutrients-amended mesocosms were each partitioned into six 10-cm-pathlength cylindrical Spectrocell spectrophotometric quartz cells (cells, ~30 mL volume each). These quartz cells and caps were cleaned following abovementioned protocols but not baked at 450 °C. Each cell was rinsed three times with sample water from the corresponding cubitainers before filling, without headspace, directly from the cubitainers. Each cell was capped with two Spectrocell caps fitted with Microsolv Teflon-lined butyl septa. Five cells for each treatment type (15 total) were placed vertically into a temperature (15°C)-controlled black aluminum block, and irradiated under an Atlas Suntest CPS+ solar simulator equipped with a 1.5 kW xenon lamp (Powers et al., 2017a; Powers et al., 2017b; Powers and Miller, 2015b). The solar simulator was fitted with a daylight filter (excluding light below ~300 nm) to provide the cells with precisely

known, full spectral light. One cell for each treatment type was wrapped in aluminum foil to serve as dark control and placed in the same water bath that provided cooling water to the aluminum block.

After irradiation, for each time point (irradiation time points see Table 2.1), 20 mL aliquots of the sample were collected from the quartz cells into acid-cleaned and 450 °C-baked 24 mL Shimadzu DOC vials, acidified to pH 2 and capped with Teflon septa-lined caps. These samples were stored in the dark at 4 °C until analyzed within a week for DOC concentrations by high-temperature catalytic oxidation method using a Shimadzu TOC-V CPH analyzer equipped with a Shimadzu ASI-V autosampler (Cauwet, 1999; Koistinen et al., 2020) at the TZS.

To provide some background photodegradation rates of added humic substances, the same Humintech GmbH HuminFeed® WSG was dissolved in Milli-Q water at a concentration of 2 mg L^{-1}, filtered through a 0.2 μm Whatman Polycap 36 AS nylon membrane cartridge filter, the same way the mesocosm samples were filtered, and irradiated in a similar fashion in temperature-controlled quartz cells under the solar simulator. DOC concentrations were determined within a week using a Shimadzu TOC-V CPH analyzer at SkIO using similar protocols as describe above.

Table 2.1. Initial chromophoric dissolved organic matter absorption coefficients at 280 nm, 400 nm and integrated over 280–400 nm (a_g(280) (m^{-1}), a_g(400) (m^{-1}) and a_g(int) (m^{-1} nm), respectively), dis- solved organic carbon concentrations ([*DOC*], mg L^{-1}) and specific ultraviolet absorbance at 254 nm ($SUVA_{254}$, L mg^{-1} m^{-1}), for JOMEX amendment experiment.

Day	Irradiation time (h)	Control					Humic					Humic+Nutrients				
		a_g280 (m^{-1})	a_g400 (m^{-1})	$a_g(int)$ (m^{-1} nm)	[DOC] (mg L^{-1})	$SUVA_{254}$ (L mg^{-1} m^{-1})	a_g280 (m^{-1})	a_g400 (m^{-1})	$a_g(int)$ (m^{-1} nm)	[DOC] (mg L^{-1})	$SUVA_{254}$ (L $mg^{-1}m^{-1}$)	a_g280 (m^{-1})	a_g400 (m^{-1})	$a_g(int)$ (m^{-1} nm)	[DOC] (mg L^{-1})	$SUVA_{254}$ (L $mg^{-1}m^{-1}$)
1	0, 2, 5, 12, 19, 27	16.5	1.19	666	5.2	2.1	21.4	2.53	988	5.5	2.4	21.3	2.43	993	6.3	2.1
3	0, 4, 8, 14, 24, 36	16.3	1.24	657	5.2	2.1	21.0	2.46	984	5.4	2.5	21.0	2.44	989	5.1	2.6
6	0, 4, 8, 14, 24, 36	15.8	1.17	630	5.0	2.1	20.2	2.28	922	5.4	2.4	20.1	2.26	921	5.2	2.5
8	0, 4, 8, 14.1, 24.1, 36.1	15.5	1.18	614	4.8	2.2	19.1	1.98	853	5.1	2.4	19.1	1.97	849	5.2	2.4
10	0, 4, 8, 14, 24, 36	15.4	0.98	611	4.9	2.1	18.0	1.70	780	5.1	2.3	17.7	1.67	763	6.8	1.7
13	0, 4, 8, 14, 24, 36	15.2	1.14	598	4.8	2.1	17.0	1.45	701	5.1	2.2	16.6	1.46	688	5.0	2.2

Optical measurements and analyses

After DOC samples were collected, absorbance ($A(\lambda)$) in the remaining sample waters were measured at 250 - 800 nm at 1.0 nm intervals, in duplicate, in a 1-cm-pathlength quartz spectrophotometric cuvette. At TZS, a Shimadzu UV-2501PC UV-VIS recording spectrophotometer with UV-Probe software was used, with air as an internal reference and Milli-Q water as blanks. At SkIO, absorbances were obtained using an Agilent 8453 UV-visible spectrophotometer with ChemStation software, with the same parameters as above and Milli-Q water as blanks. The average absorbance spectra of blanks were subtracted from the absorbance spectra of the sample water. Absorbance spectra were further corrected for potential offsets and instrument drift by subtracting the average absorbance at 690 - 710 nm (Stubbins et al., 2011), before converting $A(\lambda)$ to Napierian absorption coefficients ($a_g(\lambda)$; m^{-1}), using the following equation (Hu et al., 2002b): $a_g(\lambda) = \frac{A \ln 10}{L}$, where L (m) is the pathlength.

For laboratory irradiation experiments, the spectral downwelling irradiance $E_o(\lambda)$ (mol photons m^{-2} s^{-1} nm^{-1}) entering each cell was quantified using an Optronic Laboratories OL756 Portable UV-Vis Spectroradiometer. The calibration of the spectroradiometer, measurements of irradiance and calculations of the photon dose absorbed by CDOM in the samples ($Q_a(\lambda)$, mol photons s^{-1} nm^{-1}, Eq. (1)), and wavelength (280 - 600 nm)-integrated photon dose $Q_a(\text{int})$ (mol photons absorbed, Eq. (2)) was calculated following Powers et al. (2017) (Powers et al., 2017b) and Hu et al. (2002) (Hu et al., 2002a).

$$Q_a(\lambda) = E_0(\lambda)\left(1 - e^{-a_g(\lambda)L}\right)S \quad (1)$$

where S (m^2) is the area of the irradiated surface of the cells.

$$Q_a(\text{int}) = t\int_{280}^{600} Q_a(\lambda) \quad (2)$$

where t (s) is the irradiation time.

The *in situ* wavelength (380 - 490 nm)- and depth (3 m)-integrated photon dose (Q_a(int), mol photons absorbed) was estimated following Fichot and Miller (2010) (Fichot and Miller, 2010), using CDOM absorption measured during the LightCycle experiment ($a_g(\lambda)$ in unirradiated samples), diffuse attenuation coefficients estimated from measured absorption coefficients and downwelling irradiance estimated from modeled data,. Briefly, the diffuse attenuation coefficients (K_d) at 412 nm were estimated using measured a_g at 400 nm (equation in Figure 5 of Kowalczuk et al. 2005 (Kowalczuk et al., 2005): $\log\left(a_g(400)\right) = -0.0113 + 0.713 \times \log\left(K_d(412)\right)$), and approximation ratios (control: 0.6 - 0.9; humic-amended: 0.6 - 0.7, humic+nutrients-amended: 0.5 - 0.6) were calculated by dividing a_g(412) by K_d(412). Assuming that the contribution to K_d from CDOM absorption is consistent across the whole spectrum, K_d values across the 290 - 490 nm wavelength range were calculated by dividing the a_g values at corresponding wavelengths by these approximation ratios for the corresponding day. Cloud-corrected daily integrated downwelling irradiance (280 - 700 nm at 1 nm intervals) just below the water surface for July 15th (1996 - 2003) at 59.94 N, 23.26 E was calculated as described previously (Fichot and Miller, 2010) using clear-sky downwelling irradiance obtained from the radiative transfer model STAR (System for Transfer of Atmospheric Radiation, (Ruggaber et al., 1994)) and corrections for clouds. The *in situ* photon dose was integrated from 380 nm because the acrylic cover likely cut off all UV transmission below 380 nm.

CDOM fading in laboratory experiments was expressed as a_g fading rates (m^{-1} (mol photons absorbed)$^{-1}$), calculated by linear regressions of $a_g(\lambda)$ versus Q_a(int). Similarly, the *in situ* a_g fading rates (m^{-1} (mol photons absorbed)$^{-1}$) were calculated by linear regressions of *in situ* $a_g(\lambda)$ (values in unirradiated samples from each day's laboratory experiment) versus *in situ* Q_a(int). Laboratory a_g fading rates at 280 and 400 nm were selected as examples of the

magnitude and changes in these fading rates because CDOM absorbs most strongly at the UV range and absorption above 400 nm was very low. In case the changes in a_g differ between lower and higher wavelengths, the sum of total absorption at 280 - 400 nm (Koehler et al., 2014) was calculated as integrated a_g across 280 - 400 nm (a_g(int), m^{-1} nm) following the Simpson's Rule. a_g(int) fading rates by photon dose (m^{-1} nm (mol photons absorbed)$^{-1}$) were calculated from linear regressions of a_g(int) versus laboratory and *in situ* photon doses, respectively, to provide an idea of the total amount of CDOM fading occurring in the UV range. To account for the possibility of other *in situ* CDOM loss mechanisms, such as flocculation and biodegradation, the *in situ* a_g fading rates versus time (m^{-1} day^{-1} and m^{-1} nm day^{-1}) were also calculated (by linear regressions of *in situ* $a_g(\lambda)$ and a_g(int) vs. time (day)) to provide a general idea of CDOM loss in the mesocosms.

Chromophoric dissolved organic matter absorption spectral slope $S_{275\text{-}295}$ (nm^{-1}) values, which may reflect the molecular weights of CDOM molecules, were calculated by linear regressions of natural log-transformed absorbance (ln$A$) versus wavelength for 275 - 295 nm (Helms et al., 2008). Specific ultraviolet absorbance at 254 nm ($SUVA_{254}$; L mg^{-1} m^{-1}) has been correlated with DOM aromaticity of standard reference materials, and was calculated as the Decadic absorption coefficient at 254 nm ($A(254)/L$; m^{-1}) divided by DOC concentrations (mg L^{-1}) (Weishaar et al., 2003).

The laboratory rates of change of $S_{275\text{-}295}$ (nm^{-1} (mol photons absorbed)$^{-1}$) and $SUVA_{254}$ (L mg^{-1} m^{-1} (mol photons absorbed)$^{-1}$) were calculated using linear regressions of $S_{275\text{-}295}$ and $SUVA_{254}$ versus photons absorbed. The *in situ* values of these two parameters were from unirradiated samples in individual laboratory experiments, and the *in situ* rates of change (nm^{-1} (mol photons absorbed)$^{-1}$, nm^{-1} day^{-1}, L mg^{-1} m^{-1} (mol photons absorbed)$^{-1}$ and L mg^{-1} m^{-1} day^{-1},

respectively) were calculated using linear regressions of the *in situ* values versus *in situ* photon dose and time.

Dissolved inorganic carbon (DIC) measurements

Dissolved inorganic carbon photoproduction rates were measured at SkIO using a stable isotope dilution method, moderate dissolved inorganic carbon ($DI^{13}C$) isotope enrichment (MoDIE) (Powers et al., 2017b). Briefly, water samples were enriched to about 5000 ‰ δ^{13}C-DIC using ~7 mg L^{-1} of $NaH^{13}CO_3$, equilibrated by stirring for at least 1 h and then distributed to quartz cells using gas sampling techniques (Powers et al., 2017b) and irradiated as mentioned above. Samples were then injected into a ThermoFisher Delta V+ Isotope Ratio Mass Spectrometer through an ThermoFisher Isolink interface (Brandes, 2009), and the δ^{13}C-DIC and initial DIC concentrations of the samples were measured. The concentrations of photochemically produced DIC (M) were then calculated using mass balances of DIC and $^{13}C/^{12}C$ (Powers et al., 2017b). The DIC photoproduction rates P_{DIC} (μM (mmol photons absorbed)$^{-1}$) were calculated using linear regressions of photochemically produced DIC concentrations (M) versus photons absorbed (mol). Integrated DIC photoproduction efficiencies (DIC apparent quantum yield, AQY(int); μmol (mol photons absorbed)$^{-1}$) were calculated by multiplying P_{DIC} by the average quartz cell volume (30 mL).

Statistics

Linear regressions were performed using *lm* in R (RCoreTeam, 2021). Analysis of covariance (ANCOVA, *anova* in R; (RCoreTeam, 2021)) was used to determine whether the rates of change (slopes of linear regressions) in various parameters (over photons absorbed and

time) were different among the different treatment types. When the slopes were not statistically different between treatment groups (ANCOVA interaction term $P > 0.05$), comparison of parameter values were made between different treatment groups using analysis of variance (ANOVA, *anova* in R; (RCoreTeam, 2021)) after adjusting for photon doses or time.

Results

Chromophoric dissolved organic matter (CDOM) losses in the mesocosm

The humic- and humic+nutrients-amended mesocosms had higher absorption coefficient values than the control mesocosm at the beginning of the amendment experiment due to the added humic substances (Table 2.1 and Supplemental Figure S2.1). This trend of higher a_g values in the amended mesocosms continued throughout the amendment experiment, but the a_g values decreased over time *in situ* in all mesocosms (Figure 2.1 and 2.2, and Supplemental Figure S2.1). By day 13, absorption coefficients were more similar between all three mesocosms (Table 2.1 and Supplemental Figure S2.1), corresponding to 7.8 % $a_g(280)$ and 4.2 % $a_g(400)$ losses in the control mesocosm, 20 % $a_g(280)$ and 42 % $a_g(400)$ losses in the humic-amended mesocosm and 22 % $a_g(280)$ and 40 % $a_g(400)$ losses in the humic+nutrients-amended mesocosm. Similarly, the amended mesocosms had higher integrated absorption across the UV wavelength range 280 - 400 nm (Figures 2.1e, f, Table 2.1, and Supplemental Figure S2.1). Integrated absorption similarly decreased in all mesocosms (linear regressions, $P < 0.05$), corresponding to 10 %, 31 % and 31 % losses in the control, humic- and humic+nutrients-amended mesocosms respectively (Figures 2.1e, f, Table 2.2, and Supplemental Figure S2.1).

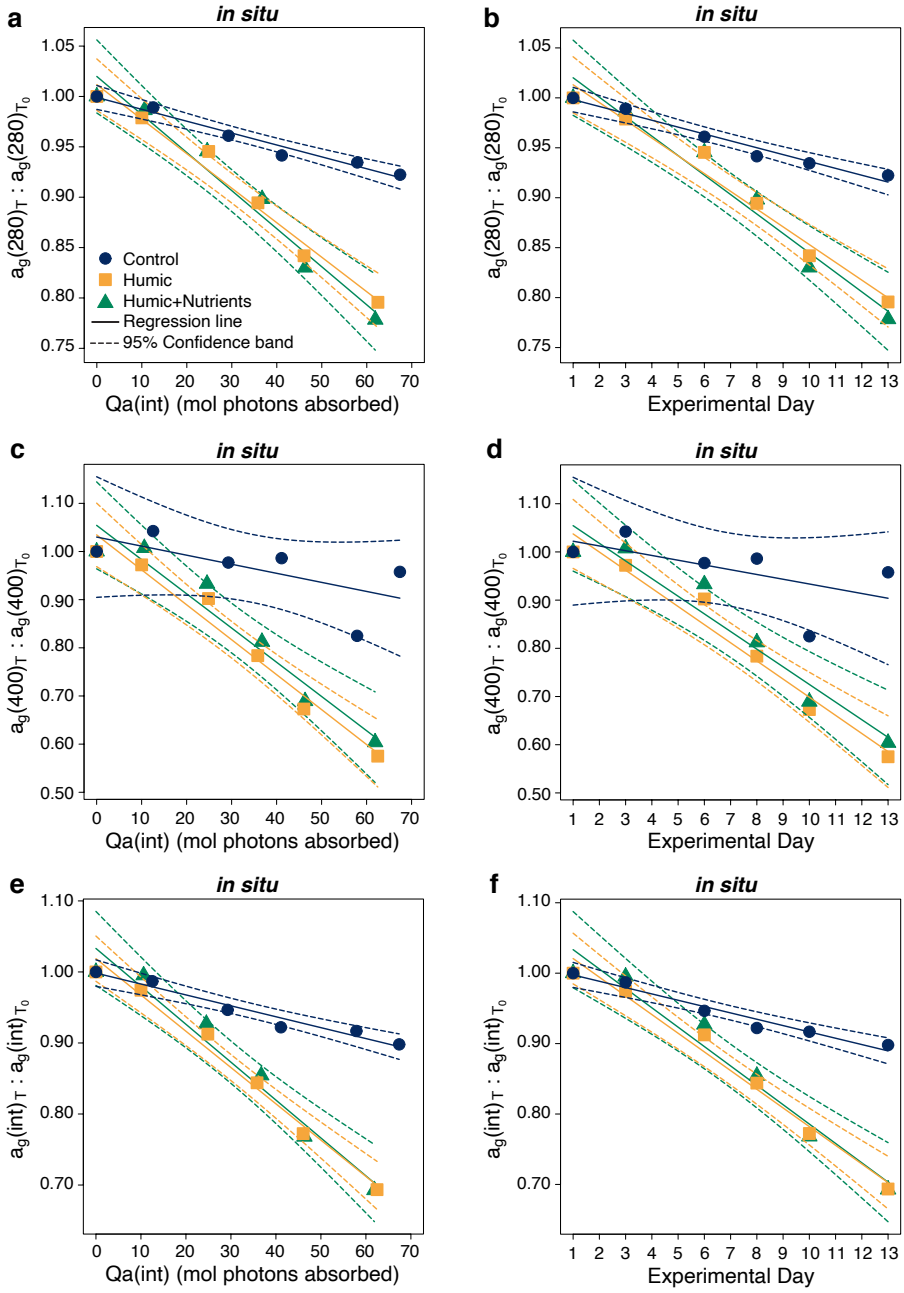

Figure 2.1. Ratios of chromophoric dissolved organic matter absorption coefficient (a, c, e) versus photon doses (Q_a(int), mol photons absorbed), and (b, d, f) versus time (day), for JOMEX amendment experiment samples that reflect the *in situ* conditions, (a, b) at 280 nm, $a_g(280)_T$: $a_g(280)_{T0}$; (c, d) at 400 nm, $a_g(400)_T$: $a_g(400)_{T0}$; (e, f) integrated from 280 nm to 400 nm, $a_g(\text{int})_T$: $a_g(\text{int})_{T0}$. Ratios were calculated as values at different days to those at experimental day 1 (immediately after amendment).

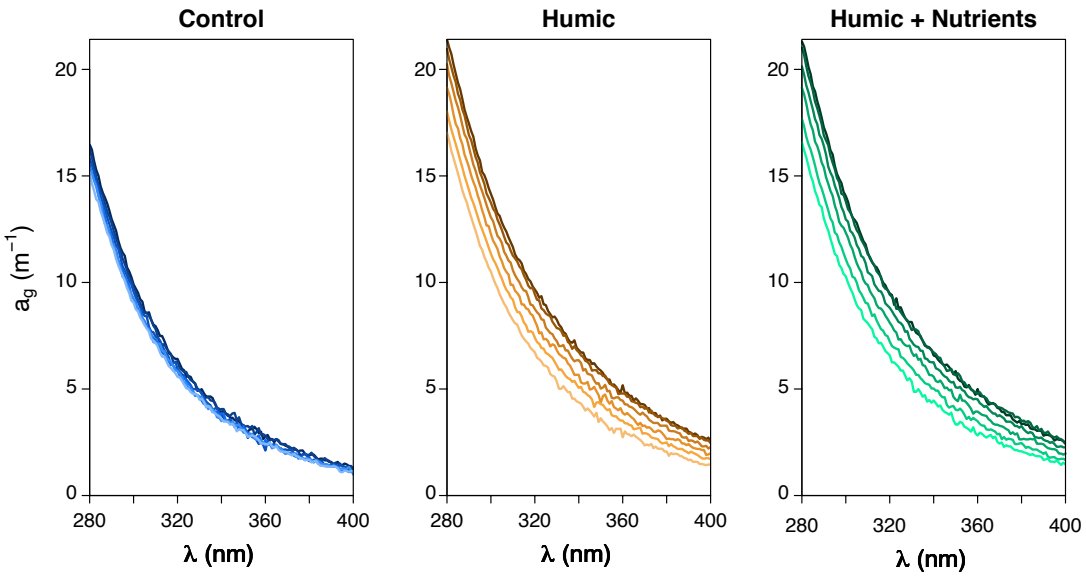

Figure 2.2. Chromophoric dissolved organic matter absorption coefficients (a_g, m^{-1}) versus wavelength λ (nm) of mesocosm samples on experimental days 1, 3, 6, 8, 10 and 13 of the JOMEX experiment. Day 1 was the day of initial amendment and corresponds to the darkest color in each treatment, the color became lighter over time and day 13 corresponds to the lightest color.

The *in situ* integrated photon doses from 380 - 490 nm for humic- and humic+nutrients-amended samples were 80 - 93 % of those absorbed by control samples, due to the higher attenuation coefficients in the amended mesocosms, which in turn was due to the higher absorption coefficients (Figure 2.1a, 2.1c, and 2.1e). The *in situ* photon doses were similar between the humic- and humic+nutrients-amended samples. Despite the relatively smaller amounts of photons absorbed, a_g fading rates (slopes of linear regressions for a_g vs. *in situ* photon dose) were much higher in the humic-amended mesocosm than in the control mesocosm (ANCOVA and linear regressions, $P < 0.05$), at 280 nm and 400 nm, and for a_g(int) (Figure 2.1, Table 2.2 and Supplemental Figure S2.1). There was no statistically significant difference in a_g

fading rates between the humic- and humic+nutrients-amended samples at either wavelength or the integrated absorption (ANCOVA, $P > 0.05$, Figure 2.1, Table 2.2 and Supplemental Figure S2.1).

Because it is not possible to separate the various CDOM loss and addition mechanisms that can potentially occur *in situ*, CDOM loss rates were also calculated versus sampling time in days (Figures 2.1b, d, f and Supplemental Figure S2.1). The trends of a_g fading rates versus time were similar to the trends in fading rates by photon dose, even though the rates were in units of m^{-1} day^{-1} (Figure 2.1 and Supplemental Figure S2.1). a_g fading rates were higher in the humic-amended mesocosm than in the control mesocosm (ANCOVA and linear regressions, $P < 0.05$), except for a non-significant slope of control sample at 400 nm. $a_g(280)$ fading rates for the control and humic-amended mesocosms were -0.11 ± 0.010 and -0.38 ± 0.030 m^{-1} day^{-1}, respectively; $a_g(400)$ fading rates for the control and humic-amended mesocosms were - 0.012 ± 0.0080 and - 0.095 ± 0.0092 m^{-1} day^{-1}, respectively (Figures 2.1b, d). However, there was no statistically significant difference in a_g fading rates versus time between the humic- and humic+nutrients-amended mesocosms at either wavelength (ANCOVA, $P > 0.05$; linear regressions, -0.42 ± 0.041 and - 0.089 ± 0.012 m^{-1} day^{-1} at 280 and 400 nm, respectively, for the humic+nutrients-amended mesocosm, $P < 0.05$. Figures 2.1b and 2.1d). Similarly, a_g(int) fading rates were higher in humic- (-27 ± 1.8 m^{-1} nm day^{-1}) and humic+nutrients-amended mesocosms (-27 ± 2.7 m^{-1} nm day^{-1}) than in the control mesocosm (-6.0 ± 0.60 m^{-1} nm day^{-1}. ANCOVA and linear regressions, $P < 0.05$. Figure 2.1f) but were not significantly different between the amended mesocosms (ANCOVA, $P > 0.05$).

CDOM losses during laboratory irradiation experiments

For laboratory irradiation experiments, amended samples had higher CDOM absorption coefficients at 280 and 400 nm than control samples throughout each experiment, and the same trend was also seen in the 280 - 400 nm integrated absorption a_g(int) (ANCOVA and ANOVA, $P < 0.05$, Supplemental Figure S2.2). Between the amended samples, humic-amended samples had higher a_g(280) and a_g(int) than the humic+nutrients-amended samples in irradiation experiments conducted using the days 10 and 13 samples, and higher a_g(400) in day 13 samples (ANCOVA and ANOVA, $P < 0.05$), humic+nutrients-amended samples had higher a_g*(400)* in day 1 samples, but otherwise the a_g values were not statistically different between the two groups during irradiation experiments (ANCOVA and ANOVA, $P > 0.05$, Supplemental Figure S2.2).

At the beginning of the amendment experiment, the amended samples absorbed more photons than the control samples in laboratory irradiation experiments because of the higher CDOM absorption, at about twice as high on day 1. This difference decreased over time, and toward the end of the amendment experiment, the photons absorbed during laboratory irradiation experiments were similar among all three groups (Figure 2.3 and Supplemental Figures S2.2 and S2.3). Chromophoric dissolved organic matter faded in laboratory irradiation experiments, as indicated by the consistent decreases in absorption a_g(280) and a_g(int) with photon dose, for all treatment groups for all experimental days (linear regressions, $P < 0.05$, Figure 2.3, Table 2.2 and Supplemental Figure S2.2 and S2.3). The changes in a_g(400) were more variable, some days there was fading (linear regressions, $P < 0.05$), but there were no statistically significant changes in a_g(400) with photon dose in days 1, 3, and 10 control samples and days 3, 10, and 13 humic-amended samples (linear regressions, $P \geq 0.05$, Figure 2.3, Table 2.2 and Supplemental Figures S2.2 and S2.3).

At 280 nm, the a_g fading rates (slopes of regression lines for a_g vs. photon dose) in the control samples were higher than those in the humic-amended samples for most of the amendment experiment (ANCOVA and linear regressions, $P < 0.05$), except for day 8 and day 13 when there was no difference between the two groups (ANCOVA, $P > 0.05$, Figures 2.3a, d, g, Table 2.2 and Supplemental Figures S2.2 and S2.3). The a_g fading rates at 400 nm were not statistically different in the humic-amended and control samples for all days (ANCOVA, $P > 0.05$, Figures 2.3b, e, h, Table 2.2 and Supplemental Figures S2.2 and S2.3). The humic+nutrients-amended samples had similar a_g fading rates to the humic-amended samples, for all days at 280 nm and 400 nm (ANCOVA, $P > 0.05$), except that the humic+nutrients-amended samples faded faster at 400 nm than the humic-amended sample on day 3 (ANCOVA and linear regressions, $P < 0.05$. Figure 2.3, Table 2.2 and Supplemental Figures S2.2 and S2.3). Integrated absorption a_g(int) faded faster in the control samples on day 1, and in the humic+nutrients-amended samples on day 13 (ANCOVA and linear regressions, $P < 0.05$), but otherwise the fading rates in a_g(int) were not statistically different among groups (ANCOVA, $P \geq 0.05$. Figure 2.3c, f, i, Table 2.2 and Supplemental Figures S2.2 and S2.3).

For a_g(280), a_g(400) and a_g(int), the fading rates in individual irradiation experiments were variable across sampling days, and about 3-5 orders of magnitudes higher than the *in situ* rates in all groups (Table 2.2). In addition, the a_g fading rates in laboratory irradiation experiment of HuminFeed in Milli-Q water was -445.58 ± 52.317 m^{-1} (mol photons absorbed)$^{-1}$ at 280 nm, -188.80 ± 37.097 m^{-1} (mol photons absorbed)$^{-1}$ at 400 nm, and -41557 ± 5461.3 m^{-1} nm (mol photons absorbed)$^{-1}$ for a_g(int) (Table 2.2). The a_g(400) and a_g(int) fading rates of HuminFeed in Milli-Q water were comparable to the laboratory a_g fading rates of humic-amended mesocosm

samples, but were only about half of the average laboratory a_g fading rates of humic-amended mesocosm samples at 280 nm (Table 2.2).

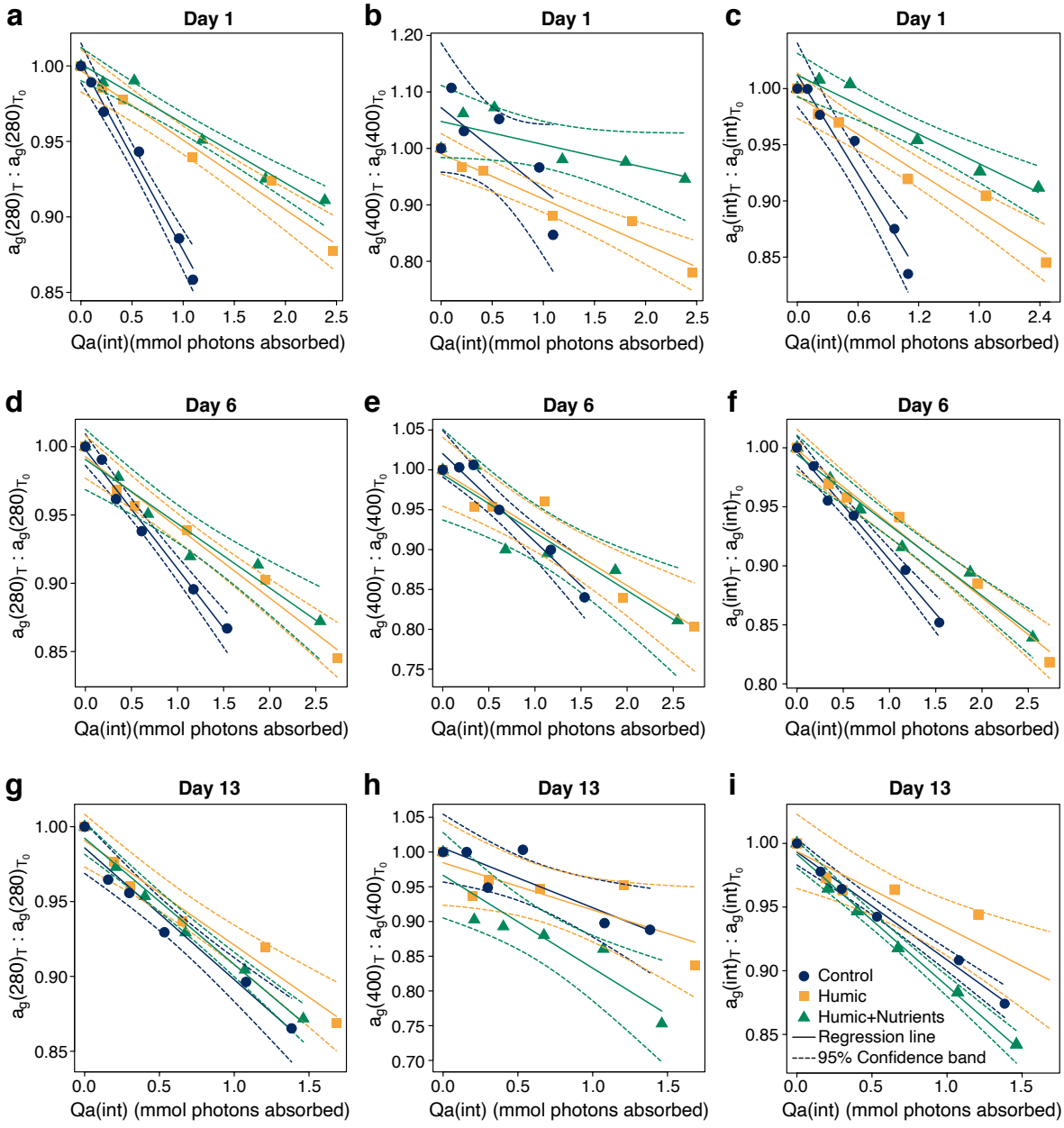

Figure 2.3. Ratios of chromophoric dissolved organic matter absorption coefficients at (a, d, g) 280 nm ($a_g(280)_T$: $a_g(280)_{T0}$), (b, e, h) 400 nm ($a_g(400)_T$: $a_g(400)_{T0}$) and (c, f, i) integrated over 280–400 nm ($a_g(\text{int})_T$: $a_g(\text{int})_{T0}$) versus photon dose (Q_a(int), mmol photons absorbed) for laboratory irradiation experiments conducted on mesocosm samples of the JOMEX experiment (day 1 was the day of initial amendment). Ratios were calculated by dividing the corresponding a_g at time T by that at time T_0.

Table 2.2. Chromophoric dissolved organic matter (CDOM) absorption coefficient a_g fading rates (mean ± 1 SE) at 280 nm (a_g(280)), 400 nm (a_g(400)) (m^{-1} (mol photons absorbed)$^{-1}$) and for integrated a_g over 280–400 nm (a_g(int)) (m^{-1} nm (mol photons absorbed)$^{-1}$), *in situ*, in laboratory irradiation experiments of the JOMEX experiment mesocosm samples after initial amendment), and in laboratory irradiation experiment of HuminFeed in Milli-Q ultrapure water (2 mg L^{-1} concentration).

Treatment	*in situ*	Laboratory irradiation experiments of mesocosm samples						HuminFeed® in water
		Day 1	Day 3	Day 6	Day 8	Day 10	Day 13	
$a_g(280)$: absorption at 280 nm								(m^{-1} (mol photons absorbed)$^{-1}$)
Control	-0.019430 ± 0.0016770	-2043.9 ± 120.87	-1104.8 ± 76.694	-1379.1 ± 78.087	-1227.8 ± 68.923	-1287.8 ± 40.721	-1336.4 ± 122.57	-
Humic	-0.073339 ± 0.0053850	-985.05 ± 80.298	-729.84 ± 114.22	-1046.2 ± 77.801	-1238.4 ± 127.95	-812.01 ± 123.13	-1188.2 ± 120.45	-445.58 ± 52.317
Humic+Nutrients	-0.080494 ± 0.0076050	-838.88 ± 63.283	-865.54 ± 72.941	-948.28 ± 114.14	-1019.8 ± 90.589	-1035.1 ± 95.695	-1398.0 ± 78.972	-
$a_g(400)$: absorption at 400 nm								(m^{-1} (mol photons absorbed)$^{-1}$)
Control	-0.0022460 ± 0.0012810	-174.44 ± 76.034	-40.906 ± 52.144	-128.53 ± 14.565	-147.71 ± 41.648	-43.833 ± 73.144	-98.114 ± 26.411	-
Humic	-0.018342 ± 0.0016410	-202.85 ± 24.095	-63.226 ± 30.507	-162.72 ± 24.192	-172.54 ± 39.923	-114.65 ± 48.516	-98.671 ± 35.571	-188.80 ± 37.097
Humic+Nutrients	-0.017235 ± 0.0021540	-99.303 ± 41.843	-167.42 ± 14.965	-164.52 ± 32.958	-157.46 ± 34.400	-213.57 ± 41.808	-195.82 ± 40.010	-
$a_g(int)$: absorption integrated over 280-400 nm								(m^{-1} nm (mol photons absorbed)$^{-1}$)
Control	-1.0232 ± 0.10660	-97988 ± 10492	-44696 ± 3653.7	-57853 ± 3466.5	-50450 ± 1415.5	-49018 ± 4872.6	-50724 ± 2889.0	-
Humic	-5.1619 ± 0.31680	-57712 ± 5447.4	-44557 ± 6121.7	-57659 ± 3971.0	-64258 ± 8544.6	-36571 ± 10301	-42085 ± 8188.1	-41557 ± 5461.3
Humic+Nutrients	-5.3015 ± 0.50950	-43482 ± 5216.5	-47918 ± 3211.3	-55002 ± 3871.3	-54307 ± 3504.7	-53626 ± 5244.9	-71232 ± 3267.2	-

Changes in CDOM spectral slopes ($S_{275\text{-}295}$) in the mesocosms and during laboratory experiments

The control mesocosm had higher initial $S_{275\text{-}295}$ values (0.024 nm^{-1}) than the amended mesocosms (0.020 and 0.021 nm^{-1} for humic- and humic+nutrients-amended mesocosms, respectively). This trend of higher $S_{275\text{-}295}$ values in the control mesocosm than in the amended mesocosms continued throughout the amendment experiment. $S_{275\text{-}295}$ values increased *in situ* with photon dose and time in the amended mesocosms (linear regressions, $P < 0.05$), but showed no statistically significant changes with photon dose or time in the control mesocosm (linear regression, $P \geq 0.05$. Figure 2.4). As a result, rates of change in $S_{275\text{-}295}$ values (slopes of linear regressions for $S_{275\text{-}295}$ vs. *in situ* photon dose) were higher in the humic-amended mesocosm ($5.6 \times 10^{-5} \pm 6.5 \times 10^{-6}$ nm^{-1} (mol photons absorbed)$^{-1}$ and $2.9 \times 10^{-4} \pm 3.6 \times 10^{-5}$ nm^{-1} day^{-1}, linear regressions, $P < 0.05$) than in the control mesocosm ($1.8 \times 10^{-5} \pm 6.6 \times 10^{-6}$ nm^{-1} (mol photons absorbed)$^{-1}$ and $1.0 \times 10^{-4} \pm 4.3 \times 10^{-5}$ nm^{-1} day^{-1}, linear regressions, $P < 0.05$) (ANCOVA, $P < 0.05$, Figure 2.4). The $S_{275\text{-}295}$ values were not statistically different between the two amended mesocosms for the duration of the amendment experiment, and the rates of change in $S_{275\text{-}295}$ values were not statistically different between the two groups (ANCOVA and ANOVA, $P > 0.05$; $5.5 \times 10^{-5} \pm 7.9 \times 10^{-6}$ nm^{-1} (mol photons absorbed)$^{-1}$ and $2.8 \times 10^{-4} \pm 4.2 \times 10^{-5}$ nm^{-1} day^{-1} for humic+nutrients-amended mesocosm, linear regressions, $P < 0.05$. Figure 2.4). At the end of the amendment experiment (day 13), $S_{275\text{-}295}$ values increased by 18 % in the humic-amended mesocosm and 16 % in the humic+nutrients-amended mesocosm, and these values became more similar to that in the control mesocosm than at the beginning of the amendment experiment.

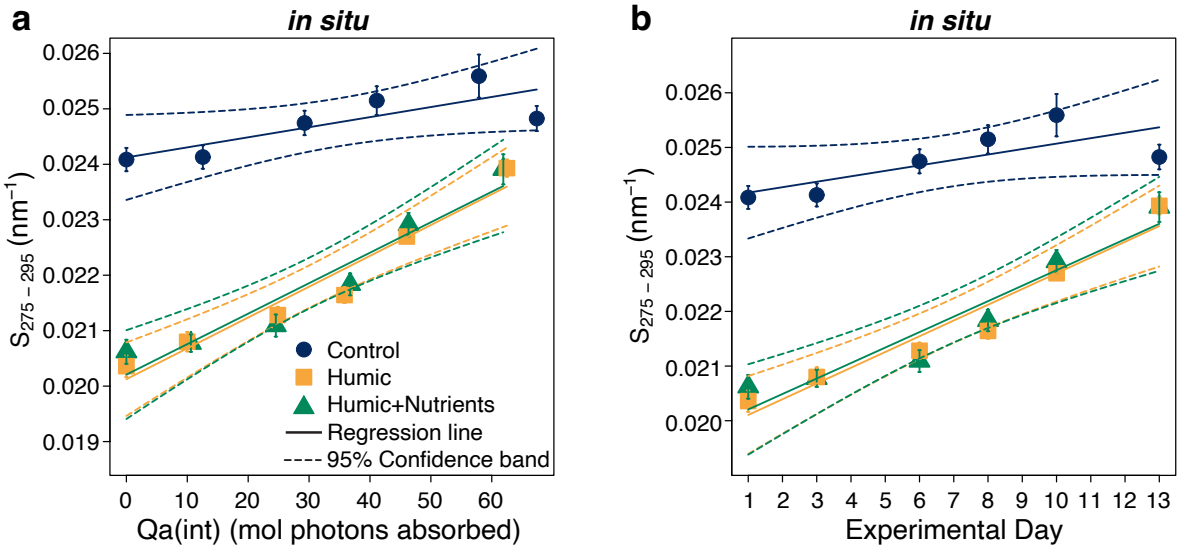

Figure 2.4. (a) Chromophoric dissolved organic matter absorption spectral slope $S_{275\text{-}295}$ (nm^{-1}) versus photon doses (Q_a(int), mol photons absorbed) for JOMEX amendment experiment samples that reflect the *in situ* conditions; (b) $S_{275\text{-}295}$ versus time (experimental day, day 1 was the day of initial amendment). Error bars were ± 1 standard error for $S_{275\text{-}295}$ (linear regression slopes of natural log-transformed absorbance versus wavelength at 275 – 295 nm).

In individual irradiation experiments, $S_{275\text{-}295}$ increased with photon dose in most treatment groups on most days sampled (linear regressions, $P < 0.05$), except on day 3 there was no change in the humic-amended samples (linear regression, $P \geq 0.05$, Figure 2.5 and Supplemental Figure S2.4). However, it is possible that the missing data point in humic-amended samples on day 3 leads to reduced statistical power and the difference in slopes on day 3 needs to be interpreted with caution. On day 10, there was no change in the control and humic-amended samples, and on day 13, there was no change in the humic-amended samples (linear regressions, $P \geq 0.05$, Figure 2.5 and Supplemental Figure S2.4).

In days 1 and 6 samples, the rates of change in $S_{275\text{-}295}$ (slopes of linear regressions for $S_{275\text{-}295}$ vs. photon dose) were higher in the control samples than in the humic-amended samples, and on day 3, the rate was higher in the humic+nutrients-amended than in the humic-amended samples (ANCOVA and linear regressions, $P < 0.05$, Figure 2.5). For the rest of the samples, the rates of change in spectral slopes were not different between control and humic-amended samples, or between humic and humic+nutrients-amended samples (ANCOVA, $P \geq 0.05$, Figure 2.5 and Supplemental Figure S2.4).

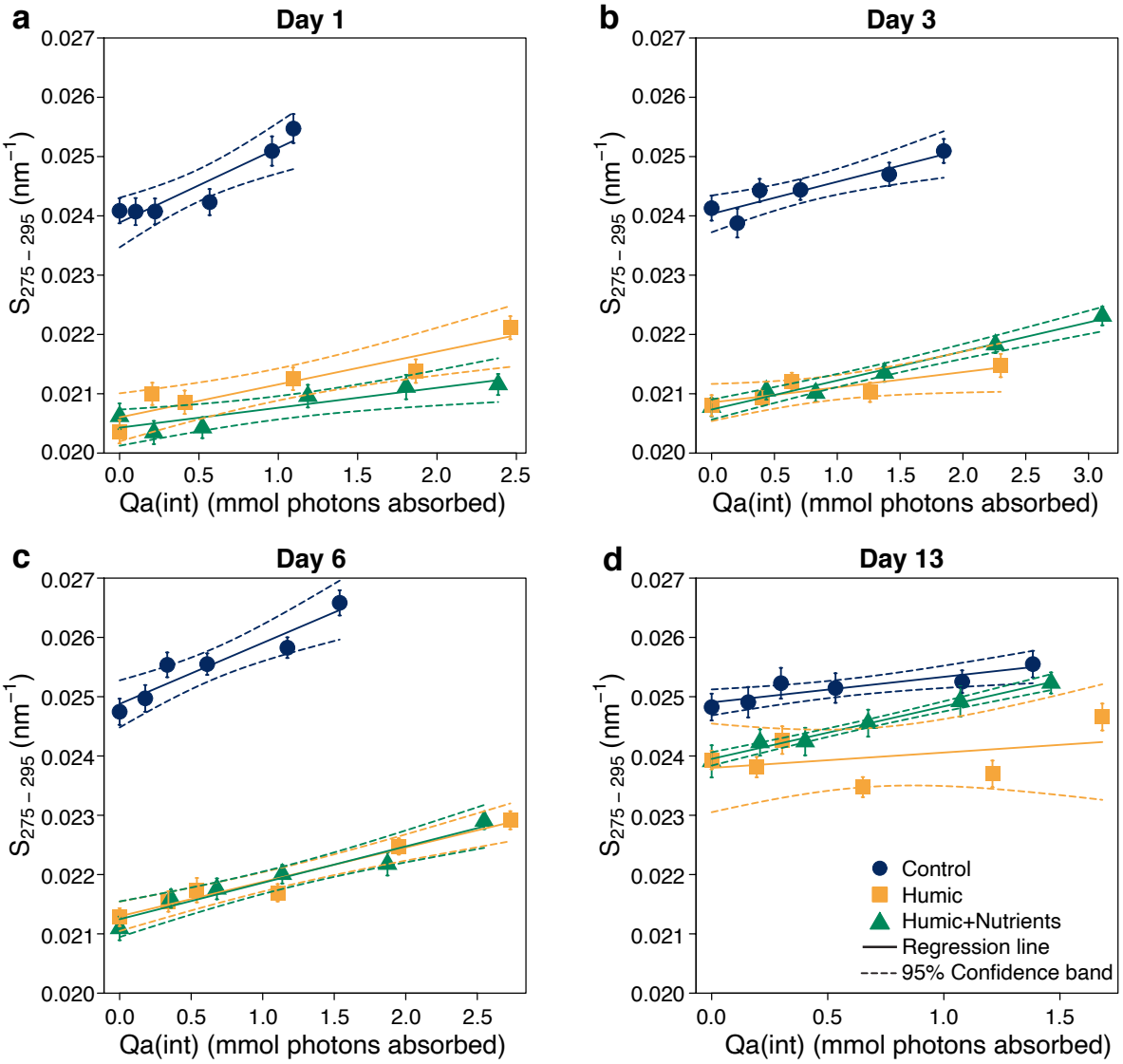

Figure 2.5. Chromophoric dissolved organic matter absorption spectral slope $S_{275\text{-}295}$ (nm^{-1}) versus photon dose (Q_a(int), mmol photons absorbed) for individual laboratory experiments, using mesocosm samples of the JOMEX amendment experiment. Error bars were 1 standard error for $S_{275\text{-}295}$ (linear regression slopes of natural log-transformed absorbance vs. wavelength at 275–295 nm).

Dissolved organic matter (DOM) degradation

The initial after amendment DOC concentrations were 5.2, 5.5 and 6.3 mg L^{-1} for control, humic-amended and humic+nutrients-amended mesocosms respectively (Figure 2.6 and Table 2.1). DOC concentrations were higher in the humic-amended mesocosm than those in the control mesocosm at the beginning and over the course of the amendment experiment (ANOVA, $P < 0.05$, Figure 2.6). DOC concentrations decreased *in situ* in both the control and humic-amended mesocosms with photon dose and time, although there was no statistically significant difference between the rates of change (-0.0064 ± 0.0015 mg L^{-1} (mol photons absorbed)$^{-1}$ and -0.038 ± 0.0085 mg L^{-1} day^{-1} in the control mesocosm, and 0.0073 ± 0.0017 mg L^{-1} (mol photons absorbed)$^{-1}$ and -0.038 ± 0.0090 mg L^{-1} day^{-1} in the humic-amended mesocosm (Linear regressions, $P < 0.05$. ANCOVA, $P = 0.7$)). DOC concentrations in the humic+nutrients-amended mesocosm were highly variable *in situ* over the course of the amendment experiment, and this variability precluded the evaluation of *in situ* DOM degradation rates based on DOC values in these samples, or comparison to other treatments.

In laboratory irradiation experiments, no clear trends in DOC concentration changes were detected (data not shown) because either changes in DOC concentrations were smaller than the signal-to-noise level of the Shimadzu TOC analyzer, or the DOC concentrations fluctuated a lot over the course of the irradiation but were not significantly different before and after irradiation, so that it was impossible to calculate the photodegradation rates of DOM directly, or to make comparisons among the different treatments for laboratory experiments.

The initial DOC concentration of HuminFeed in Milli-Q water (2 mg L^{-1}) was 0.30 ± 0.033 mg L^{-1}. This concentration is consistent with the difference between the initial DOC concentrations in control and humic-amended mesocosms. There was no consistent change in

DOC concentrations with photon dose when the HuminFeed in Milli-Q water samples were irradiated (linear regression, $P = 0.4$).

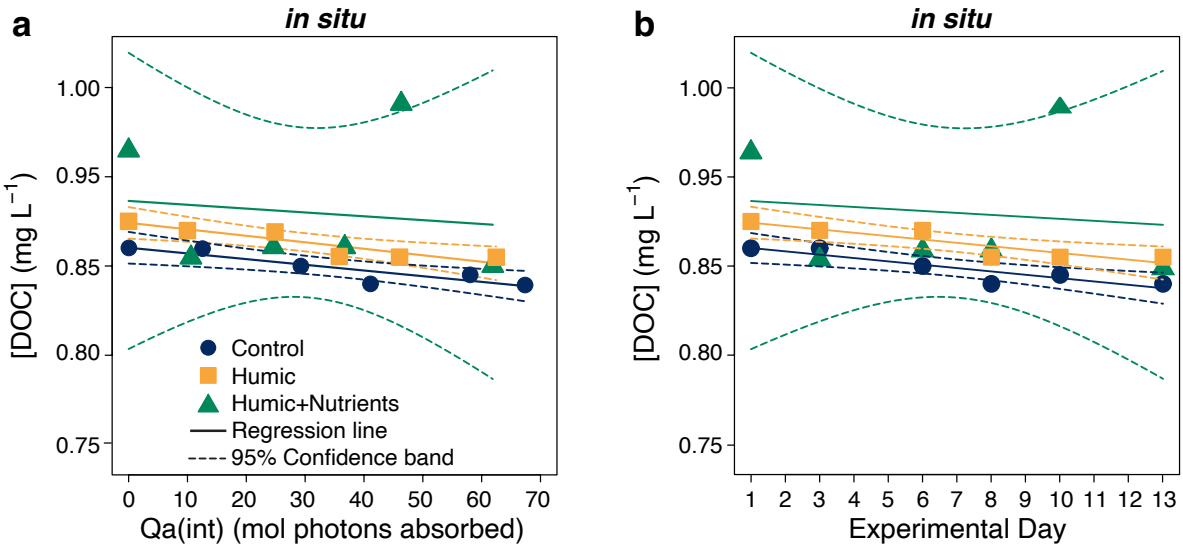

Figure 2.6. Dissolved organic carbon (DOC) concentrations (mg L^{-1}) (a) versus photon dose (Q_a(int), mol photons absorbed), and (b) versus time (day), for JOMEX amendment experiment samples that reflect the *in situ* conditions. Day 1 was the day of initial amendment.

The initial after amendment specific ultraviolet absorbance at 254 nm ($SUVA_{254}$) values were 2.1, 2.4 and 2.1 L mg^{-1} m^{-1} for control, humic-amended and humic+nutrients-amended mesocosms respectively (Figure 2.7 and Table 2.1). The *in situ* $SUVA_{254}$ values were higher in the humic-amended mesocosm than in the control mesocosm at the beginning and throughout the amendment experiment (ANOVA, $P < 0.05$, Figure 2.7). $SUVA_{254}$ decreased in the humic-amended mesocosm with photon dose and time (-0.0038 ± 0.00088 L mg^{-1} m^{-1} (mol photons absorbed)$^{-1}$ and - 0.020 ± 0.0047 L mg^{-1} m^{-1} day^{-1}; Linear regressions, $P < 0.05$), but there was no change in $SUVA_{254}$ values in the control mesocosm (linear regressions, $P > 0.05$) (Figure 2.7a, b).

As a result, the rates of change were higher in the humic-amended mesocosm with both photon dose and time (ANCOVA, $P < 0.05$). The $SUVA_{254}$ value in the humic-amended mesocosm (2.2 L mg^{-1} m^{-1}) became more similar to that in the control mesocosm (2.1 L mg^{-1} m^{-1}) at the end of the amendment experiment. $SUVA_{254}$ values in the humic+nutrients-amended mesocosm were again highly variable over the course of the amendment experiment, and this variability precluded the calculation of a linear rate, or comparison to other treatments.

In laboratory irradiation experiments, the changes in $SUVA_{254}$ values with photon dose fluctuated over the course of the amendment experiment. $SUVA_{254}$ values decreased with photon dose in the control and humic+nutrients-amended samples on day 6, 8, and 13, decreased in the humic-amended samples on day 8 only (linear regressions, $P < 0.05$), and otherwise showed no changes with photon dose (linear regressions, $P \geq 0.05$) (Figure 2.7c-f and Supplemental Figure S2.5). The rates of change were not different among the treatments (ANCOVA, $P \geq 0.05$) except for day 6, when the rate of change was higher in control than in the humic-amended samples (ANCOVA, $P < 0.05$) (Figure 2.7c-f).

The initial $SUVA_{254}$ of HuminFeed in Milli-Q water was 10 ± 2.3 L mg^{-1} m^{-1}. There was no consistent change in $SUVA_{254}$ values with photon dose when the samples were irradiated (linear regression, $P = 0.4$).

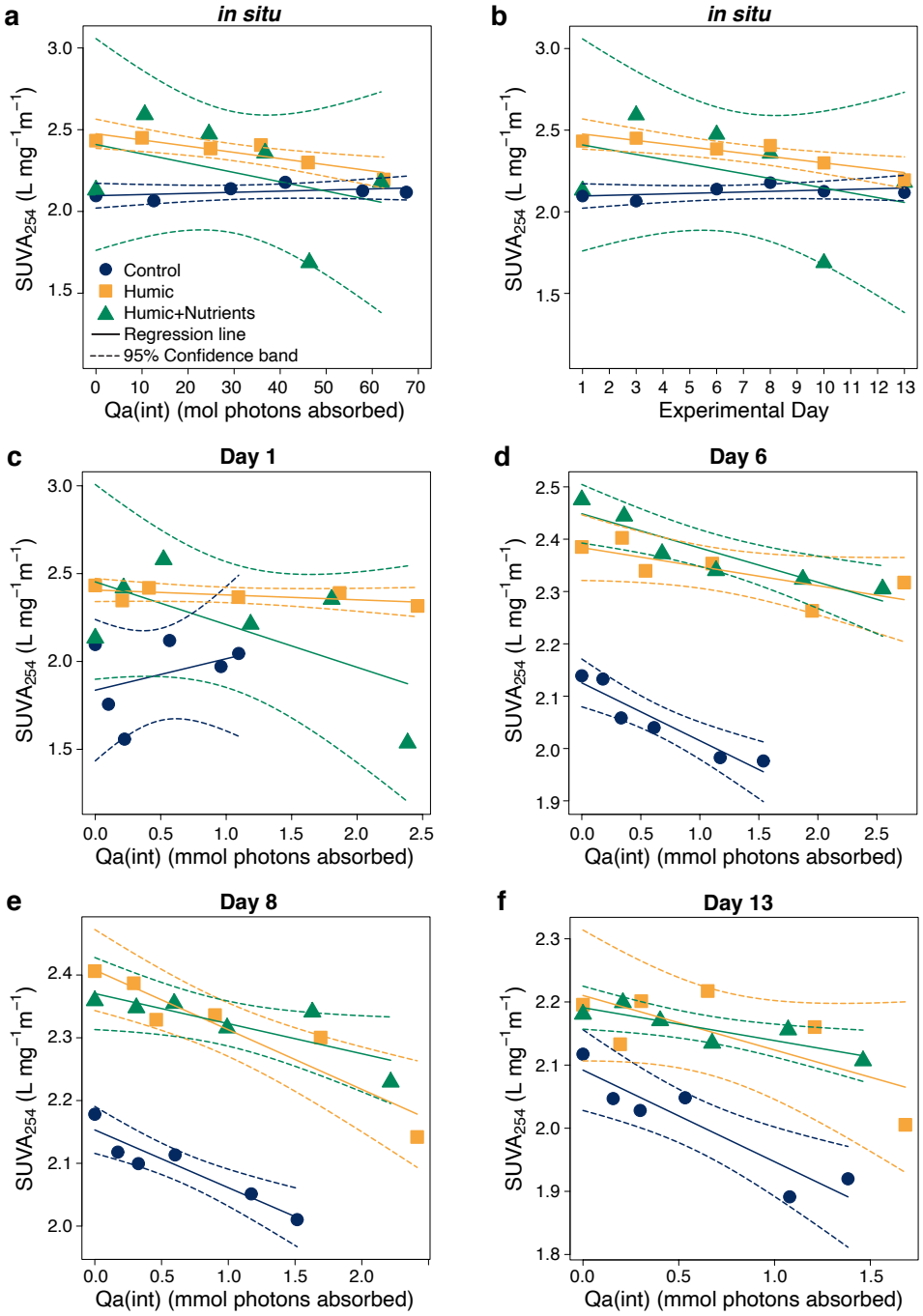

Figure 2.7. Specific ultraviolet absorbance $SUVA_{254}$ (L mg^{-1} m^{-1}) (a) versus photon doses (Q_a(int), mol photons absorbed), and (b) versus time (day), for JOMEX amendment experiment samples that reflect the *in situ* conditions. Day 1 was the day of initial amendment. (c–f) $SUVA_{254}$ versus photon dose (Q_a(int), mmol photons absorbed) for laboratory irradiation experiments using mesocosm samples of the JOMEX amendment experiment.

Although direct measurement of DOM photodegradation rates in laboratory experiments proved impossible given the variability of the DOC concentrations, DIC photoproduction rates measured using the MoDIE method provided some clue to the rates of DOM photodegradation in the treatment groups and the changes in these rates. Immediately after amendment (day 1), all groups had similar DIC photoproduction rates, at 1.4 ± 0.089 μM (mmol photons absorbed)$^{-1}$ (AQY(int) = 43 ± 2.7 μmol DIC (mol photons absorbed)$^{-1}$) for control samples, 1.5 ± 0.11 μM (mmol photons absorbed)$^{-1}$ (AQY(int) = 44 ± 3.4 μmol DIC (mol photons absorbed)$^{-1}$) for humic-amended samples and 1.6 ± 0.17 μM (mmol photons absorbed)$^{-1}$ (AQY(int) = 48 ± 5.1 μmol DIC (mol photons absorbed)$^{-1}$) for humic+nutrients-amended samples respectively (Figure 2.8). By day 6, the rates in control and humic-amended samples increased to 2.7 ± 0.23 μM (mmol photons absorbed)$^{-1}$ (AQY(int) = 82 ± 6.8 μmol DIC (mol photons absorbed)$^{-1}$), and 2.5 ± 0.11μM (mmol photons absorbed)$^{-1}$ (AQY(int) = 74 ± 3.3 μmol DIC (mol photons absorbed)$^{-1}$), corresponding to 93 % increase and 67 % increase, respectively. The rate in humic+nutrients-amended samples remained the same (1.6 ± 0.15 μM (mmol photons absorbed)$^{-1}$, AQY(int) = 47 ± 4.6 μmol DIC (mol photons absorbed)$^{-1}$) (Figure 2.8).

In addition, the DIC photoproduction rate in the irradiation experiment of HuminFeed in Milli-Q water was 3.5 ± 0.34 μM (mmol photons absorbed)$^{-1}$ (AQY(int) = 106 ± 10 μmol DIC (mol photons absorbed)$^{-1}$). This rate was over two times higher than the laboratory DIC photoproduction rates of humic-amended mesocosm samples on day 1.

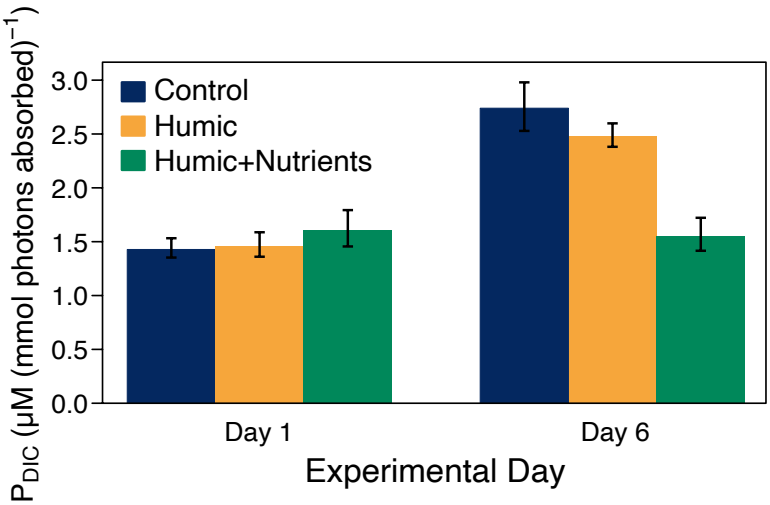

Figure 2.8. Dissolved inorganic carbon (DIC) photoproduction rates (P_{DIC}, µM (mmol photon absorbed)$^{-1}$) for laboratory irradiation experiments using mesocosm samples from JOMEX amendment experiment. Day 1 was the day of initial amendment. Rates were slopes of linear regressions of photochemically produced DIC concentrations ($[DIC]_{photo}$, µM) versus photon absorbed by CDOM (mmol photons absorbed), error bars were ± 1 standard error of the slope.

Discussion

CDOM losses during the mesocosm experiment and laboratory irradiation experiments

Humic- and humic+nutrients-amended mesocosm samples had higher initial a_g values (Figure 2.2, Table 2.1 and Supplemental Figure S2.1) and lower $S_{275\text{-}295}$ values (Figure 2.4), consistent with added humic substances leading to higher absorption and with observed browning effects in surface waters (de Wit et al., 2016; Monteith et al., 2007). The amended samples absorbed less photons *in situ* than the control samples (Figure 2.1) despite the higher absorption, most likely due to the higher attenuation coefficients in the amended samples, so light decreased with depth much faster in the amended mesocosms. The higher attenuation in turn was likely due to the higher CDOM absorption from humic substance addition, but possibly

also from particle formation induced by the added HuminFeed (Scharnweber et al., 2021), although the estimation of *in situ* light dose in this study assumed a constant contribution from CDOM absorption to attenuation. The decrease in light availability at depth caused by higher light attenuation is also consistent with the effect of browning on light availability in the water column (Jones, 1992).

CDOM absorption coefficients generally decreased over time *in situ* and in laboratory irradiation experiments (Figure 2.1, 2.2, 2.3, Table 2.2 and Supplemental Figures S2.1, S2.2, and S2.3), suggesting CDOM degradation *in situ* and by photoirradiation. The added humic substances led to changes in CDOM absorption fading rates, however the effect is different *in situ* and in laboratory irradiation experiments of filtered samples. The *in situ* a_g fading rates of amended samples were higher than those of control samples even though the photon doses were lower in the amended mesocosms (Figure 2.1, Table 2.2 and Supplemental Figure S2.1), whereas in laboratory experiments, control samples generally had higher a_g fading rates than the amended samples at 280 nm, and the fading rates were generally not different among all three groups for $a_g(400)$ and $a_g(\text{int})$, with a few exceptions (Figure 2.3, Table 2.2 and Supplemental Figures S2.2 and S2.3). If the dominant CDOM loss process *in situ* were photodegradation, we should have seen differences in rates similar to those in laboratory experiments when comparing the loss rates among different treatments. These results suggest that the *in situ* CDOM fading might not be entirely due to photodegradation, but have contributions from other processes such as biological degradation (Lu et al., 2016; Sankar et al., 2019; Scharnweber et al., 2021) or particle formation (Asmala et al., 2014b; Scharnweber et al., 2021; Sholkovitz, 1976), especially considering the reduced light availability in the mesocosms because of the cut off of short-wavelength UV light by the acrylic cover.

The addition of humic substances seemed to lower the a_g fading rate in laboratory irradiation experiments, and this pattern was more pronounced at the lower UV range, for example, at 280 nm. The slower a_g fading at the lower UV range may mean more UV protection for organisms from the added humic substances, while the impact on the availability of photosynthetically active radiation may still be significant. However, "recovery" to an original state of CDOM absorption might be faster at higher wavelengths in the visible.

When comparing the results from the laboratory irradiation experiment of HuminFeed in Milli-Q water to those from laboratory experiments of mesocosm samples, it is interesting that the a_g fading rates were similar at 400 nm and when integrated from 280 to 400 nm, but the rate at 280 nm in Milli-Q water was half that of the humic-amended mesocosm sample rate (Table 2.2). It is possible that much higher background CDOM fading rates at 280 nm in the humic-amended mesocosm samples, that is, fading in the native mesocosm water comparable to control mesocosm samples (Figure 2.3 and Table 2.2), contributed to this higher fading rate.

It is also worth noting that the a_g fading rates in laboratory irradiation experiments were three to five orders of magnitude higher than the *in situ* a_g fading rates in all samples (Table 2.2). One possible explanation is that processes other than photochemistry are responsible for the CDOM removal *in situ*, as mentioned above, and the rates of these processes were lower than photodegradation (Benner and Kaiser, 2011; Lu et al., 2016; Yang et al., 2021). The composition of the native and added CDOM/DOM likely played a role in the degradation rates. Their results were based on riverine DOM, but Benner and Kaiser (2011) found that while biodegradation is mainly responsible for the loss of total DOC and the amino acid components of DOM, CDOM and lignin phenols degrade faster photochemically (Benner and Kaiser, 2011). These results were consistent with our results of faster CDOM fading in laboratory irradiation experiments. Since

allochthonous tDOM makes a significant contribution to the high molecular weight DOM pool in the surface Baltic Sea water (Deutsch et al., 2012), and tDOM frequently contains humic substances, such as lignin polyphenols (Coble, 2007), it would not be surprising that the mesocosm samples in this study contained a high percentage of lignin phenols, and led to faster photodegradation.

In addition, it is likely that while photodegradation was occurring *in situ*, the reduced wavelength range of solar radiation reaching the mesocosms led to more indirect photochemical loss, whereas full spectral solar irradiation in laboratory experiments could cause both direct and indirect photochemical degradation (Vione, 2016). The *in situ* integrated (290 - 490 nm) photon dose could be 23 - 25 % higher than the current estimated Q_a(int), if there were no acrylic cover over the mesocosms. Other factors and processes will likely affect the *in situ* photodegradation of DOM (Bauer and Bianchi, 2011; Minor et al., 2006; Seidel et al., 2017), but high laboratory photodegradation rates suggests that there is a high potential for photodegradation of the added humic substances, at least of the colored portion. While the samples in our Baltic Sea study are different, previous work found very little degradation of HuminFeed when kept in the dark, but observed CDOM and DOC decreases accompanied by increases in particulate matter, when exposed to visible light (Scharnweber et al., 2021).

It is also possible that CDOM is produced *in situ* by microbial activities (Nelson et al., 2004), and thus CDOM degradation is counteracted by CDOM production and led to lowered net loss *in situ*. Without dark incubation experiments to measure biological degradation and/or production, it is not possible to separate the photochemical from the biological effects in the mesocosms or to determine the relative importance of photodegradation in removing the added humic substances.

There was no difference in CDOM loss rates between humic-amended and humic+nutrients-amended samples *in situ* (Figure 2.1, Table 2.2 and Supplemental Figure S2.1), suggesting that either nutrients did not enhance CDOM biodegradation or that biodegradation of HuminFeed DOM is not that important. Similarly, nutrient additions in general did not affect CDOM fading in laboratory irradiation experiments, suggesting that CDOM photodegradation is not affected or negligibly affected by nutrient additions.

Chromophoric dissolved organic matter absorption coefficients became similar in all treatments toward the end of the amendment experiment (Figure 2.1), suggesting that the increase in color from the added humic substances diminished over time, and the mesocosms returned close to their original states at least in terms of color.

Changes in CDOM spectral slopes ($S_{275\text{-}295}$) in the mesocosms and during laboratory experiments

Spectral slopes were lower in amended samples than in control samples (Figure 2.4, 2.5 and Supplemental Figure S2.4), likely due to the increased absorption from the addition of HuminFeed, but may also suggest an addition of higher molecular weight CDOM to the amended samples (Helms et al., 2008), as HuminFeed is characterized as having a high abundance of higher molecular weight aromatic compounds (Scharnweber et al., 2021). Spectral slopes increased with photons absorbed and time in amended samples *in situ* and in laboratory irradiation experiments (with some exceptions) (Figure 2.4, 2.5 and Supplemental Figure S2.4), suggesting *in situ* degradation and photobleaching of CDOM, and may suggest a decrease in molecular weight of CDOM as CDOM degraded (Helms et al., 2008).

Similar to the trends in *in situ* CDOM losses, the rates of change in CDOM spectral slopes were higher in the humic-amended mesocosm than in control, but there were no differences between the two amended mesocosms (Figure 2.4). In comparison, in laboratory experiments, the rates of change in $S_{275\text{-}295}$ were mostly not different among treatments with a few exceptions (Figure 2.5 and Supplemental Figure S2.4). The differences between the *in situ* and laboratory rates of change again supported the hypothesis that other processes might be responsible for the changes in optical properties and possibly in molecular weight in the mesocosms.

DOM degradation

The DOC concentration was higher in the humic-amended mesocosm than in the control mesocosm, and the difference in DOC concentrations at the beginning of the amendment experiment corresponded well with the DOC concentration of 2 mg L^{-1} HuminFeed dissolved in Milli-Q water (Figure 2.6). This result supports that the added humic substance led to increased DOC concentration. DOC decreased *in situ* with photon dose and time in control and humic-amended samples (Figure 2.6), suggesting *in situ* degradation of DOM, although the addition of humic substances did not seem to change the rate of DOC degradation as the change rates were not different between control and humic-amended samples. Because there were no clear change patterns in laboratory irradiation experiments, the *in situ* DOC decreases occurred in the control and humic-amended mesocosms may be mainly due to processes other than photodegradation. The potential input and subsequent degradation of phytoplankton-origin DOM (Carlson and Hansell, 2015) may be responsible for the highly fluctuating change patterns in the

humic+nutrients-amended mesocosm (Figure 2.6), if phytoplankton blooms occurred in response to the nutrient additions.

There was no clear trend in DOC concentration changes in laboratory irradiation experiments. It is possible that the irradiation was not long enough for DOC concentrations to change significantly, as Moran et al. 2000 (Moran et al., 2000) showed that there were only 9.4 - 30.7 % DOC loss during their 6 - 70 days long-term irradiation experiment. The addition of humic substances or humic and nutrients did not appear to change the photoreactivity of the DOM at the time scale tested, and this hypothesis is further supported by the lack of statistically significant change in DOC concentrations in the HuminFeed in Milli-Q water experiment. The nature of the native DOM in this Baltic Sea site likely plays an important role in affecting the DOC concentration change in the photoirradiation experiments. The DOM molecules at this Baltic Sea site may contain relatively high proportion of unsaturated aliphatic compounds (Seidel et al., 2017), and aliphatic compounds tend to be more photoresistant (Stubbins et al., 2010a). In addition, large phytoplankton blooms can occur from spring to autumn in the Baltic Sea (Seidel et al., 2017), so it would not be entirely surprising to find high concentrations of plankton DOM at this site, particularly in the nutrients added mesocosms. However, studies have found conflicting results for the photoreactivity of phytoplankton-sourced DOM and thus could also be a reason why DOM photodegradation showed no clear trend in this dynamic system. Obernosterer and Benner (2004) found that plankton DOM exposed to light showed no loss in DOC (Obernosterer and Benner, 2004), but Johannessen et al. (2007) found that algal-derived DOM had higher photodegradation efficiency than river DOM did (Johannessen et al., 2007). Furthermore, it is possible that the mesocosms in this study also had complex changes in DOM composition due to *in situ* DOM addition and removal, as suggested by a previous CDOM

addition study at the IGB LakeLab (Stella Berger, personal communication), and *in situ* processing of DOM (Bauer and Bianchi, 2011) may have changed the photoreactivity of DOM molecules to further complicate the matter. For example, cyanobacteria could produce extracellular and intracellular DOM that are not readily degraded by photoirradiation (Bittar et al., 2015).

The humic-amended mesocosm had higher specific ultraviolet absorbance $SUVA_{254}$ than control, $SUVA_{254}$ values decreased in the humic-amended mesocosm and the humic-amended samples had higher rate of decrease in *in situ* $SUVA_{254}$ values than the control samples, although there was no statistically significant change in $SUVA_{254}$ values in control samples over the course of the amendment experiment (Figure 2.7 and Table 2.1). These trends were again consistent with the addition of humic substances to the mesocosm, and may suggest an increase in aromaticity when humic substance was added (Weishaar et al., 2003) and a decrease in aromaticity during subsequent *in situ* degradation of the added humic substance (Helms et al., 2014; Stubbins et al., 2010a), as HuminFeed is abundant in aromatic compounds (Scharnweber et al., 2021). The $SUVA_{254}$ values became similar again between the control and humic-amended mesocosms toward the end of the amendment experiment (Figure 2.7a, b). This pattern again may suggest a "recovery" from the added humic substances to the original state in terms of specific ultraviolet absorbance. $SUVA_{254}$ values in the humic+nutrients-amended mesocosm were fluctuating with time (Figure 2.6), again may point to complex DOM changes brought on by a potential nutrients-induced phytoplankton bloom (Carlson and Hansell, 2015).

The response of $SUVA_{254}$ values with photon dose varied in laboratory irradiation experiments, there were decreases in some samples for some days, mostly in the control and humic+nutrients-amended samples, and in the second half of the amendment experiment (Figure

2.7c-f and Supplemental Figure S2.5). These results again may be caused by the differences in photoreactivity of the mesocosm samples due to complex changes and *in situ* processing of DOM molecules (Bauer and Bianchi, 2011). The general lack of change pattern in the humic-amended samples, lack of difference between the rates of change in the control and humic-amended samples and no significant change in $SUVA_{254}$ values with photon dose in the HuminFeed in Milli-Q water experiment, point to the likelihood that the changes in $SUVA_{254}$ values in the control and humic+nutrients-amended samples were likely caused by other properties in the samples than humic substance addition. Nutrient addition did not appear to change the $SUVA_{254}$ values either because the specific ultraviolet absorbance changes in the control and humic+nutrients-amended samples seemed to track each other.

The DIC photoproduction rates at day 1 were similar among all samples (Figure 2.8), even though the control samples had higher a_g fading rates (Figure 2.3 and Table 2.2). The production rates increased in control and humic-amended samples at day 6 but remained the same in humic+nutrients-amended samples (Figure 2.8), again not in total agreement with the higher a_g fading rates in the control samples (Figure 2.3 and Table 2.2). In addition, while integrated AQY for control (43 – 82 μmol DIC (mol photons absorbed)$^{-1}$) in this mesocosm study is lower than that for estuarine water from the South Atlantic Bight (128 ± 3.43 μmol DIC (mol photons absorbed)$^{-1}$, (Powers et al., 2017b)), and integrated AQY for humic-amended samples (44 - 75 μmol DIC (mol photons absorbed)$^{-1}$) is lower than that for a dark water river (initial $a_g(325)$ = 129 m^{-1}, 279 ± 14.0 μmol DIC (mol photons absorbed)$^{-1}$, (Powers et al., 2017b)), the difference is much larger between the integrated AQY values of humic-amended samples and the dark water river. Therefore, it is reasonable to hypothesize that photons absorbed in the samples may lead to other photochemically induced changes in CDOM/DOM

but not complete remineralization, and DOM source may have a large impact on changes in DOM photodegradation rates. In fact, chemical analysis of HuminFeed revealed that it is relatively low in carboxylic acid groups that can efficiently carry out photodecarboxylation reactions (Budac and Wan, 1992), when compared to fresh terrestrial DOM isolated using reverse osmosis (Scharnweber et al., 2021), which could explain why the addition of HuminFeed seemed to have little influence on DIC photoproduction rate despite lowering the a_g fading rates.

It is interesting though that the DIC photoproduction rates almost doubled in the control and humic-amended samples from day 1 to day 6, but remained relatively constant in the humic+nutrients-amended samples. It is possible that similar natural processes in the control and humic-amended mesocosms caused the DIC photoproduction rates to increase, and the presence of added humic substances in the humic-amended mesocosm had little effect on this increase, but the addition of nutrients stimulated microbial growth and consumption of DOM (Carlson and Hansell, 2015) in the humic+nutrients-amended mesocosms. This DOM consumption may have decreased the photoreactivity of DOM in terms of DIC production over time. For example, changes in CDOM/DOM structures, such as consumption of low molecular weight carboxylic acids (Bertilsson and Tranvik, 1998), could lead to fewer CDOM/DOM molecules capable of complete photooxidation to CO_2 (Budac and Wan, 1992).

It is reasonable to hypothesize that the trends and changes in DIC photoproduction reflected to some degree the negligible effect of humic addition on DOM photodegradation rates and the negative effects of nutrient addition. However, it is important to keep in mind that DOM photodegradation could also lead to production of biolabile DOM molecules, such as low molecular weight compounds (Miller et al., 2002; Mopper and Kieber, 2002b; Mopper et al., 2015), instead of complete oxidation to CO_2, so that the actual DOM degradation rates could be

much higher in both the control and the amended samples. Without further experiments to test the lability of photoreacted DOM in this system, it is impossible to make complete quantitative estimates of the actual DOM photodegradation rates.

In addition, the DIC photoproduction rates were higher in the HuminFeed in Milli-Q water samples than in the humic-amended mesocosm samples. Properties of the background Baltic seawater, such as salinity (Aarnos et al., 2012; Minor et al., 2006), may have affected the ability of the humic substances to produce DIC photochemically. It is especially interesting that the a_g fading rates in laboratory experiments of HuminFeed in Milli-Q water were about half that of the humic-amended mesocosm samples at 280 nm. This offers further support that DOM and CDOM photodegradation is complex in this dynamic system, especially with added humic substances. CDOM photobleaching does not completely equal DOM photodegradation, and DOM photodegradation does not always lead to complete remineralization.

Even though the optical properties in the amended mesocosms seemed to be "recovering" to the "original" state, that is, similar to the control samples, these "recoveries" don't necessarily mean complete remineralization of the added CDOM/DOM. Instead, the degraded CDOM/DOM and photoproduction of biolabile DOM molecules may have further impact on the ecosystem during and after the "recovery". Previous works in lakes and rivers show that browning can impact phytoplankton and bacterial communities (Andersson et al., 2013; Brothers et al., 2014; Feuchtmayr et al., 2019; Karlsson et al., 2009; Urrutia-Cordero et al., 2017), and it is likely that some of these impacts are brought on by the alteration of the added DOM molecules, such as the production of biolabile DOM (Aarnos et al., 2012). This impact and the role of DOM photodegradation may also be the case in estuarine systems even if the light field and optics differ from lakes and rivers.

Readdress the hypotheses

From the results of our laboratory experiments, it is clear that rapid CDOM/DOM photodegradation can occur after the addition of allochthonous CDOM/DOM to the Baltic Sea. Yet, even in mesocosms with much of the UV radiation removed, the system seems to return to a "normal" state or "recover" from the excess CDOM/DOM, that is, the CDOM absorption, spectral slopes and specific ultraviolet absorbance values became similar to those in the control mesocosm toward the end of the amendment experiment. Our results agree with what Aarnos et al. found in their 2012 study that the combined DOC photomineralization and subsequent bacterial utilization of photoproduced labile DOM exceeds the annual river input of photoreactive DOC to the Baltic Sea (Aarnos et al., 2012). However, the relative contribution of photodegradation to added allochthonous CDOM/DOM degradation could not be determined from this study. Furthermore, it is important to keep in mind that HuminFeed differs in many ways from natural CDOM/DOM and degrades differently in natural water (Scharnweber et al., 2021), and further tests are necessary to more completely address the impact of browning and photochemical removal of added CDOM/DOM on coastal environments.

Comparison of changes in CDOM and DOM properties between *in situ* and laboratory irradiation experiments gives some indication that processes other than photodegradation may be responsible for degradation of added CDOM and DOM in the humic-amended mesocosms, even though photodegradation has a high potential for removal of added CDOM/DOM. Scharnweber et al. (2021) found that lake water with added HuminFeed had significantly higher rate of particle formation and that HuminFeed stimulated bacterial production in the presence of light (Scharnweber et al., 2021), and these processes may be responsible for at least some of the CDOM and DOM changes we saw in our study. It is possible that the availability of full spectral

solar radiation at this Baltic Sea site may lead to more photodegradation of the added humic substances, and change the relative contribution of photodegradation to added and native CDOM/DOM degradation with respect to other *in situ* processes.

The addition of nutrients did not lead to any major differences in the optical properties and their change rates in humic+nutrients-amended samples when compared to those in the humic-amended samples, and therefore did not seem to compound the effects of added humic substances on DOM optical properties in this experiment. However, nutrient addition seemed to cause the DOC concentration, specific ultraviolet absorbance and DIC photoproduction to fluctuate over time in the humic+nutrients-amended mesocosm. This trend was not observed in the control or humic-amended mesocosms. This phenomenon may have been caused by DOM addition or removal during any potential phytoplankton changes induced by the nutrient addition (Carlson and Hansell, 2015).

To better constrain the importance of photodegradation to added humic substances in this Baltic Sea ecosystem, future studies could include concurrent photoirradiation and dark incubation experiments, quantum yield experiments combined with *in situ* light measurements to better estimate *in situ* photodegradation/photoproduction rates and use of mesocosm covers that allow full spectral solar radiation penetration. In addition, future studies to measure the changes in fluorescent dissolved organic matter of photoirradiated samples may also help to differentiate photodegradation from biological degradation (Coble, 2007). Compositional and structural studies of DOM using Fourier-transform ion cyclotron resonance mass spectrometry and nuclear magnetic resonance spectroscopy, respectively, to analyze samples before and after irradiation and over the course of the amendment experiment, may complement optical and DIC

photoproduction measurements, and provide a more complete picture of the DOM changes after browning and photoirradiation of this Baltic Sea ecosystem.

Acknowledgements

The authors would like to thank the scientists and staff at Tvärminne Zoological Station and the JOMEX team for providing equipment and facilities, assisting experimental setup and sample collection. We also thank Jaana Koistinen at Tvärminne Zoological Station for DOC sample analysis. In addition, we would like to thank Lee Ann DeLeo for assistance with graphics. This work was supported by the Transnational Access Programme of the AQUACOSM project grant 731065 funded by the European Union's Horizon 2020 Research and Innovation Programme, and Unite States National Science Foundation chemical oceanography grant 1635618. This study has utilized research infrastructure facilities provided by FINMARI (Finnish Marine Research Infrastructure network).

REFERENCES

Aarnos, H., Ylostalo, P. and Vähätalo, A.V., 2012. Seasonal phototransformation of dissolved organic matter to ammonium, dissolved inorganic carbon, and labile substrates supporting bacterial biomass across the Baltic Sea. Journal of Geophysical Research-Biogeosciences, 117: 14.

Aitkenhead, J.A. and McDowell, W.H., 2000. Soil C : N ratio as a predictor of annual riverine DOC flux at local and global scales. Global Biogeochemical Cycles, 14(1): 127-138.

Amon, R.M.W. and Benner, R., 1996. Bacterial utilization of different size classes of dissolved organic matter. Limnology and Oceanography, 41(1): 41-51.

Anderson, S. et al., 2001. Indicators of UV exposure in corals and their relevance to global climate change and coral bleaching. Human and Ecological Risk Assessment, 7(5): 1271-1282.

Andersson, A. et al., 2013. Can Humic Water Discharge Counteract Eutrophication in Coastal Waters? PLOS ONE, 8(4): e61293.

Asmala, E., Autio, R., Kaartokallio, H., Stedmon, C.A. and Thomas, D.N., 2014a. Processing of humic-rich riverine dissolved organic matter by estuarine bacteria: effects of predegradation and inorganic nutrients. Aquatic Sciences, 76(3): 451-463.

Asmala, E., Bowers, D.G., Autio, R., Kaartokallio, H. and Thomas, D.N., 2014b. Qualitative changes of riverine dissolved organic matter at low salinities due to flocculation. Journal of Geophysical Research-Biogeosciences, 119(10): 1919-1933.

Bauer, J.E. and Bianchi, T.S., 2011. Dissolved Organic Carbon Cycling and Transformation. In: E. Wolanski and D. McLusky (Editors), Treatise on Estuarine and Coastal Science, Vol 5: Biogeochemistry. Elsevier Academic Press Inc, San Diego, pp. 7-67.

Bélanger, S. et al., 2006. Photomineralization of terrigenous dissolved organic matter in Arctic coastal waters from 1979 to 2003: Interannual variability and implications of climate change. Global Biogeochemical Cycles, 20(4): 13.

Benner, R. and Kaiser, K., 2011. Biological and photochemical transformations of amino acids and lignin phenols in riverine dissolved organic matter. Biogeochemistry, 102(1-3): 209-222.

Bertilsson, S. and Tranvik, L.J., 1998. Photochemically produced carboxylic acids as substrates for freshwater bacterioplankton. Limnology and Oceanography, 43(5): 885-895.

Bittar, T.B., Vieira, A.A.H., Stubbins, A. and Mopper, K., 2015. Competition between photochemical and biological degradation of dissolved organic matter from the cyanobacteria Microcystis aeruginosa. Limnology and Oceanography, 60(4): 1172-1194.

Blough, N.V. and Del Vecchio, R., 2002. Chapter 10 - Chromophoric DOM in the Coastal Environment. In: D.A. Hansell and C.A. Carlson (Editors), Biogeochemistry of Marine Dissolved Organic Matter. Academic Press, San Diego, pp. 509-546.

Brandes, J.A., 2009. Rapid and precise delta C-13 measurement of dissolved inorganic carbon in natural waters using liquid chromatography coupled to an isotope-ratio mass spectrometer. Limnology and Oceanography-Methods, 7: 730-739.

Brothers, S. et al., 2014. A feedback loop links brownification and anoxia in a temperate, shallow lake. Limnology and Oceanography, 59(4): 1388-1398.

Budac, D. and Wan, P., 1992. PHOTODECARBOXYLATION - MECHANISM AND SYNTHETIC UTILITY. Journal of Photochemistry and Photobiology a-Chemistry, 67(2): 135-166.

Carlson, C.A. and Hansell, D.A., 2015. Chapter 3 - DOM Sources, Sinks, Reactivity, and Budgets. Biogeochemistry of Marine Dissolved Organic Matter: 65-126.

Carstensen, J. et al., 2020. Factors regulating the coastal nutrient filter in the Baltic Sea. Ambio, 49(6): 1194-1210.

Cauwet, G., 1999. Determination of dissolved organic carbon and nitrogen by high temperature combustion. In: K. Grasshoff, K. Kremling and M. Ehrhardt (Editors), Methods of Seawater Analysis. Wiley-VCH, Weinheim, pp. 407-420.

Cherrier, J. and Bauer, J.E., 2004. Bacterial utilization of transient plankton-derived dissolved organic carbon and nitrogen inputs in surface ocean waters. Aquatic Microbial Ecology, 35(3): 229-241.

Chupakova, A.A., Chupakov, A.V., Neverova, N.V., Shirokova, L.S. and Pokrovsky, O.S., 2018. Photodegradation of river dissolved organic matter and trace metals in the largest European Arctic estuary. Science of the Total Environment, 622: 1343-1352.

Coble, P.G., 2007. Marine optical biogeochemistry: The chemistry of ocean color. Chemical Reviews, 107(2): 402-418.

Dalzell, B.J., Minor, E.C. and Mopper, K.M., 2009. Photodegradation of estuarine dissolved organic matter: a multi-method assessment of DOM transformation. Organic Geochemistry, 40(2): 243-257.

de Wit, H.A. et al., 2016. Current Browning of Surface Waters Will Be Further Promoted by Wetter Climate. Environmental Science & Technology Letters, 3(12): 430-435.

Deininger, A. and Frigstad, H., 2019. Reevaluating the Role of Organic Matter Sources for Coastal Eutrophication, Oligotrophication, and Ecosystem Health. Frontiers in Marine Science, 6: 11.

Deutsch, B., Alling, V., Humborg, C., Korth, F. and Morth, C.M., 2012. Tracing inputs of terrestrial high molecular weight dissolved organic matter within the Baltic Sea ecosystem. Biogeosciences, 9(11): 4465-4475.

Farjalla, V.F., Amado, A.M., Suhett, A.L. and Meirelles-Pereira, F., 2009. DOC removal paradigms in highly humic aquatic ecosystems. Environmental Science and Pollution Research, 16(5): 531-538.

Feuchtmayr, H. et al., 2019. Effects of brownification and warming on algal blooms, metabolism and higher trophic levels in productive shallow lake mesocosms. Science of the Total Environment, 678: 227-238.

Fichot, C.G. and Benner, R., 2014. The fate of terrigenous dissolved organic carbon in a river-influenced ocean margin. Global Biogeochemical Cycles, 28(3): 300-318.

Fichot, C.G. and Miller, W.L., 2010. An approach to quantify depth-resolved marine photochemical fluxes using remote sensing: Application to carbon monoxide (CO) photoproduction. Remote Sensing of Environment, 114(7): 1363-1377.

Hansell, D.A. and Carlson, C.A., 1998. Deep-ocean gradients in the concentration of dissolved organic carbon. Nature, 395(6699): 263-266.

Hansell, D.A., Carlson, C.A., Repeta, D.J. and Schlitzer, R., 2009. Dissolved organic matter in the ocean: a controversy stimulates new insights. Oceanography, 22(4): 202-211.

Hedges, J.I., 1992. GLOBAL BIOGEOCHEMICAL CYCLES - PROGRESS AND PROBLEMS. Marine Chemistry, 39(1-3): 67-93.

Helms, J.R. et al., 2014. Loss of optical and molecular indicators of terrigenous dissolved organic matter during long-term photobleaching. Aquatic Sciences, 76(3): 353-373.

Helms, J.R. et al., 2008. Absorption spectral slopes and slope ratios as indicators of molecular weight, source, and photobleaching of chromophoric dissolved organic matter. Limnology and Oceanography, 53(3): 955-969.

Hu, C., Muller-Karger, F.E. and Zepp, R.G., 2002a. Absorbance, absorption coefficient, and apparent quantum yield: A comment on common ambiguity in the use of these optical concepts. Limnology and Oceanography, 47(4): 1261-1267.

Hu, C.M., Muller-Karger, F.E. and Zepp, R.G., 2002b. Absorbance, absorption coefficient, and apparent quantum yield: A comment on common ambiguity in the use of these optical concepts. Limnology and Oceanography, 47(4): 1261-1267.

Johannessen, S.C., Pena, M.A. and Quenneville, M.L., 2007. Photochemical production of carbon dioxide during a coastal phytoplankton bloom. Estuarine Coastal and Shelf Science, 73(1-2): 236-242.

Jones, R.I., 1992. THE INFLUENCE OF HUMIC SUBSTANCES ON LACUSTRINE PLANKTONIC FOOD-CHAINS. Hydrobiologia, 229: 73-91.

Karlsson, J. et al., 2009. Light limitation of nutrient-poor lake ecosystems. Nature, 460(7254): 506-U80.

Koehler, B., Landelius, T., Weyhenmeyer, G.A., Machida, N. and Tranvik, L.J., 2014. Sunlight-induced carbon dioxide emissions from inland waters. Global Biogeochemical Cycles, 28(7): 696-711.

Koistinen, J., Sjöblom, M. and Spilling, K., 2020. Determining Inorganic and Organic Carbon. In: K. Spilling (Editor), Biofuels from Algae: Methods and Protocols. Springer New York, New York, NY, pp. 63-70.

Kowalczuk, P., Olszewski, J., Darecki, M. and Kaczmarek, S., 2005. Empirical relationships between coloured dissolved organic matter (CDOM) absorption and apparent optical properties in Baltic Sea waters. International Journal of Remote Sensing, 26(2): 345-370.

Kritzberg, E.S. et al., 2014. Warming and browning of lakes: consequences for pelagic carbon metabolism and sediment delivery. Freshwater Biology, 59(2): 325-336.

Kroer, N., 1993. Bacterial-growth efficiency on natural dissolved organic matter. Limnology and Oceanography, 38(6): 1282-1290.

Kullenberg, G., 1981. Chapter 3 Physical Oceanography. In: A. Voipio (Editor), Elsevier Oceanography Series. Elsevier, pp. 135-181.

Lauerwald, R., Hartmann, J., Ludwig, W. and Moosdorf, N., 2012. Assessing the nonconservative fluvial fluxes of dissolved organic carbon in North America. Journal of Geophysical Research-Biogeosciences, 117: 19.

Lu, C.J. et al., 2016. Sources and Transformations of Dissolved Lignin Phenols and Chromophoric Dissolved Organic Matter in Otsuchi Bay, Japan. Frontiers in Marine Science, 3.

Massicotte, P., Asmala, E., Stedmon, C. and Markager, S., 2017. Global distribution of dissolved organic matter along the aquatic continuum: Across rivers, lakes and oceans. Science of the Total Environment, 609: 180-191.

Mayorga, E. et al., 2010. Global Nutrient Export from WaterSheds 2 (NEWS 2): Model development and implementation. Environmental Modelling & Software, 25(7): 837-853.

Miller, W.L. and Moran, M.A., 1997. Interaction of photochemical and microbial processes in the degradation of refractory dissolved organic matter from a coastal marine environment. Limnology and Oceanography, 42(6): 1317-1324.

Miller, W.L., Moran, M.A., Sheldon, W.M., Zepp, R.G. and Opsahl, S., 2002. Determination of apparent quantum yield spectra for the formation of biologically labile photoproducts. Limnology and Oceanography, 47(2): 343-352.

Minor, E.C., Dalzell, B.L., Stubbins, A. and Mopper, K., 2007. Evaluating the photoalteration of estuarine dissolved organic matter using direct temperature-resolved mass spectrometry and UV-visible spectroscopy. Aquatic Sciences, 69(4): 440-455.

Minor, E.C., Pothen, J., Dalzell, B.J., Abdulla, H. and Mopper, K., 2006. Effects of salinity changes on the photodegradation and ultraviolet-visible absorbance of terrestrial dissolved organic matter. Limnology and Oceanography, 51(5): 2181-2186.

Monteith, D.T. et al., 2007. Dissolved organic carbon trends resulting from changes in atmospheric deposition chemistry. Nature, 450(7169): 537-U9.

Mopper, K. and Kieber, D.J., 2000. Marine photochemistry and its impact on carbon cycling. In: M. Vernet, S. Demers and S. De Mora (Editors), The Effects of UV Radiation in the Marine Environment. Cambridge Environmental Chemistry Series. Cambridge University Press, Cambridge, pp. 101-129.

Mopper, K. and Kieber, D.J., 2002. Chapter 9 - Photochemistry and the Cycling of Carbon, Sulfur, Nitrogen and Phosphorus. Biogeochemistry of Marine Dissolved Organic Matter: 455-507.

Mopper, K., Kieber, D.J. and Stubbins, A., 2015. Marine Photochemistry of Organic Matter: Processes and Impacts. In: D.A. Hansell and C.A. Carlson (Editors), Biogeochemistry of Marine Dissolved Organic Matter, 2nd Edition. Academic Press Ltd-Elsevier Science Ltd, London, pp. 389-450.

Moran, M.A., Sheldon, W.M. and Sheldon, J.E., 1999. Biodegradation of riverine dissolved organic carbon in five estuaries of the southeastern United States. Estuaries, 22(1): 55-64.

Moran, M.A., Sheldon, W.M. and Zepp, R.G., 2000. Carbon loss and optical property changes during long-term photochemical and biological degradation of estuarine dissolved organic matter. Limnology and Oceanography, 45(6): 1254-1264.

Nelson, N.B., Carlson, C.A. and Steinberg, D.K., 2004. Production of chromophoric dissolved organic matter by Sargasso Sea microbes. Marine Chemistry, 89(1): 273-287.

Obernosterer, I. and Benner, R., 2004. Competition between biological and photochemical processes in the mineralization of dissolved organic carbon. Limnology and Oceanography, 49(1): 117-124.

Osburn, C.L. and Bianchi, T.S., 2016. Editorial: Linking Optical and Chemical Properties of Dissolved Organic Matter in Natural Waters. Frontiers in Marine Science, 3: 3.

Osburn, C.L., Retamal, L. and Vincent, W.F., 2009. Photoreactivity of chromophoric dissolved organic matter transported by the Mackenzie River to the Beaufort Sea. Marine Chemistry, 115(1-2): 10-20.

Pinsonneault, A.J. et al., 2020. Dissolved organic carbon sorption dynamics in tidal marsh soils. Limnology and Oceanography: 12.

Powers, L.C., Brandes, J.A., Miller, W.L. and Stubbins, A., 2017a. Using liquid chromatography-isotope ratio mass spectrometry to measure the delta C-13 of dissolved inorganic carbon photochemically produced from dissolved organic carbon. Limnology and Oceanography-Methods, 15(1): 103-115.

Powers, L.C., Brandes, J.A., Stubbins, A. and Miller, W.L., 2017b. MoDIE: Moderate dissolved inorganic carbon ((DIC)-C-13) isotope enrichment for improved evaluation of DIC photochemical production in natural waters. Marine Chemistry, 194: 1-9.

Powers, L.C. and Miller, W.L., 2015. Photochemical production of CO and CO2 in the Northern Gulf of Mexico: Estimates and challenges for quantifying the impact of photochemistry on carbon cycles. Marine Chemistry, 171: 21-35.

RCoreTeam, 2021. R: A language and environment for statistical computing. The R Foundation for Statistical Computing, Vienna, Austria.

Rolff, C. and Elmgren, R., 2000. Use of riverine organic matter in plankton food webs of the Baltic Sea. Marine Ecology Progress Series, 197: 81-101.

Ruggaber, A., Dlugi, R. and Nakajima, T., 1994. MODELING RADIATION QUANTITIES AND PHOTOLYSIS FREQUENCIES IN THE TROPOSPHERE. Journal of Atmospheric Chemistry, 18(2): 171-210.

Sankar, M.S. et al., 2019. Effect of photo-biodegradation and biodegradation on the biogeochemical cycling of dissolved organic matter across diverse surface water bodies. Journal of Environmental Sciences, 77: 130-147.

Santonja, M., Minguez, L., Gessner, M.O. and Sperfeld, E., 2017. Predator-prey interactions in a changing world: humic stress disrupts predator threat evasion in copepods. Oecologia, 183(3): 887-898.

Santos, L., Santos, E.B.H., Dias, J.M., Cunha, A. and Almeida, A., 2014. Photochemical and microbial alterations of DOM spectroscopic properties in the estuarine system Ria de Aveiro. Photochemical & Photobiological Sciences, 13(8): 1146-1159.

Scharnweber, K. et al., 2021. Comprehensive analysis of chemical and biological problems associated with browning agents used in aquatic studies. bioRxiv: 2021.02.26.433092.

Seidel, M. et al., 2017. Composition and Transformation of Dissolved Organic Matter in the Baltic Sea. Frontiers in Earth Science, 5(31).

Sholkovitz, E.R., 1976. FLOCCULATION OF DISSOLVED ORGANIC AND INORGANIC MATTER DURING MIXING OF RIVER WATER AND SEAWATER. Geochimica Et Cosmochimica Acta, 40(7): 831-845.

Stubbins, A., Law, C.S., Uher, G. and Upstill-Goddard, R.C., 2011. Carbon monoxide apparent quantum yields and photoproduction in the Tyne estuary. Biogeosciences, 8(3): 703-713.

Stubbins, A. et al., 2010. Illuminated darkness: Molecular signatures of Congo River dissolved organic matter and its photochemical alteration as revealed by ultrahigh precision mass spectrometry. Limnology and Oceanography, 55(4): 1467-1477.

Thomas, H., Pempkowiak, J., Wulff, F. and Nagel, K., 2010. The Baltic Sea. In: K.-K. Liu, L. Atkinson, R.Q. ones and L. Talaue-McManus (Editors), Carbon and Nutrient Fluxes in Continental Margins: a Global Synthesis. Springer, pp. 1-741.

Tranvik, L.J. et al., 2009. Lakes and reservoirs as regulators of carbon cycling and climate. Limnology and Oceanography, 54(6): 2298-2314.

Urrutia-Cordero, P. et al., 2017. Phytoplankton diversity loss along a gradient of future warming and brownification in freshwater mesocosms. Freshwater Biology, 62(11): 1869-1878.

Vasconcelos, F.R., Diehl, S., Rodriguez, P., Karlsson, J. and Bystrom, P., 2018. Effects of Terrestrial Organic Matter on Aquatic Primary Production as Mediated by Pelagic-Benthic Resource Fluxes. Ecosystems, 21(6): 1255-1268.

Vione, D., 2016. Photochemical Reactions in Sunlit Surface Waters. In: G. Bergamini and S. Silvi (Editors), Applied Photochemistry-When Light Meets Molecules, pp. 343-376.

Weishaar, J.L. et al., 2003. Evaluation of specific ultraviolet absorbance as an indicator of the chemical composition and reactivity of dissolved organic carbon. Environmental Science & Technology, 37(20): 4702-4708.

Williams, P.M. and Druffel, E.R.M., 1987. Radiocarbon in dissolved organic matter in the central North Pacific Ocean. Nature, 330(6145): 246-248.

Yang, L., Zhang, J. and Yang, G.P., 2021. Mixing behavior, biological and photolytic degradation of dissolved organic matter in the East China Sea and the Yellow Sea. Science of the Total Environment, 762: 19.

CHAPTER 3

COMPARISONS OF PHOTODEGRADATION RATES AND EFFICIENCIES AMONG SOLID PHASED EXTRACT-AMENDED, ELECTRODIALYSIS REVERSE OSMOSIS EXTRACT-AMENDED, AND UNAMENDED COASTAL WATER SAMPLES

Introduction

Oceanic dissolved organic matter (DOM) is an important component of the global carbon cycle and serves many important functions (Ridgwell and Arndt, 2015), such as food for microbes (Amon and Benner, 1996; Kroer, 1993) and protection for biota from UV and reactive oxygen radicals (Arrigo and Brown, 1996; Del Vecchio and Blough, 2002). As DOM contains ~50 % carbon by weight, it is commonly reported as dissolved organic carbon (DOC) (Moody and Worrall, 2017; Vetter et al., 2007). DOC is the second largest pool of bioreactive carbon in the ocean at ~ 662 ± 32 Pg C, making it comparable to the CO_2 pool in the atmosphere (Carlson and Hansell, 2015; Hansell and Carlson, 1998; Hansell et al., 2009a). A globally-significant flux of CO_2 can be generated from degradation of even a small fraction of oceanic DOC (Hansell, 2002; Hedges, 2002).

Photochemistry is one of the most significant abiotic reaction mechanisms in the surface ocean and an important sink for DOM (Carlson and Hansell, 2015; Gonsior et al., 2014; Mopper et al., 2015; Mopper et al., 1991; Zafiriou et al., 2003). Chromophoric DOM (CDOM) photochemistry can affect light availability to photosynthesis and penetration of UV radiation in the water column, impact elemental cycling, and produce reactive species and biolabile

compounds (Miller et al., 2002; Mopper et al., 2015). In addition, greenhouse gases, such as CO_2, can be produced from DOM photodegradation (Clark et al., 2004; Johannessen and Miller, 2001; Powers et al., 2017a; Powers et al., 2017b; Powers and Miller, 2015b; Reader and Miller, 2012; White et al., 2010; Ziolkowski and Miller, 2007). CDOM is the light absorbing component of DOM, highly photoreactive, and thus presumably the dominant photoreactant (Coble, 2007; Mopper and Kieber, 2000; Nelson and Siegel, 2013). CDOM can also serve as a photosensitizer and trigger degradation and transformations of other DOM components (Carlson and Hansell, 2015; Coble, 2007; Mopper et al., 2015). CDOM optical property changes, such as decreasing absorption during photoirradiation, can provide information on changes in CDOM and DOM during photochemistry (Coble, 2007; Mopper et al., 2015; Obernosterer and Benner, 2004).

Dissolved inorganic carbon (DIC) is a major product of DOC photodegradation (Miller and Zepp, 1995). However, the *in situ* rates and magnitude of DIC photoproduction in the global oceans are poorly constrained due to the analytical challenges posed by determining rates on the order of nM h^{-1} to μM h^{-1} against a high marine DIC background of ~2 mM. It is conceivable that when the DOM in a seawater sample is concentrated, i.e., more DOM molecules to react and make photoproducts, more DIC could be produced, so that photoproduced DIC concentration could increase to a more easily measurable level. Such concentration of DOM is possible if DOM were extracted from seawater and then the extracts added to the same seawater. Several methods, such as solid-phase extraction and electrodialysis coupled with reverse osmosis, have been developed to efficiently extract DOM from seawater (Green et al., 2014), and may be used for the purpose of concentrating DOM.

Solid-phase extraction (SPE) using Bond Elut™ PPL sorbent (modified styrene-divinylbenzene polymer) is a convenient and efficient method to extract DOM from large

volumes of seawater without major instrumentation, and can be deployed with ease in the field (Chen et al., 2016; Dittmar et al., 2008; Green et al., 2014; Stubbins and Dittmar, 2012). Coastal samples containing higher proportion of terrigenous DOM typically have higher recovery rates (> 60 %) than open ocean samples (> 40 %) (Chen et al., 2016; Dittmar et al., 2008; Green et al., 2014). SPE using PPL resin results in the complete desalting of seawater samples (Dittmar et al., 2008) and extracts can be dried and stored in a dark freezer before further use. This method has a tendency to extract more small and polar compounds (Arrieta et al., 2015; Chambers et al., 2016).

An alternative method to extract DOM from seawater and desalt at the same time is electrodialysis coupled with reverse osmosis (EDRO) (Chambers et al., 2016; Green et al., 2014; Helms et al., 2015; Koprivnjak et al., 2006; Koprivnjak et al., 2009; Vetter et al., 2007; Young and Ingall, 2010). Using ion-exchange and reverse osmosis membranes, EDRO efficiently desalts the water, significantly reduces sample volume while effectively concentrating DOM, and is a relatively mild treatment that doesn't subject the samples to acid treatment as does SPE. Concentrated samples can then be freeze dried and stored in a dark freezer for long periods of time without compromising the quality of extracted DOM (Koprivnjak et al., 2006). DOC recovery rates using EDRO span a wide range (40 – 93 %) depending on the type of water extracted, and open seawater tends to have higher recovery than coastal waters (Chambers et al., 2016; Helms et al., 2015; Vetter et al., 2007; Young and Ingall, 2010). Depending on the setting, capability of the equipment, and initial and final sample volumes, the amount of salt remaining after processing can be very low (Vetter et al., 2007). EDRO has relatively lower recoveries for small, charged molecules, but extracts a more representative sample of the original DOM compared to SPE (Chambers et al., 2016; Green et al., 2014; Helms et al., 2015; Helms et al.,

2013; Koprivnjak et al., 2009). Size or compositional bias is significantly reduced in EDRO extraction compared to SPE (Chambers et al., 2016). Furthermore, electrodialysis is more capable of extracting carboxylic acids than SPE (Tfaily et al., 2012).

Photochemical degradation of seawater samples amended with extracted DOM from SPE (SPE-DOM) or EDRO (EDRO-DOM) could potentially have rates, efficiencies and changes in optical and chemical properties different from photodegradation of the original seawater, because of the selective extraction of DOM molecules and potential bias of any isolation method used. Potential differences need to be investigated before meaningful inferences about the photodegradation of the original seawater can be made from photochemical experiments using the amended samples. In this first study of such kind, we compared the changes in optical properties and DIC photoproduction among unamended estuarine seawater sample, SPE-DOM-amended sample, and EDRO-DOM-amended sample. The question we aim to answer is whether photodegradation rates and efficiencies are comparable among the amended and unamended samples; a question we need to answer first if we were to extrapolate the rates and efficiencies of amended samples to the original water samples, for properties that are difficult to measure. Furthermore, we aimed to determine if there were differences in the photochemistry between the SPE-DOM-amended and EDRO-DOM-amended samples due to the different selection biases of DOM molecules for the different methods.

Methods

Site and Sampling

Surface (0.5 m) water samples were collected from the Skidaway River Estuary (SRE) at the boat dock of Skidaway Institute of Oceanography (SkIO), Savannah GA, USA

(31°59'24.3"N 81°01'20.6"W) on March 8th, 2020, using 10 L polyethylene Hedwin Cubitainers™. The time of collection was approximately an hour after the high tide, and there had been continuous heavy rains for two days prior to collection. The water temperature was 13.4 °C, salinity was 18 ppt, and pH was 7.52. The samples were transported to a SkIO lab and immediately filtered through 0.2 μm Whatman Polycap 36 AS nylon membrane cartridge filters, using a Masterflex L/S Digital Standard Drive peristaltic pump with Easy Load II and Masterflex L/S 17 silicone tubing at 100 mL min^{-1}. All filtered sample waters were stored in 10 L polypropylene carboys in the dark at 4 °C before use for a period of up to 10 months.

All labware for sampling and photoirradiation experiments were first rinsed with copious amount of MilliporeSigma 18.2-MΩ.cm Milli-Q® Type 1 ultrapure water (Milli-Q water), and soaked overnight in 10 % HCl solution, before rinsed again with an excess of Milli-Q water. Plasticware was stored with a small amount of fresh 0.1 % HCl (pH 2) solution to prevent bacterial growth before use. Glassware was dried and baked at 450 °C for at least 5 h. Plasticware was rinsed again with copious amounts of Milli-Q water before use, and all labware was rinsed three times with a small volume of sample water prior to use. Quartz spectrophotometric cells used in photochemistry experiments were cleaned following the same procedure with glassware but not baked. All acid solutions were made using Fisher Chemical Certified ACS Plus Safe-Cote® HCl and Milli-Q water.

Dissolved organic carbon (DOC) extraction

Electrodialysis reverse osmosis

Electrodialysis reverse osmosis was performed on 11th and 12th of March 2020, at Dr. Ellery Ingall's lab at Georgia Institute of Technology following protocols in Chambers et al.

(2016) with modifications. A Deukum electrodialysis stack (Deukum GmbH, Frickenhausen, Germany) coupled to a circulation system was used for electrodialysis. The stack consisted of alternating anion (Fumasep FAS-PET-130) and cation (Fumasep FKS-PET-130) exchange membranes. Membranes were separated by 0.7-mm-thick flexible turbulence promoting spacers. The stack of alternating membranes and spacers was sandwiched between two opposing flow regulating end blocks that house a platinized titanium mesh anode in one and a stainless steel cathode in the other. The circulation system consisted of three Iwaki WMD water pumps, an Accumet AP75 conductivity meter, and three high-density polyethylene (HDPE) tanks for diluate, concentrate, and electrode rinse storage. The cross-sectional active membrane area of the stack was approximately 200 cm^2, and the electric potential across the stack was supplied by a 1.2-kW Sorensen DCS150-8EM1 solid-state power supply. A FILMTEC™ TW30-2514 membrane and a Fluid-o-Tech rotary vein pump was used for reverse osmosis.

The EDRO system was rinsed with copious amount of Milli-Q water before sample extraction. The system was rinsed twice by circulating 2 L each of the sample water through for about 5 min, and the rinse samples were drained and discarded after each rinse. 10 L of the sample was placed in the diluate tank and circulated through the system for 5 min to ensure thorough mixing, before a 40 mL DOC sample for initial DOC concentration ($[DOC]_{initial}$, mg L^{-1}) was taken. Electricity was then supplied to the system. The diluate and concentrate conductivity and the applied amperage were closely monitored. The applied amperage was increased then decreased according to the conductivity of the diluate and concentrate and the pre-determined limiting current density (LCD) function (Chambers et al., 2016). An end point was reached when the conductivity of the sample reached between 0.5 and 1 mS. Another 40 mL DOC sample for final DOC concentration ($[DOC]_{final,}$ mg L^{-1}) was taken. The extracts were then

freeze dried and stored in a -18 °C freezer until used in photodegradation experiments. DOC concentrations were measured as non-purgeable organic carbon using high temperature catalytic oxidation with a Shimadzu TOC-VCSN analyzer (Benner and Strom 1993; Grasshoff et al. 1999). The DOC recovery rate was 59 % and was calculated with the following equation:

$$\text{DOC recovery rate (\%)} = \frac{[DOC]_{\text{final}} \times V_{\text{final}}}{[DOC]_{\text{initial}} \times V_{\text{initial}}} \times 100$$

where V_{final} (L) was the volume of the EDRO extract before freeze drying, and V_{initial} (L) was the volume of the SRE water extracted by EDRO.

Since EDRO doesn't completely desalt the samples, a small amount of salt was still present in the dried EDRO extracts, however, the salt added to the amended samples with the extract is less than 1 % of the background concentration and it is unlikely that this small amount of salt would have an effect on the optical properties and DIC photoproduction rate of EDRO-DOM-amended samples.

Solid-phase extraction

The 0.2 μm-filtered water samples for SPE were acidified to pH 2 with Fisher Chemical Certified ACS Plus Safe-Cote® HCl immediately after filtration. DOC was extracted by SPE on March 16th, 2020, at SkIO, using Agilent Bond Elut™ PPL Straight Barrel 1 g/6 mL cartridges. Cartridges were rinsed and activated using 10 mL of Fisher Chemical Optima® LC/MS methanol and then rinsed with 10 mL of 0.1 % HCl solution. Approximately 10 L of acidified filtered water sample was gravity filtered through a single cartridge. Two 40 mL DOC samples were taken prior to filtration to determine initial DOC concentration ($[DOC]_{\text{initial}}$, mg L^{-1}). The cartridges were then rinsed with 0.1 % HCl solution and dried with zero air and eluted using 10 mL of Fisher Chemical Optima® LC/MS methanol. The final volume of extract in methanol was

7.495 mL. Extracts in methanol were stored in a -18 °C freezer until used in photodegradation experiments. To determine recovery rate, 100 μL of the extract in methanol was dried in a 40 mL DOC vial at room temperature inside a hood, then the dried extract was dissolved in 40 mL Milli-Q water and the DOC concentration of the solution was measured ($[DOC]_{\mathrm{InMQ}}$, mg L^{-1}). DOC concentrations were again determined by high temperature catalytic oxidation method, using a Shimadzu TOC-V CPN Total Organic Carbon Analyzer (Stubbins et al., 2012) at SkIO within a week of extraction. The DOC recovery rate was 77 % and calculated as following:

$$\text{DOC recovery rate (\%)} = \frac{\frac{[DOC]_{\mathrm{InMQ}} \times 0.040}{0.000100} \times 0.007495}{[DOC]_{\mathrm{initial}} \times V_{\mathrm{initial}}} \times 100$$

where V_{initial} (L) was the volume of the SRE water extracted by SPE, 0.040 was the volume (L) of Milli-Q water used to dissolve the dried extract, and 0.007495 was the final volume (L) of extract in methanol.

Amendment and enrichment

A portion of the filtered original SRE sample was set aside to be used as background water for the amended samples. This water was filtered again immediately before amendment using abovementioned apparatus and procedures. SPE extracts in methanol were dried in 1 L glass bottles in a 60 °C vented oven. Dried SPE extracts and EDRO extracts were dissolved in the re-filtered sample water so that the final absorbances of the amended samples were around 0.1 at 325 nm (1 cm pathlength), similar to that of the original SRE sample. About 2 L of each sample was transferred to 4 L polyethylene Hedwin Cubitainers™, and approximately 9.8 mg L^{-1} $NaH^{13}CO_3$ was then added to achieve ^{13}C enrichment levels of 8000 – 9000 ‰. The enriched samples were stirred overnight to equilibrate.

Photodegradation experiment

Time series experiment

Time series (TS) photodegradation experiment followed protocols modified from Powers et al. (2017b). The experiment was conducted to determine the time required to produce measurable DIC photoproduction using an isotope dilution method, moderate dissolved inorganic carbon ($DI^{13}C$) isotope enrichment (MoDIE) (Powers et al., 2017b), and the maximum photon dose before the rate becomes nonlinear. The TS experiment also allowed the determination of optical property changes and the calculation of DIC photoproduction rates under full-spectrum solar radiation. Samples of each amendment type were distributed to 8 cylindrical 10-cm-pathlength Spectrocell spectrophotometric quartz cells (cells), ~30 mL volume each. Each cell was overfilled with 3 times cell volume from the bottom with Teflon tubing to prevent bubble formation and excess turbulence, and to minimize CO_2 exchange with the atmosphere (Brandes, 2009). The cells were then capped with Spectrocell caps fitted with Microsolv Teflon-lined butyl septa and stored under Milli-Q water to reduce atmospheric gas exchange. The cells were then vertically aligned inside two custom made aluminum blocks to ensure the optical windows of the cells were perpendicular with incoming solar radiation when placed inside the solar simulator, to eliminate off-axis photons and ensure each cell received a known photon dose. Water from a water bath was circulated through the aluminum blocks to maintain temperature (21 °C) throughout the experiment. The aluminum block with cells were immersed inside another room temperature water bath (~ 21 °C) to minimize CO_2 exchange between the cell and the atmosphere during the experiment. Irradiation was carried out under an Atlas Suntest CPS+ solar simulator and an Atlas Suntest CPS solar simulator, both equipped with a 1.5 kW xenon lamp and a daylight filter (excluding light below ~300 nm). The placement

of samples for each amendment type under the two solar simulators was randomly assigned. Cells were irradiated for 2 and 4 hours. Each time point had two duplicate cells from each amendment type. Each time point also had a dark control by wrapping cells in aluminum foils and placing them in the water bath cooling the aluminum blocks.

Apparent quantum yield determination

Apparent quantum yield spectra (AQY, mol DIC (mol photons absorbed)$^{-1}$) were determined to reflect the DIC photoproduction efficiencies. AQY experiments were carried out following Powers and Miller (2015b) and Powers et al. (2017a), using the same set up as the time series experiment, except that a polychromatic system with Schott long-pass optical filters were used instead of the daylight filters. These filters have cut-on wavelengths (the wavelength of 50% peak transmission) of 280, 295, 305, 320, 380, 400, 435, and 480 nm, respectively, and duplicates were used for each type of filter except for 400 and 435 nm. Three AQY experiments were conducted. Each AQY experiment used only one type of enriched sample water and 15 cells. Each filter was placed directly over a corresponding cell, and one cell was covered with black electric tape to serve as a dark control. Cells under 280, 295, 305, and 320 nm filters were irradiated for 3 h, while cells under 380, 400, 435, and 480 filters were irradiated for 4 h. These time points were selected because the time series experiment had shown that the DIC photoproduction rate was measurable and linear under 4-h irradiation. An Atlas Suntest CPS+ solar simulator was used for these experiments and cut-on filters were randomly placed.

Measurements

Optical measurements

Absorbances ($A(\lambda)$) were measured between wavelength (λ) 250 - 800 nm of samples before and after irradiation using an Agilent 8453 UV-visible spectrophotometer with ChemStation software, at 1.0 nm intervals, in duplicate, in a 1-cm-pathlength quartz cuvette. Milli-Q water was used as blanks. The absorbance spectra were first corrected by subtracting the average absorbance spectra of blanks from the absorbance spectra of the sample water, then by subtracting the average absorbance at 690 - 710 nm to correct for potential offsets and instrument drift (Stubbins et al., 2011). Napierian absorption coefficients ($a_g(\lambda)$; m^{-1}) were calculated using the following equation (Hu et al., 2002b): $a_g(\lambda) = \frac{A(\lambda)\ \ln 10}{L}$, where L (m) is the pathlength. $a_g(\lambda)$ % fading was calculated as the percent difference between $a_g(\lambda)$ values at irradiation time T and T0. $a_g(\lambda)$ fading rates were calculated by linear regressions of $a_g(\lambda)$ versus the integrated photon dose (Q_a(int). *lm* in R, RCoreTeam (2021)).

The integrated photon dose Q_a(int) (mol photons absorbed) for wavelengths 280 - 600 nm absorbed by the samples in each experimental cell, corrected for self-shading, was calculated following Powers et al. (2017b) and Hu et al. (2002a) (Equations 1 and 2)

$$Q_a(\lambda) = E_0(\lambda)\left(1 - e^{-a_g(\lambda)L}\right)S \quad (1)$$

$$Q_a(\text{int}) = t\int_{280}^{600} Q_a(\lambda) \quad (2)$$

where $Q_a(\lambda)$ is the photon dose absorbed by CDOM in the samples at each wavelength (mol photons absorbed s^{-1} nm^{-1}), $E_o(\lambda)$ is the spectral downwelling irradiance entering each cell (mol photons m^{-2} s^{-1} nm^{-1}) quantified using an Optronic Laboratories OL756 Portable UV-Vis Spectroradiometer (Powers et al., 2017b), S (m^2) is the area of the irradiated surface of the cells, t (s) is the irradiation time.

Absorption spectral slopes $S_{275\text{-}295}$ and $S_{350\text{-}400}$ (nm^{-1}) were calculated by linear regressions of natural-log-transformed absorption ($\ln a_g(\lambda)$) versus wavelength for 275 - 295 nm and 350 – 400 nm, respectively (Helms et al., 2008). Spectral ratios S_R were calculated by dividing $S_{275\text{-}295}$ by $S_{350\text{-}400}$ (Helms et al., 2008). Specific ultraviolet absorbance at 254 nm ($SUVA_{254}$; L mg^{-1} m^{-1}) was calculated as the Decadic absorption coefficient at 254 nm ($A(254)/L$; m^{-1}) divided by DOC concentrations (mg L^{-1}) (Weishaar et al., 2003).

Dissolved organic carbon measurement

Duplicate DOC samples (40 mL) were taken from the unamended and amended SRE water samples before irradiation and analyzed for DOC concentrations within a week. DOC concentrations ([*DOC*]) were determined by high temperature catalytic oxidation method using a Shimadzu TOC-V CPH analyzer equipped with a Shimadzu ASI-V autosampler (Stubbins et al., 2012). DOC concentration in the original water samples (unamended samples) was 4.02 ± 0.06 mg L^{-1}, and the amended samples had more than twice the [*DOC*] of the original samples (Table 3.1).

Table 3.1. Dissolved organic carbon concentrations ([*DOC*], mg L^{-1}) and specific ultraviolet absorbance at 254 nm ($SUVA_{254}$, L mg^{-1} m^{-1}), at time 0 of photochemical irradiation time series experiment, using solid phased extract-amended (SPE), electrodialysis reverse osmosis extract-amended (EDRO), and unamended Skidaway River Estuary water. Mean ± 1SE.

	EDRO	SPE	Unamended
[*DOC*] (mg L^{-1})	10.73 ± 0.02	9.22 ± 0.09	4.02 ± 0.06
$SUVA_{254}$ (L mg^{-1} m^{-1})	3.23 ± 0.00	3.88 ± 0.04	3.44 ± 0.05

Photoproduced dissolved inorganic carbon measurements

Photoproduced dissolved inorganic carbon was measured using MoDIE, following protocols modified from Powers et al. (2017b). A liquid chromatography - isotope ratio mass spectrometry (LC-IRMS) system using a Thermo Scientific™ Surveyor HPLC-Isolink LC interface coupled to a Thermo Scientific™ Delta V+ IRMS was used to measure the initial DIC concentrations and DIC-$\delta\,^{13}$C in the samples. Before sample analysis, the IRMS was conditioned to moderate enrichment levels by running continuous injections using enriched SRE water of similar enrichment level (8000 – 9000 ‰) for an hour. This conditioning was shown to reduce instrumental drift and increase precision of sample runs in previous experiments. Samples were injected directly from the cells through a six-valve port on the Isolink LC interface through small diameter Teflon tubing sipper and a peristaltic pump after the valve.

The concentrations of photoproduced DIC ($[DIC]_{\text{photo}}$) at each irradiation time point were calculated using the following equation (Powers et al., 2017a; Powers et al., 2017b):

$$[DIC]_{\text{photo}} = \left(\frac{(^{13}\text{C}/^{12}\text{C})_{\text{final}} - (^{13}\text{C}/^{12}\text{C})_{\text{start}}}{(^{13}\text{C}/^{12}\text{C})_{\text{photo}} - (^{13}\text{C}/^{12}\text{C})_{\text{final}}}\right)[DIC]_{\text{start}} \qquad (3)$$

where $(^{13}\text{C}/^{12}\text{C})_{\text{start}}$, $(^{13}\text{C}/^{12}\text{C})_{\text{final}}$ are the carbon isotope ratios of DIC in the enriched water samples before and after irradiation, $(^{13}\text{C}/^{12}\text{C})_{\text{photo}}$ is that of photoproduced DIC, and $[DIC]_{\text{start}}$ is the starting DIC concentration in the water sample before irradiation. Powers et al. (2017b) demonstrated that the calculation of $[DIC]_{\text{photo}}$ using the MoDIE method has very low sensitivity to the choice of $\delta\,^{13}$C-DIC$_{\text{photo}}$. Therefore, since neither the $[DIC]_{\text{photo}}$ or $\delta\,^{13}$C-DIC$_{\text{photo}}$ can be measured directly for this estuarine sample, the $(^{13}\text{C}/^{12}\text{C})_{\text{photo}}$ was calculated from a $\delta\,^{13}$C-DIC$_{\text{photo}}$ value of −33.3 ‰ (Powers et al., 2017b).

Dissolved inorganic carbon photoproduction rates and efficiencies

Rate calculations for time series experiments

Dissolved inorganic carbon photoproduction rates (P_{DIC}, M DIC (mol photons absorbed)$^{-1}$) were calculated using linear regressions (*lm* in R, RCoreTeam (2021)) of $[DIC]_{photo}$ (M) versus photon doses Q_a(int) (mol photons absorbed). DOC normalized DIC photoproduction (P_{DIC}/[*DOC*], mol L mg^{-1}) was also calculated by dividing the amount of photoproduced DIC (P_{DIC}, mol) in each cell by time 0 DOC concentration (mg L^{-1}).

Apparent quantum yield determinations

Measured DIC photoproduction rates for cells under each optical filter (mol DIC s^{-1}) were calculated using linear regressions (*lm* in R, RCoreTeam (2021)) of $N_{DICphoto}$ (mol) versus irradiation time (h), where $N_{DICphoto}$ is $[DIC]_{photo}$ (M) multiplied by cell volume (~30 mL, determined precisely for each cell using weight subtraction). Predicted DIC photoproduction rates (d*P*/d*t*, mol DIC s^{-1}) were determined using equations (4) and (5) (Powers and Miller, 2015b).

$$\frac{dP}{dt} = \int_{280nm}^{600nm} [\phi(\lambda) \times Q_a(\lambda)] d\lambda \qquad (4)$$

$$\phi(\lambda) = e^{-(m_1 + m_2(\lambda - 290))} \qquad (5)$$

where m_1 and m_2 were fitting parameters.

A nonlinear weighted least squares regression model comparing the measured and predicted DIC photoproduction rates was used to determine the apparent quantum yield fitting parameters (*nls* in R, RCoreTeam (2021)). The model uses a relative-offset convergence criterion to iteratively determine the parameters m_1 and m_2 (Ritz and Streibig, 2008). 95 % confidence intervals were obtained using the profile likelihood method (Ritz and Streibig, 2008).

Normalized root mean square errors (nRMSE, %) were used to determine the statistical robustness of the determined AQY spectrum. The R^2 for linear regressions of measured DIC photoproduction versus predicted DIC photoproduction for each cell was also used to determine the model fit. Predicted DIC photoproduction was calculated by integrating the product of AQY spectrum and $Q_a(\lambda)$ over the 280-600 nm range.

Predicted DIC photoproduction rates (nmol h^{-1}) for all amendment types were estimated using equations (1), (4) and (5), with AQY spectra calculated from the AQY fitting parameters, full spectral downwelling irradiance from the solar simulator (with daylight filter that cuts off wavelength below ~300 nm), and CDOM absorption coefficients of unirradiated unamended samples. Uncertainties were propagated using Monte Carlo evaluation, with randomly generated m_1 and m_2 values using the mean and standard errors determined above for the fitting parameters, assuming normal distribution for both parameters.

Results

Optical property comparisons

Chromophoric dissolved organic matter absorption coefficient ($a_g(\lambda)$) values at 280, 300, 325, and 350 nm decreased with photon dose during photoirradiation (faded) in all samples (linear regressions, $P < 0.05$. Figures 3.1, 3.2, and Table 3.2). a_g fading was small in all wavelengths. For example, a_g % fading at 325 nm after 4 hours were 5.4 ± 0.3 % for EDRO-DOM-amended samples, 5.1 ± 1.6 % for SPE-DOM-amended samples, and 9.3 ± 2.4 % for unamended samples. a_g fading at 280, 300, 325, and 350 nm occurred at rates (m^{-1} (mol photons absorbed)$^{-1}$) that are statistically not different among the amendment types when all time points were included (ANCOVA, $P > 0.05$. Figure 3.2).

Similarly, there was no statistical difference in a_g fading rates (a_g versus photon dose, m^{-1} (mol photons absorbed)$^{-1}$) among amendment types when fading rates were evaluated between adjacent irradiation time points, for either the 0-2 h or 2-4 h time periods (linear regressions for rate determination, $P < 0.05$. ANCOVA for rate comparisons, $P > 0.05$. Figure 3.3). a_g fading rates decreased from the 0-2 h time period to the 2-4 h time period in the EDRO-DOM-amended samples at 280, 300, 325, and 350 nm (ANCOVA, $P < 0.05$), but didn't change significantly for the other two amendment types (ANCOVA, $P > 0.05$), except for SPE-DOM-amended samples at 350 nm where the rate decreased from 0-2 h to 2-4 h (ANCOVA, $P < 0.05$. Figure 3.3).

Initial absorption spectral slope $S_{275\text{-}295}$ values were similar between the unamended and EDRO-DOM-amended samples (one-way ANOVA, $P = 0.002$, followed by Tukey HSD, $P = 1$), but both were higher than those of SPE-DOM-amended samples (Tukey HSD, $P = 0.002$. Figure 3.4a). Initial $S_{350\text{-}400}$ values were not statistically different among amendment types (one-way ANOVA, $P = 0.07$. Figure 3.4b). Initial S_R values were highest in EDRO-DOM-amended samples, and lowest in SPE-DOM-amended samples (one-way ANOVA, $P = 0.003$, followed by Tukey HSD, $P < 0.05$. Figure 3.4c). $S_{275\text{-}295}$ and S_R values increased with photon dose for all three amendment types (linear regressions, $P < 0.05$), but $S_{350\text{-}400}$ values had no statistically significant changes with photon dose (linear regressions, $P > 0.05$. Figure 3.4).

When all time points are considered, $S_{275\text{-}295}$ values increased faster in the unamended samples than in the amended samples (ANCOVA, $P < 0.05$), but the change rates were not different between the amended samples (ANCOVA, $P > 0.05$. Figure 3.4a). The rates of change in S_R showed similar trend with the rates of change in $S_{275\text{-}295}$ when compared among amendment types (Figure 3.4c), but there was no statistically significant difference in the rates of change in $S_{350\text{-}400}$ among the different amendment types (ANCOVA, $P > 0.05$. Figure 3.4b).

Initial specific ultraviolet absorbance values at 254 nm ($SUVA_{254}$) were highest in SPE-DOM-amended samples, and lowest in EDRO-DOM-amended samples (one-way ANOVA, $P = 0.0003$, followed by Tukey HSD, $P < 0.05$. Table 3.1).

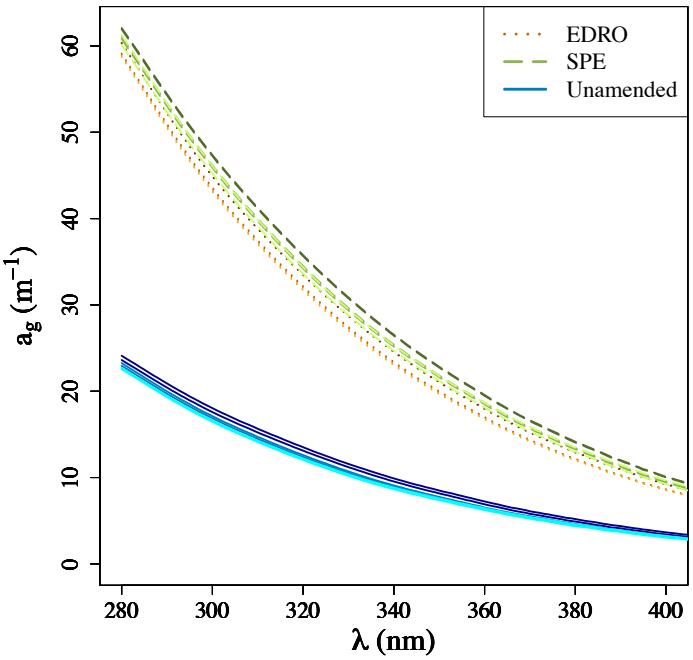

Figure 3.1. Chromophoric dissolved organic matter absorption coefficients (a_g, m^{-1}) versus wavelength (λ, nm), for photochemical irradiation time series experiment, using solid phased extract-amended (SPE), electrodialysis reverse osmosis extract-amended (EDRO), and unamended Skidaway River Estuary water. Darkest color for each amendment type represents time 0 of photoirradiation experiments, color progressively gets lighter as irradiation progresses, and lightest color represents the last time point.

Table 3.2. Chromophoric dissolved organic matter absorption coefficients at 325 nm ($a_g(325)$, m^{-1}) at different irradiation time points, for photochemical irradiation time series experiment, using solid phased extract-amended (SPE), electrodialysis reverse osmosis extract-amended (EDRO), and unamended Skidaway River Estuary water. Mean ± 1 SE.

Irradiation time (h)	$a_g(325)$ (m^{-1})		
	EDRO	SPE	Unamended
0	31.0 ± 0.0	33.2 ± 0.1	12.3 ± 0.3
2	29.7 ± 0.1	31.8 ± 0.2	11.5 ± 0.1
4	29.3 ± 0.1	31.5 ± 0.5	11.2 ± 0.1

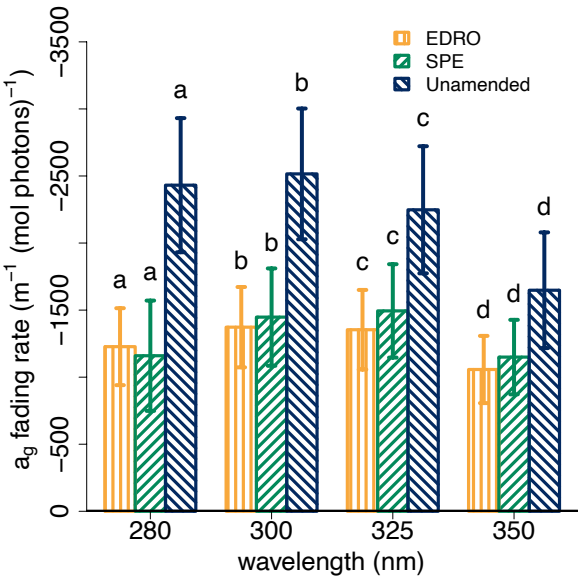

Figure 3.2. Chromophoric dissolved organic matter absorption coefficient a_g fading rates (a_g versus photon dose, m^{-1} (mol photons absorbed)$^{-1}$) at 280 nm, 300 nm, 325 nm, and 350 nm. For photochemical irradiation time series experiment, using solid phased extract-amended (SPE), electrodialysis reverse osmosis extract-amended (EDRO), and unamended Skidaway River Estuary water. Rates were calculated by including values at all time points. Shared letter on top of bars denotes rates that are not significantly different from each other (ANCOVA, $P \geq 0.05$). Rates were not compared among the different wavelengths. Error bars were ± 1SE.

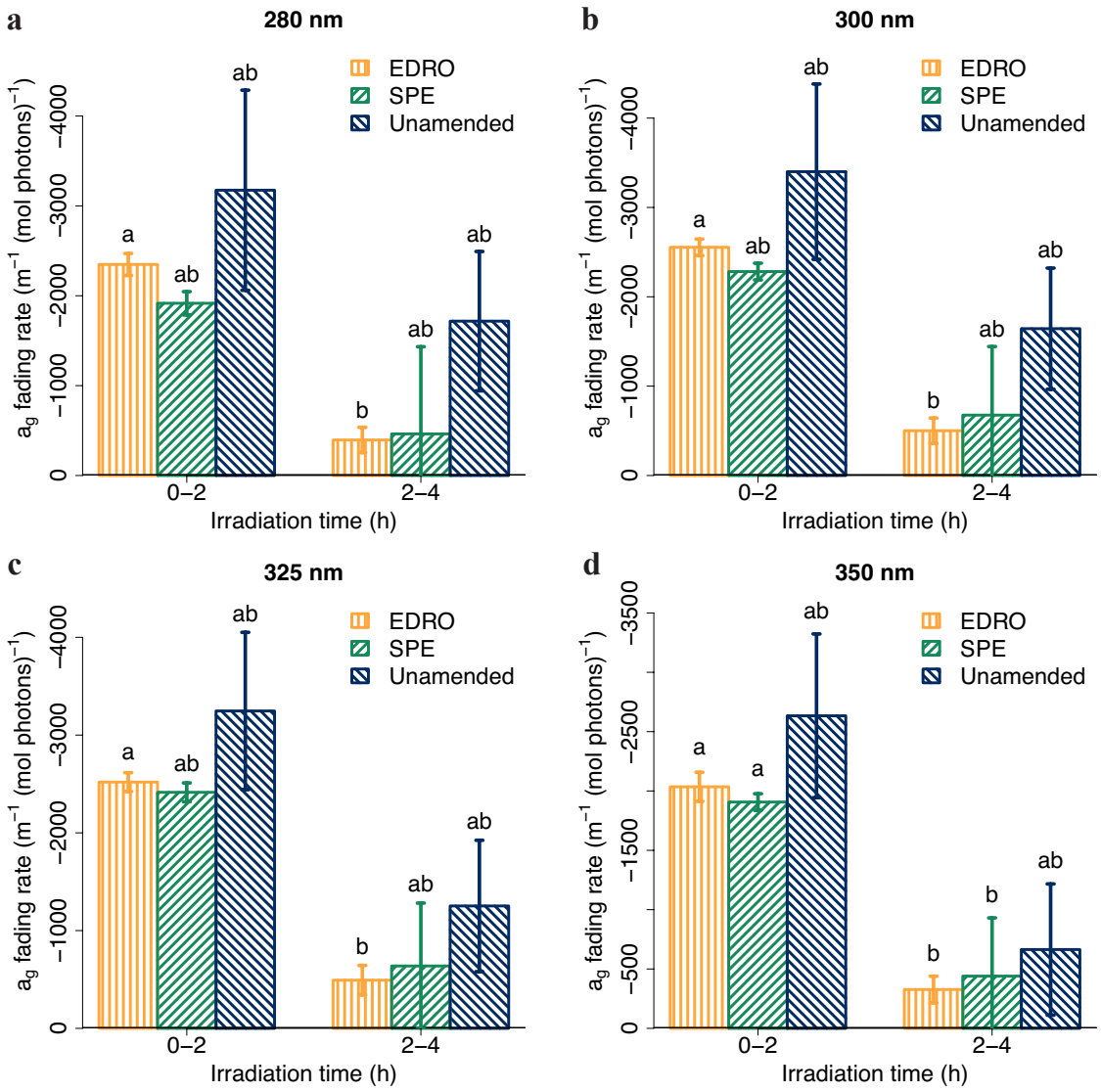

Figure 3.3. Chromophoric dissolved organic matter absorption coefficient a_g fading rates (a_g versus photon dose, m^{-1} (mol photons absorbed)$^{-1}$) at (a) 280 nm, (b) 300 nm, (c) 325 nm, and (d) 350 nm. For photochemical irradiation time series experiment, using solid phased extract-amended (SPE), electrodialysis reverse osmosis extract-amended (EDRO), and unamended Skidaway River Estuary water. Rates were calculated between two adjacent time points. Different letters on top of bars denote rates that are significantly different from each other (ANCOVA, $P < 0.05$), shared letters denote rates that are not significantly different from each other (ANCOVA, $P \geq 0.05$). Error bars were ± 1SE.

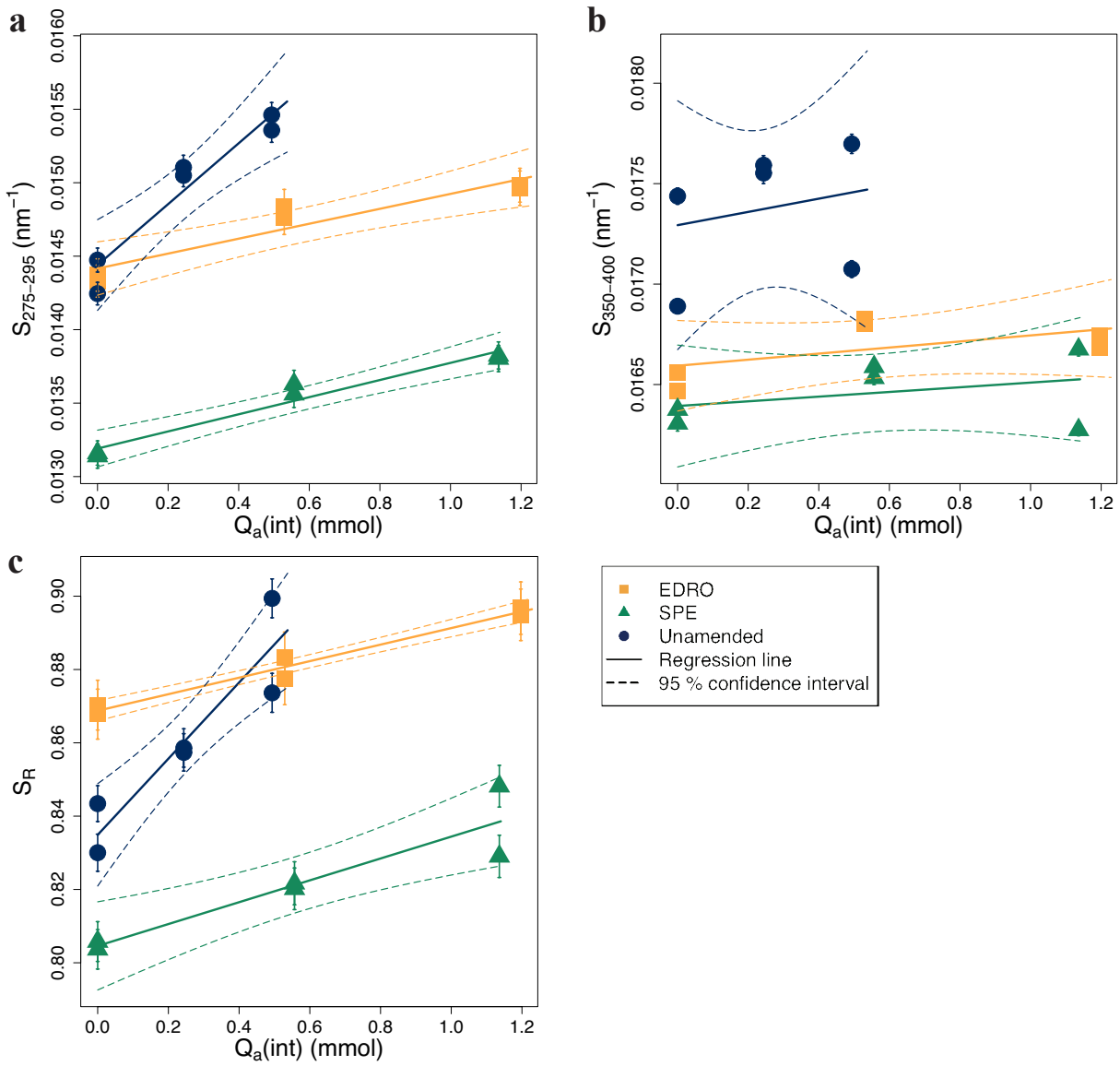

Figure 3.4. Chromophoric dissolved organic matter (CDOM) spectral slopes (a) $S_{275\text{-}295}$ (nm^{-1}), (b) $S_{350\text{-}400}$ (nm^{-1}), and (c) S_R, versus photon dose (Q_a(int), mmol, photons absorbed by CDOM in the sample, integrated from 280 nm to 600 nm). For photochemical irradiation time series experiment, using solid phased extract-amended (SPE), electrodialysis reverse osmosis extract-amended (EDRO), and unamended Skidaway River Estuary water. Error bars were ± 1SE.

Dissolved inorganic carbon photoproduction comparisons

Dissolved inorganic carbon photoproduction rates (P_{DIC}) were higher in EDRO-DOM-amended than SPE-DOM-amended samples when all time points are considered (ANCOVA, $P < 0.05$), but were not statistically different between unamended and either amendment types (ANCOVA, $P > 0.05$. Figure 3.5a). For the 0-2 h time period, P_{DIC} was higher in the EDRO-DOM-amended samples than in either the SPE-DOM-amended or unamended samples (ANCOVA, $P < 0.05$), but was not different between the SPE-DOM-amended and unamended samples (ANCOVA, $P > 0.05$. Figure 3.5b). P_{DIC} remained unchanged in unamended samples from 0-2 h to 2-4 h (ANCOVA, $P > 0.05$), but decreased in amended samples (ANCOVA, $P < 0.05$. Figure 3.5b). P_{DIC} was higher in the unamended than in the amended samples for the 2-4 h period (ANCOVA, $P < 0.05$), but was not different between the amended samples (ANCOVA, $P > 0.05$. Figure 3.5b).

Dissolved organic carbon normalized DIC photoproduction rate (P_{DIC}/[*DOC*]) was higher in the unamended than in the amended samples when all time points are considered (ANCOVA, $P < 0.05$), but was not different between the amended types (ANCOVA, $P > 0.05$. Figure 3.5c). The same trend was observed when considering the 0-2 h and 2-4 h time periods separately (Figure 3.5 d). P_{DIC}/[*DOC*] remained unchanged in unamended samples from 0-2 h to 2-4 h (ANCOVA, $P > 0.05$), but decreased in amended samples (ANCOVA, $P < 0.05$. Figure 3.5d).

Predicted DIC photoproduction calculated from the AQY spectra (Eq. (4) and (5)) agreed well with measured values ($R^2 > 0.80$ for linear regressions of predicted versus measured DIC photoproduction. Table 3.3). The AQY spectra were similar among the three amendment types (Table 3.3, Figure 3.6). The ranges of predicted DIC photoproduction rates overlapped among

the three amendment types (32.3 ± 18.5 nmol h^{-1}, 21.7 ± 8.0 nmol h^{-1}, and 18.9 ± 7.7 nmol h^{-1} for EDRO-DOM-amended, SPE-DOM-amended, and unamended samples, respectively. Figure 3.7).

Table 3.3. Dissolved inorganic carbon apparent quantum yield (AQY) fitting parameters (m_1 and m_2) for photochemical irradiation experiments, using solid phased extract-amended (SPE), electrodialysis reverse osmosis extract-amended (EDRO), and unamended Skidaway River Estuary water. R^2 values were from linear regressions of predicted versus measured DIC photoproduction.

	m_1	m_2	R^2	nRMSE (%)
EDRO	6.43 ± 0.33	0.0180 ± 0.0042	0.87	26.0
SPE	6.50 ± 0.23	0.0225 ± 0.0035	0.94	18.3
Unamended	6.54 ± 0.22	0.0239 ± 0.0042	0.94	19.5

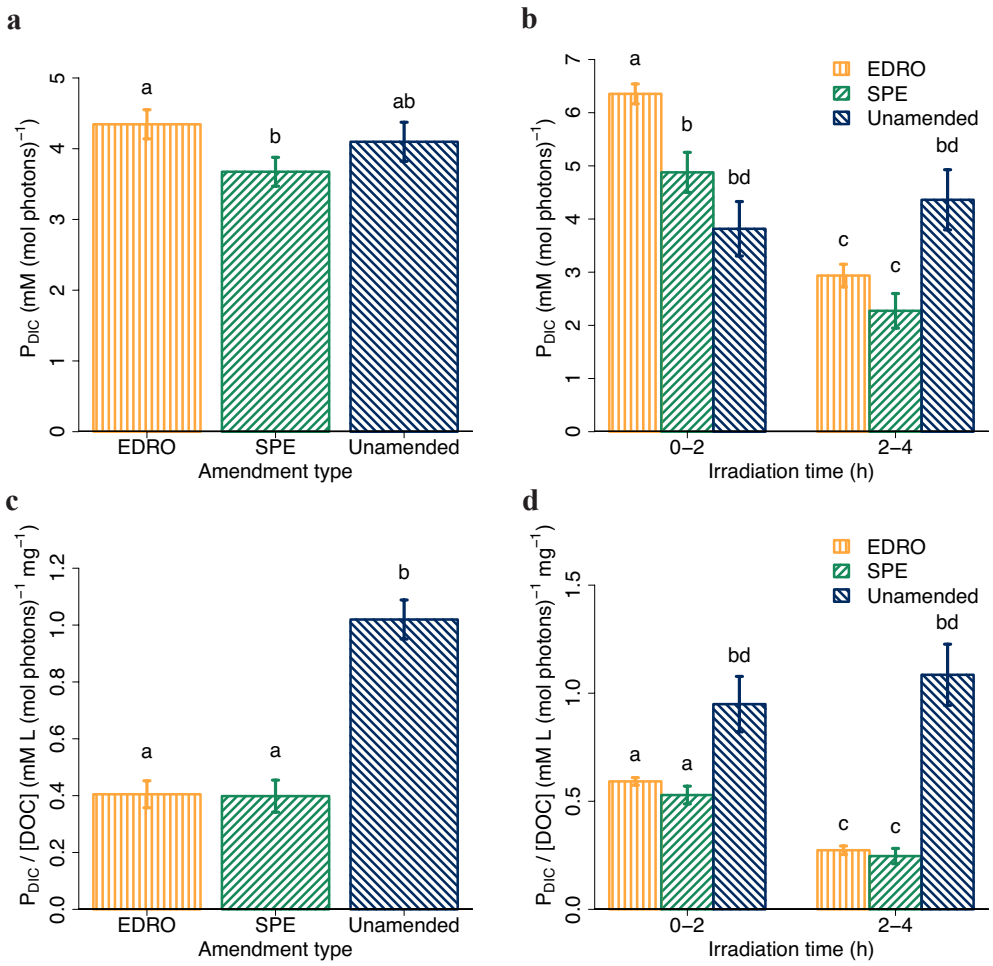

Figure 3.5. (a) Dissolved inorganic carbon (DIC) photoproduction rates (P_{DIC}, mM DIC (mol photons absorbed)$^{-1}$), normalized to CDOM absorption and corrected for self-shading, (b) P_{DIC}/[*DOC*] (mM L (mol photons absorbed)$^{-1}$ mg^{-1}), P_{DIC} normalized to time 0 DOC concentration (mg L^{-1}) in the samples. For photochemical irradiation time series experiment, using solid phased extract-amended (SPE), electrodialysis reverse osmosis extract-amended (EDRO), and unamended Skidaway River Estuary water. (a, c) P_{DIC} and P_{DIC}/[*DOC*] values calculated using all time point data, (b, d) P_{DIC} and P_{DIC}/[*DOC*] values calculated between two adjacent time points. Different letters on top of bars denote rates that are significantly different from each other (ANCOVA, $p < 0.05$), shared letters denote rates that are not significantly different from each other (ANCOVA, $p \geq 0.05$). Error bars were ± 1SE.

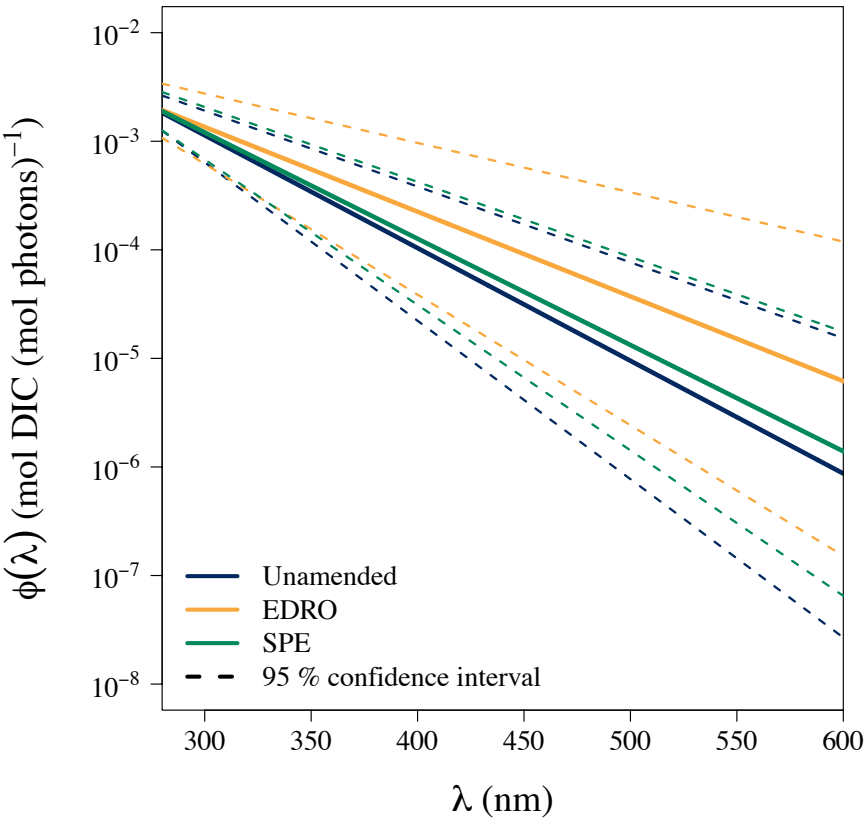

Figure 3.6. Dissolved inorganic carbon apparent quantum yield (AQY, $\phi(\lambda)$) spectra (vs. wavelength λ) for photochemical irradiation experiments, using solid phased extract-amended (SPE), electrodialysis reverse osmosis extract-amended (EDRO), and unamended Skidaway River Estuary water.

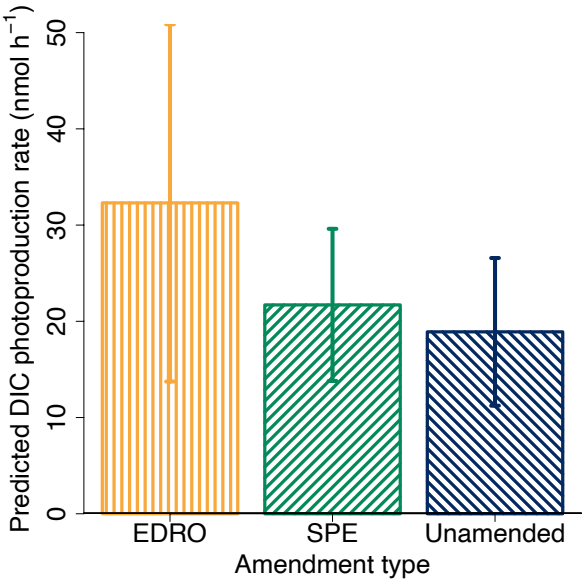

Figure 3.7. Predicted dissolved inorganic carbon (DIC) photoproduction rates (nmol h^{-1}), estimated using apparent quantum yield spectra calculated from the fitting parameters, full spectral downwelling irradiance (with daylight filter that cuts off wavelength below ~300 nm), and colored DOM absorption coefficients of unirradiated unamended samples. For photochemical irradiation experiments, using solid phased extract-amended (SPE), electrodialysis reverse osmosis extract-amended (EDRO), and unamended Skidaway River Estuary water. Error bars were ± 1SE.

Discussion

Optical properties comparison

Chromophoric dissolved organic matter absorption decreased with photon dose in all samples as expected (Table 3.2, Figures 3.1, 3.2, and 3.3), indicating photobleaching of CDOM in the samples. There were no differences in a_g fading rates at the wavelength tested among the amendment types (Figure 3.2 and 3.3). It is likely that even though SPE and EDRO could lead to

incomplete extraction of CDOM molecules (Helms et al., 2015; Wünsch et al., 2018), and SPE decreases absorbance (Wünsch et al., 2018), they can still extract a representative suite of CDOM molecules and thus do not significantly impact CDOM fading in the short term (hours). It is worth noting that a_g fading rate decreased over time in EDRO-DOM-amended samples for all wavelength tested, and in SPE-DOM-amended samples at 350 nm, suggesting that the changes in photoreactivity over time are different depending on the amendment type. It is possible that EDRO and SPE preferentially extracted a collection of DOM molecules that can photobleach rapidly and thus are consumed rapidly, so that fading decreases over time.

The similar initial spectral slope $S_{275\text{-}295}$ and $S_{350\text{-}400}$ values between EDRO-DOM-amended and unamended samples (Figure 3.4a, b) suggests a similarity of optical properties at the UV range between EDRO-extracted CDOM and the original whole water CDOM, and a difference between EDRO-extracted and SPE-extracted CDOM. This agrees with the finding of Chambers et al. (2016) that EDRO can extract a representative suite of fluorescent DOM molecules, which is a fraction of CDOM, from the original whole water. The lower initial $S_{275\text{-}295}$ values in SPE-DOM-amended samples agrees with the finding of Wünsch et al. (2018) that the SPE extraction efficiency is spectrally variable and SPE decreases $S_{275\text{-}295}$. Unlike in Wünsch et al. (2018), there was no statistical difference in $S_{350\text{-}400}$ values between SPE-DOM-amended and unamended samples, but the difference in results could in fact support their hypothesis that SPE leads to complex changes in the quality of CDOM, and these changes could be affected by chemical properties of the original water extracted. The large error in $S_{350\text{-}400}$ values in the unamended samples may have also affected the statistical power of the comparisons. The difference in S_R values between the EDRO-DOM-amended and unamended samples (Figure 3.4c) may also have been caused by the large errors in $S_{350\text{-}400}$ values in unamended samples, but

could also suggest that complex changes occur to CDOM molecules when they are EDRO extracted.

The similarity in spectral slope values between EDRO-DOM-amended and unamended samples may also suggest a similar distribution of molecular weights between EDRO-DOM and the original whole water DOM, as a correlation was suggested between $S_{275\text{-}295}$ values and molecular weights (Helms et al., 2008). These results again suggest that EDRO-DOM is representative of the whole water DOM, although the effect of EDRO on molecular weights could be more complicated because S_R values differed between the unamended and EDRO-DOM-amended samples. It is interesting though that the lower $S_{275\text{-}295}$ values in SPE-DOM-amended samples would appear to suggest an average higher molecular weight of SPE-DOM compared to the original whole water DOC, even though SPE is thought to be biased towards small molecules (Arrieta et al., 2015). This result is again supportive of the hypothesis of Wünsch et al. (2018) that the changes occur during SPE are likely complex and qualitative, instead of simply biased towards certain size fractions.

Spectral slope $S_{275\text{-}295}$ and slope ratio S_R increased with photon dose (Figure 3.4a, c). This is consistent with observed changes in slopes during photoirradiation from other studies, and may also reflect the preferential degradation of higher molecular weight DOM and preservation or production of lower molecular weight DOM typically occurs during DOM photodegradation (Helms et al., 2008; Stubbins et al., 2010b). The rates of change were higher in unamended samples, but not different between the amended samples, suggesting effects of extraction on optical property and potentially molecular weight of DOM during photoirradiation, and similarities of these effects between the two extraction methods.

Since $SUVA_{254}$ is a ratio of CDOM absorption at 254 nm to [*DOC*], it could provide some insight into the relative proportion of CDOM to DOC in a sample. SPE-DOM has a higher ratio of CDOM:DOC than both the EDRO-DOM and the original whole water DOM (Table 3.1), because of a preferential extraction of CDOM by SPE. On the other hand, EDRO-DOM had the lowest CDOM:DOC ratio and may suggest a better retention of non-chromophoric DOM that are smaller and less hydrophobic.

$SUVA_{254}$ values in unamended samples of this study (Table 3.1) were higher than those reported in Skidaway River Estuary (SRE) in March, but were within the range of $SUVA_{254}$ values found at SRE year round (Bittar et al., 2016). Values in all sample types were similar to reported values of humic substances, particularly riverine fulvic acids (Weishaar et al., 2003). These results suggest a high terrestrial input of DOM at the sample site, likely due to the continuous heavy rains that carried terrestrial organic matter to the estuary prior to sample collection, similar to what Bittar et al. (2016) found at the site during high freshwater discharge period. In addition, the higher initial $SUVA_{254}$ values in SPE-DOM-amended samples (Table 3.1) may suggest increased aromaticity after extraction, since $SUVA_{254}$ has been positively correlated with aromaticity (Weishaar et al., 2003). This was consistent with the observed effect of SPE on $SUVA_{254}$ values, which was attributed to either the effect of salt on sorption efficiencies of aromatic DOM, or the selective sorption of aromatic DOM due to intrinsic differences in DOM quality (Arellano et al., 2018; Cawley et al., 2009).

Dissolved inorganic carbon photoproduction rates and apparent quantum yield comparisons

The apparent quantum yield spectra for unamended water samples (Table 3.3) were in relatively good agreement with previously published results of coastal estuarine systems in the region (Reader and Miller, 2012). There were 13.3 %, 9.77 %, and 9.42 % differences in the fitting parameter m_1 values between our result and the March 2009 high tide Dolby Sound, Altamaha Sound, and Sapelo Sound samples in Reader and Miller (2012), respectively; and 38.1 %, 0.418 %, 25.5 % differences in m_2 values. Dolby Sound is more similar to the SRE in terms of freshwater input, so the differences in fitting parameters, particularly in m_2, between our results and Reader and Miller (2012), could be the results of the slightly different AQY equations used. There's a third parameter m_3 in the AQY equation used in Reader and Miller (2012), and the estimated m_3 value for Dolby Sound was 297.253. In contrast, we used a 290 fixed value in place of the m_3 parameter (Powers and Miller, 2015b). The differences in m_1 and m_2 values between SRE in our study and Altamaha Sound in Reader and Miller (2012) were much smaller, likely due to the similarity of the fitted m_3 value for Altamaha Sound (290.118) and the 290 value used in our study.

Since the calculations of DIC photoproduction rates (P_{DIC}, mol DIC (mol photons absorbed)$^{-1}$, measured from the time series experiment, Figure 3.5a, b; and nmol h^{-1}, predicted from apparent quantum yield spectra, Figure 3.7) used integrated photon doses which incorporated CDOM absorption in the equation (equations 1 and 2), the rates were scaled by CDOM absorption, thus can be evaluated as if the samples had the same initial CDOM absorption. It is interesting that DIC photoproduction does not completely track with CDOM photobleaching. While a_g fading rates were not different among the amendment types and the

rates of change in $S_{275\text{-}295}$ and S_R were higher in unamended samples but not different between the amended samples, EDRO-DOM-amended samples had higher P_{DIC} than SPE-DOM-amended samples when all time point values were considered and for the 0-2 h period. In addition, EDRO-DOM-amended samples had higher P_{DIC} than unamended samples for the 0-2 h period, and both amended types had lower P_{DIC} than unamended for the 2-4 h period.

These differences in DIC photoproduction rates among the samples, and the difference between the trends in CDOM photobleaching and DIC photoproduction, may be attributed to the different types of molecules preferentially extracted by the two methods. It is conceivable that EDRO extracts a collection of DOM molecules that are more efficient at producing DIC upon photoirradiation, as compared to SPE and the original seawater where photochemical reactions that do not lead to DIC photoproduction might be more common. For example, although the comparisons were based on peatland porewater samples, Tfaily et al. (2012) found that EDRO extracted a high abundance of carboxylic acids, which can efficiently carry out photodecarboxylation and/or other photooxidation reactions, and produce DIC upon photoirradiation (Budac and Wan, 1992; Xie et al., 2004). Tfaily et al. (2012) also found that SPE using PPL had much lower extraction efficiency for carboxylic acids compared to EDRO. The significant reduction of DIC photoproduction rate from 0-2 h to 2-4 h in the amended samples while the rates in unamended samples remain unchanged between the two time periods, suggests the preferential extraction by EDRO of a DOM fraction that photolyzes rapidly and subsequently depleted faster in the amended samples.

In contrast to color-scaled DIC photoproduction rates (normalized to CDOM), the difference among the amendment types changed when DIC photoproduction rate was normalized to DOC concentrations ($P_{DIC}/[DOC]$, mM L (mol photons)$^{-1}$ mg^{-1}, Figure 3.4c, d). Both amended

types had lower P_{DIC}/[*DOC*] than unamended samples whether all data were included or only data between 0-2 h or 2-4 h were considered. This contrast suggests that both SPE and EDRO extracts had lower CDOM:DOC ratios than the original SRE water. This result is contrary to that suggested by $SUVA_{254}$ that SPE-DOM has a higher ratio of CDOM:DOC than both the EDRO-DOM and the original whole water DOM (Table 3.1). However, $SUVA_{254}$ only provides the optical information on CDOM at 254 nm, while comparison of the two sets of normalized P_{DIC} values likely provide a better evaluation of CDOM:DOC since the rates were normalized to the full absorption spectrum.

The recovery rate for SPE in this study was high (77 %), as usually is the case for high-terrestrial-content waters (> 60 %, Dittmar et al., 2008). The whole water sample used in this study likely contained high terrestrial DOM, as the salinity was relatively low, and continuous heavy rain occurred prior to sampling. Recovery rates for EDRO (59 % and 60 %) were higher than the 51 % recovery rate of the SRE water in Young and Ingall (2010), likely due to the reduced system volume and membrane surface area (50 L versus 10 L for our system). It is difficult to completely drain the sample from the system, and the added membrane surface area could lead to more sample loss. On the other hand, the EDRO recovery rates were lower than those in Chambers et al. (2016) (71.3 ± 6.5 %) where SRE water was also used, likely due to sample loss to the added reverse osmosis membranes in our study.

Conclusions

When using DIC photoproduction rates of the amended samples to extrapolate to the rates in the original water sample, our results suggest that extrapolation by color/CDOM can be time sensitive. Extrapolation based on rates in the EDRO-DOM-amended samples can be a good

approximation or overestimation of the original water rate, depending on which time period the rate is calculated for (i.e., 0-4 h versus 0-2 h). SPE-DOM-amendment approximates the rates in the original water well, both for the 0-4 h and 0-2 h periods, thus SPE-DOM-amendment could be a better option for experiments to estimate initial DIC photoproduction rates and determine AQY. Extrapolation by [*DOC*], on the other hand, can significantly underestimate DIC photoproduction rates in the original water, using amended samples from extracts of either extraction method.

Both the extraction and amendment methods performed well to approximate the DIC photoproduction efficiency, as suggested by the similar AQY spectra and overlapping ranges of predicted DIC photoproduction (Figure 3.7). The results of this study suggest that DOM extraction and amendment to the original seawater could effectively concentrate CDOM and DOM in the samples, but does not significantly change the CDOM fading rate or DIC photoproduction efficiencies. Therefore, DOM extraction and amendment offers an excellent opportunity to investigate the photochemical properties of seawater, especially when the property is difficult to investigate in the original whole water, such as DIC photoproduction. By concentrating CDOM and DOM, the method could increase the amount of photoproduced DIC in the sample, to a level more easily measurable by the MoDIE method. Future studies with iterations of this study, such as using samples from a variety of locations (inshore to offshore), amended to different extract concentrations, and using different irradiation times, could reveal more information about the differences among sample types (or lack thereof).

The extraction efficiency of SPE tends to be much lower for open-ocean DOM than for coastal DOM (Chen et al., 2016; Dittmar et al., 2008; Green et al., 2014; Stubbins and Dittmar, 2012), whereas EDRO tends to have higher recovery in open seawater than coastal waters

(Chambers et al., 2016; Helms et al., 2015; Vetter et al., 2007; Young and Ingall, 2010). The types and abundance of molecules extracted could also be different between open ocean and coastal water samples depending on the extraction method (Dittmar et al., 2008; Koprivnjak et al., 2009). For example, SPE can extract terrigenous DOM more efficiently than marine DOM (Dittmar et al., 2008), whereas EDRO can extract representative fractions of DOM for both terrestrially-derived and marine DOM efficiently (Koprivnjak et al., 2009). The whole water sample used in this study likely contained high terrestrial DOM, therefore, results might be different when applying the method in this study to samples in the open ocean. Nonetheless, given the difficulties in examining DIC photoproduction rates and efficiencies in the open ocean, it is worth the effort to test this method in the open ocean.

Acknowledgements

This work was supported by United States National Science Foundation Chemical Oceanography grant #1635618. I would like to thank Dr. Ellery Ingall for teaching me electrodialysis reverse osmosis, providing space and equipment for the extraction, and helping me with extraction; Carl Lehman for help with the electrodialysis reverse osmosis system testing. I would also like to thank Dr. Leanne Powers for her editorial help.

REFERENCES

Amon, R.M.W. and Benner, R., 1996. Bacterial utilization of different size classes of dissolved organic matter. Limnology and Oceanography, 41(1): 41-51.

Arellano, A.R., Bianchi, T.S., Hutchings, J.A., Shields, M.R. and Cui, X.Q., 2018. Differential effects of solid-phase extraction resins on the measurement of dissolved lignin-phenols and organic matter composition in natural waters. Limnology and Oceanography-Methods, 16(1): 22-34.

Arrieta, J.M. et al., 2015. Dilution limits dissolved organic carbon utilization in the deep ocean. Science, 348(6232): 331-333.

Arrigo, K.R. and Brown, C.W., 1996. Impact of chromophoric dissolved organic matter on UV inhibition of primary productivity in the sea. Marine Ecology Progress Series, 140(1-3): 207-216.

Bittar, T.B. et al., 2016. Seasonal dynamics of dissolved, particulate and microbial components of a tidal saltmarsh-dominated estuary under contrasting levels of freshwater discharge. Estuarine Coastal and Shelf Science, 182: 72-85.

Brandes, J.A., 2009. Rapid and precise delta C-13 measurement of dissolved inorganic carbon in natural waters using liquid chromatography coupled to an isotope-ratio mass spectrometer. Limnology and Oceanography-Methods, 7: 730-739.

Budac, D. and Wan, P., 1992. PHOTODECARBOXYLATION - MECHANISM AND SYNTHETIC UTILITY. Journal of Photochemistry and Photobiology a-Chemistry, 67(2): 135-166.

Carlson, C.A. and Hansell, D.A., 2015. Chapter 3 - DOM Sources, Sinks, Reactivity, and Budgets. Biogeochemistry of Marine Dissolved Organic Matter: 65-126.

Cawley, K.M., Hakala, J.A. and Chin, Y.-P., 2009. Evaluating the triplet state photoreactivity of dissolved organic matter isolated by chromatography and ultrafiltration using an alkylphenol probe molecule. Limnology and Oceanography: Methods, 7(6): 391-398.

Chambers, L.R. et al., 2016. Enhanced Dissolved Organic Matter Recovery from Saltwater Samples with Electrodialysis. Aquatic Geochemistry, 22(5-6): 555-572.

Chen, M., Kim, S., Park, J.E., Jung, H.J. and Hur, J., 2016. Structural and compositional changes of dissolved organic matter upon solid-phase extraction tracked by multiple analytical tools. Analytical and Bioanalytical Chemistry, 408(23): 6249-6258.

Clark, C.D. et al., 2004. CDOM distribution and CO(2) production on the southwest Florida shelf. Marine Chemistry, 89(1-4): 145-167.

Coble, P.G., 2007. Marine optical biogeochemistry: The chemistry of ocean color. Chemical Reviews, 107(2): 402-418.

Del Vecchio, R. and Blough, N.V., 2002. Photobleaching of chromophoric dissolved organic matter in natural waters: kinetics and modeling. Marine Chemistry, 78(4): 231-253.

Dittmar, T., Koch, B., Hertkorn, N. and Kattner, G., 2008. A simple and efficient method for the solid-phase extraction of dissolved organic matter (SPE-DOM) from seawater. Limnology and Oceanography-Methods, 6: 230-235.

Gonsior, M. et al., 2014. Photochemical production of polyols arising from significant photo-transformation of dissolved organic matter in the oligotrophic surface ocean. Marine Chemistry, 163: 10-18.

Green, N.W. et al., 2014. An intercomparison of three methods for the large-scale isolation of oceanic dissolved organic matter. Marine Chemistry, 161: 14-19.

Hansell, D.A., 2002. DOC in the global ocean carbon cycle. In: D.A. Hansell and C.A. Carlson (Editors), Biogeochemistry of marine dissolved organic matter. Academic Press, pp. 685-716.

Hansell, D.A. and Carlson, C.A., 1998. Deep-ocean gradients in the concentration of dissolved organic carbon. Nature, 395(6699): 263-266.

Hansell, D.A., Carlson, C.A., Repeta, D.J. and Schlitzer, R., 2009. DISSOLVED ORGANIC MATTER IN THE OCEAN A CONTROVERSY STIMULATES NEW INSIGHTS. Oceanography, 22(4): 202-211.

Hedges, J.I., 2002. Why dissolved organics matter? . In: D.A. Hansell and C.A. Carlson (Editors), Biogeochemistry of marine dissolved organic matter. Academic Press, pp. 1-34.

Helms, J.R. et al., 2015. Spectroscopic characterization of oceanic dissolved organic matter isolated by reverse osmosis coupled with electrodialysis. Marine Chemistry, 177: 278-287.

Helms, J.R. et al., 2013. Photochemical bleaching of oceanic dissolved organic matter and its effect on absorption spectral slope and fluorescence. Marine Chemistry, 155: 81-91.

Helms, J.R. et al., 2008. Absorption spectral slopes and slope ratios as indicators of molecular weight, source, and photobleaching of chromophoric dissolved organic matter. Limnology and Oceanography, 53(3): 955-969.

Hu, C., Muller-Karger, F.E. and Zepp, R.G., 2002a. Absorbance, absorption coefficient, and apparent quantum yield: A comment on common ambiguity in the use of these optical concepts. Limnology and Oceanography, 47(4): 1261-1267.

Hu, C.M., Muller-Karger, F.E. and Zepp, R.G., 2002b. Absorbance, absorption coefficient, and apparent quantum yield: A comment on common ambiguity in the use of these optical concepts. Limnology and Oceanography, 47(4): 1261-1267.

Johannessen, S.C. and Miller, W.L., 2001. Quantum yield for the photochemical production of dissolved inorganic carbon in seawater. Marine Chemistry, 76(4): 271-283.

Koprivnjak, J.F., Perdue, E.M. and Pfromm, P.H., 2006. Coupling reverse osmosis with electrodialysis to isolate natural organic matter from fresh waters. Water Research, 40(18): 3385-3392.

Koprivnjak, J.F. et al., 2009. Chemical and spectroscopic characterization of marine dissolved organic matter isolated using coupled reverse osmosis-electrodialysis. Geochimica Et Cosmochimica Acta, 73(14): 4215-4231.

Kroer, N., 1993. Bacterial-growth efficiency on natural dissolved organic matter. Limnology and Oceanography, 38(6): 1282-1290.

Miller, W.L., Moran, M.A., Sheldon, W.M., Zepp, R.G. and Opsahl, S., 2002. Determination of apparent quantum yield spectra for the formation of biologically labile photoproducts. Limnology and Oceanography, 47(2): 343-352.

Miller, W.L. and Zepp, R.G., 1995. Photochemical production of dissolved inorganic carbon from terrestrial organic matter: significance to the oceanic organic carbon cycle Geophysical Research Letters, 22(4): 417-420.

Moody, C.S. and Worrall, F., 2017. Modeling rates of DOC degradation using DOM composition and hydroclimatic variables. Journal of Geophysical Research: Biogeosciences, 122(5): 1175-1191.

Mopper, K., Kieber, D.J. and Stubbins, A., 2015. Marine Photochemistry of Organic Matter: Processes and Impacts. In: D.A. Hansell and C.A. Carlson (Editors), Biogeochemistry of Marine Dissolved Organic Matter, 2nd Edition. Academic Press Ltd-Elsevier Science Ltd, London, pp. 389-450.

Mopper, K. et al., 1991. Photochemical degradation of dissolved organic carbon and its impact on the oceanic carbon cycle. Nature, 353(6339): 60-62.

Obernosterer, I. and Benner, R., 2004. Competition between biological and photochemical processes in the mineralization of dissolved organic carbon. Limnology and Oceanography, 49(1): 117-124.

Powers, L.C., Brandes, J.A., Miller, W.L. and Stubbins, A., 2017a. Using liquid chromatography-isotope ratio mass spectrometry to measure the delta C-13 of dissolved inorganic carbon photochemically produced from dissolved organic carbon. Limnology and Oceanography-Methods, 15(1): 103-115.

Powers, L.C., Brandes, J.A., Stubbins, A. and Miller, W.L., 2017b. MoDIE: Moderate dissolved inorganic carbon ((DIC)-C-13) isotope enrichment for improved evaluation of DIC photochemical production in natural waters. Marine Chemistry, 194: 1-9.

Powers, L.C. and Miller, W.L., 2015. Photochemical production of CO and CO2 in the Northern Gulf of Mexico: Estimates and challenges for quantifying the impact of photochemistry on carbon cycles. Marine Chemistry, 171: 21-35.

RCoreTeam, 2021. R: A language and environment for statistical computing. The R Foundation for Statistical Computing, Vienna, Austria.

Reader, H.E. and Miller, W.L., 2012. Variability of carbon monoxide and carbon dioxide apparent quantum yield spectra in three coastal estuaries of the South Atlantic Bight. Biogeosciences, 9(11): 4279-4294.

Ridgwell, A. and Arndt, S., 2015. Why dissolved organics matter: DOC in ancient oceans and past climate change. In: D.A. Hansell and C.A. Carlson (Editors), Biogeochemistry of marine dissolved organic matter. Academic Press.

Ritz, C. and Streibig, J.C., 2008. Nonlinear Regression with R. Use R! Springer, 144 pp.

Stubbins, A. and Dittmar, T., 2012. Low volume quantification of dissolved organic carbon and dissolved nitrogen. Limnology and Oceanography-Methods, 10: 347-352.

Stubbins, A., Law, C.S., Uher, G. and Upstill-Goddard, R.C., 2011. Carbon monoxide apparent quantum yields and photoproduction in the Tyne estuary. Biogeosciences, 8(3): 703-713.

Stubbins, A., Niggemann, J. and Dittmar, T., 2012. Photo-lability of deep ocean dissolved black carbon. Biogeosciences, 9(5): 1661-1670.

Stubbins, A. et al., 2010. Illuminated darkness: Molecular signatures of Congo River dissolved organic matter and its photochemical alteration as revealed by ultrahigh precision mass spectrometry. Limnology and Oceanography, 55(4): 1467-1477.

Tfaily, M.M., Hodgkins, S., Podgorski, D.C., Chanton, J.P. and Cooper, W.T., 2012. Comparison of dialysis and solid-phase extraction for isolation and concentration of dissolved organic matter prior to Fourier transform ion cyclotron resonance mass spectrometry. Analytical and Bioanalytical Chemistry, 404(2): 447-457.

Vetter, T.A., Perdue, E.M., Ingall, E., Koprivnjak, J.F. and Pfromm, P.H., 2007. Combining reverse osmosis and electrodialysis for more complete recovery of dissolved organic matter from seawater. Separation and Purification Technology, 56(3): 383-387.

Weishaar, J.L. et al., 2003. Evaluation of specific ultraviolet absorbance as an indicator of the chemical composition and reactivity of dissolved organic carbon. Environmental Science & Technology, 37(20): 4702-4708.

White, E.M., Kieber, D.J., Sherrard, J., Miller, W.L. and Mopper, K., 2010. Carbon dioxide and carbon monoxide photoproduction quantum yields in the Delaware Estuary. Marine Chemistry, 118(1-2): 11-21.

Wünsch, U.J. et al., 2018. Quantifying the impact of solid-phase extraction on chromophoric dissolved organic matter composition. Marine Chemistry, 207: 33-41.

Xie, H.X., Zafiriou, O.C., Cai, W.J., Zepp, R.G. and Wang, Y.C., 2004. Photooxidation and its effects on the carboxyl content of dissolved organic matter in two coastal rivers in the Southeastern United States. Environmental Science & Technology, 38(15): 4113-4119.

Young, C.L. and Ingall, E.D., 2010. Marine Dissolved Organic Phosphorus Composition: Insights from Samples Recovered Using Combined Electrodialysis/Reverse Osmosis. Aquatic Geochemistry, 16(4): 563-574.

Zafiriou, O.C., Andrews, S.S. and Wang, W., 2003. Concordant estimates of oceanic carbon monoxide source and sink processes in the Pacific yield a balanced global "blue-water" CO budget. Global Biogeochemical Cycles, 17(1).

Ziolkowski, L.A. and Miller, W.L., 2007. Variability of the apparent quantum efficiency of CO photoproduction in the Gulf of Maine and Northwest Atlantic. Marine Chemistry, 105(3-4): 258-270.

CHAPTER 4

TEXTILE-DERIVED MICROPLASTIC FIBER (MICROFIBER) PHOTODEGRADATION AND CONCOMITANT PHOTOPRODUCTION OF DISSOLVED ORGANIC CARBON IN AQUATIC ENVIRONMENTS

Introduction

In recent years, the ubiquity of microplastic pollution in aquatic ecosystems has raised both environmental concerns and research interests (Aves et al., 2022; Bonanno and Orlando-Bonaca, 2018; Dauvergne, 2018; Karbalaei et al., 2018; van Sebille et al., 2015; Wang et al., 2021). Microplastics are defined as plastic fragments smaller than 5 mm in size (Arthur et al., 2009; van Sebille et al., 2015) and could have significant adverse effects on aquatic organisms (Cole et al., 2011 and references within; Huang et al., 2021and references within). Ecotoxicity of microplastics could manifest due to direct ingestion of microplastics (Betts, 2008; Cole et al., 2015; Rehse et al., 2016; Thompson et al., 2009), biohazardous chemicals released from microplastic and plasticizer (plastic additives) leachates (Barnes et al., 2009; Lithner et al., 2009; Lithner et al., 2011; Schrank et al., 2019; Talsness et al., 2009), and other pollutants adhered on microplastics, which can include toxic metals (Ashton et al., 2010; Betts, 2008; Brennecke et al., 2016), endocrine disrupting chemicals (Ng and Obbard, 2006), and persistent organic pollutants (Rios et al., 2007).

One microplastic particle morphology found in the environment is microfiber. There is an abundance of microfiber source materials globally. In 2015 alone, the production of plastics for textiles was 5.9×10^7 metric tons, and on average these textile plastics are only used for 5 years

before discarded (Geyer et al., 2017). Hartline et al. (2016) reported that machine washing synthetic clothes could generate enough microfibers per wash to account for, on average, 0.2 % of the unwashed garment mass, so that washing of synthetic clothing could be a major source of microfibers in the environment (Browne et al., 2011). Despite the ability of conventional wastewater treatment facilities to remove significant amount of microplastics, treated wastewater may still act as a significant source of microplastics because the large volumes of effluents that are discharged (Browne et al., 2011; Talvitie et al., 2017). Polyester and polyamide are the most common commercially available textile plastics in clothing (Ravandi and Valizadeh, 2011), and polyester and acrylic microfibers dominate sediments in marine habitats receiving sewage effluent (Browne et al., 2011).

There could be as many as 1.5×10^{18} microfibers in the ocean (Mishra et al., 2019). Research has indicated the presence of up to 1×10^{12} microplastic particles in Georgia's intercoastal waterways, with the majority of these microfibers (Brandes and Sanders, 2019; Sanders and Brandes, 2020). Microfibers are ubiquitous even in the remote Arctic Ocean (Ross et al., 2021) and found in the diet of the King penguin in the Southern Ocean (Le Guen et al., 2020).

Estimated oceanic inventories of plastic account for less than 1% of the land-based plastic waste estimated to enter the ocean annually (van Sebille et al., 2015). It is thus apparent that there are significant removal pathways for plastics in the ocean. Since microplastics are frequently found in surface samples of the water column where they are exposed to sunlight (Bohdan, 2022; Enders et al., 2015; Song et al., 2015; Song et al., 2014), photodegradation could be an important abiotic removal pathway (Andrady, 2015; Gewert et al., 2015; Hakkarainen and Albertsson, 2004; Lee and Kim, 2021; Ranby and Lucki, 1980; Wayman and Niemann, 2021).

However, photodegradation of microplastics in the aquatic environments remains poorly quantified duo to a scarcity of environmentally relevant research (i.e., research conducted under realistic temperatures and solar radiation spectrum). The majority of current research has been conducted by polymer engineers who have different emphases and goals for studying polymer degradation than environmental chemists (Gewert et al., 2015). For example, polymer engineers might be interested in discoloration/coloration and fragmentation of plastics, and conditions that would help prevent such decline in product quality, whereas environmental chemists might want to know what chemicals are released into the environment as the plastic polymers degrade (Lee and Kim, 2021).

Microplastics can affect organic matter cycling in the ocean (Boldrini et al., 2021; Galgani et al., 2018; Galgani and Loiselle, 2019; Romera-Castillo et al., 2018). Chromophoric dissolved organic matter (CDOM) and dissolved organic carbon (DOC) can leach from microplastics (Galgani and Loiselle, 2019; Romera-Castillo et al., 2018). The presence of microplastic can stimulate bacterial activity and enhance the microbial release of CDOM (Galgani et al., 2018). On the other hand, the leached DOC can enhance microbial activity, which could lead to increased processing of CDOM and thus decreased CDOM (Boldrini et al., 2021). However, few studies have examined whether and how microplastic photodegradation alone impacts the carbon cycling through DOC and CDOM production (Zhu et al., 2020b). With the experiments reported here, we aim to fill this knowledge gap.

Microfibers, by their morphology, have larger surface to volume ratios than typical macroplastics such as bottles, bags, and Styrofoam cups, and this alone may affect microfiber photochemistry (Fahem and Yousif, 2017). Two potential products from microfiber

photodegradation were examined in this study, DOC and CDOM. Comparisons were made between the DOC/CDOM photoproduction rates in ultrapure water and in seawater.

Methods

Yarnbee™ Eternal Bliss art #43 100 % polyester red/18 yarn and Joann™ 1508-0229 100 % polyester Sumi Casa sanded satin bright white fabric were purchased from commercial craft stores. The yarn and fabric were chosen because they were readily available and popular. Raman microscopy confirmed that the polyesters were polyethylene terephthalate (PET). The yarn or fabric was cut into small pieces using a sharp blade, then hand pulled into loose threads and ground using a Spex Certiprep 6750 freezer mill to obtain microfibers. The default setting was used that included 3 cycles of grinding (15 min pre-cooling, 2 min grinding, and 1 min cooling each). The grinding cycles were repeated until most of the samples placed in the freezer mill were of microfiber sizes. The microfibers obtained from the red yarn were then dried in a 60 °C oven for two days before used. The microfibers obtained from the white fabric were stirred and soaked in MilliporeSigma 18.2-MΩ.cm Milli-Q® Type 1 ultrapure water (Milli-Q water) overnight, then filtered onto a Whatman GF/F 0.7 μm filter, before dried in a 60 °C oven. The ground and dried microfibers have a powdery appearance, and most microfibers were in the tens of μm to < 1 mm length range, having an ~ 20 μm diameter.

About 10 mg of microfibers were weighed onto pre-combusted aluminum foil and poured into a cylindrical 10-cm-pathlength Spectrocell spectrophotometric quartz cell (cell, ~30 mL volume). Any remaining microfibers on the aluminum foil were rinsed off with Milli-Q water or seawater into the cell. The cell was then filled with either Milli-Q water or seawater and capped with Spectrocell caps fitted with Microsolv Teflon-lined butyl septa. Effort was made to

eliminate headspace, by adding liquid until meniscus form before the cell was capped; however, the cell couldn't be overfilled to reduce loss of microfibers, and it was difficult to completely eliminate air bubbles trapped in the caps. The seawater used in the experiments was surface (5 m) Atlantic subtropical gyre water from a Bermuda Atlantic Time-series (BATS) station obtained on 13 May 2017. The seawater sample was re-filtered on 12 May 2020 using a 0.2 μm Whatman Polycap 36 AS nylon membrane cartridge filter.

Photodegradation experiments followed protocols modified from Powers et al. (2017b). Cells were irradiated under an Atlas Suntest CPS+ or CPS solar simulator, both equipped with a 1.5 kW xenon lamp and a daylight filter (excluding light below ~300 nm). The cells were vertically aligned inside a custom aluminum block to ensure the optical windows of the cells were perpendicular to incoming radiation when placed inside the solar simulator, to eliminate off-axis photons and ensure each cell receives a known photon dose. Water was circulated through the aluminum blocks to maintain temperature (21 °C) throughout the experiment. Experiment 1 used Milli-Q water only (6.25, 121.38, and 219.38 h irradiation), experiment 2 used seawater only (42.33, 90.33, 138.33, and 186.33 h irradiation), and experiments 3 and 4 used Milli-Q water and seawater (4, 8, 12, 24, 36, and 60 h irradiation, 12.1, 24.1, 36, 48, and 60.2 h irradiation, respectively). Experiment 1 and 2 used microfibers from the red yarn, and experiment 3 and 4 used microfibers from the white fabric. Triplicate cells were used for each time point. Triplicate dark controls for experiment 1 and 2, and duplicate dark controls for experiment 3 and 4, were sampled for the last time point, using cells wrapped in aluminum foil and placed in the water bath supplying cold water to the aluminum block.

The downwelling irradiance entering each cell was quantified using an Optronic Laboratories OL756 Portable UV-Vis Spectroradiometer. The mean integrated incident

irradiances (250-800 nm) at the cell surface were 395 W m^{-2} for CPS+ and 405 W m^{-2} for CPS solar simulators. For reference, a 219.38-h irradiation under the solar simulator was equivalent to 12.4 and 12.7 July days respectively, under natural sunlight in Bermuda (32.3, -64.8).

Sample from each cell was filtered through a Whatman GF/F 1825-025 (25 mm diameter, 0.7 μm pore size) filter. Approximately 20 mL of the filtrate was poured directly into a 24 mL combusted borosilicate glass vial for DOC concentration measurements, and the remaining filtrate was poured into another vial for CDOM measurements. In experiment 1, the cell was rinsed with Milli-Q water multiple times to dislodge the microfibers adhering to the cell wall, and the rinse water was filtered through the original filter to collect these microfibers. The microfibers collected after irradiation were dried and weighed to determine the mass of microfiber remaining after irradiation. It is worth mentioning that even after diligent rinsing with Milli-Q water to collect as many microfibers as possible, some very small microfibers remained in the cell and the filtration funnel. The filtration set was rinsed with copious amount of Milli-Q water before used for the next cell.

Chromophoric dissolved organic matter absorbance (CDOM) ($A(\lambda)$) in the filtrates was measured using an Agilent 8453 UV-visible spectrophotometer with ChemStation software, between 250 - 800 nm, at 1.0 nm intervals, in duplicate, and in a 1-cm-pathlength quartz cuvette. Milli-Q water was used as blanks. The absorbance spectra were first corrected by subtracting the average absorbance spectra of blanks from the absorbance spectra of the sample water, then by subtracting the average absorbance at 690 - 710 nm to correct for potential offsets and instrument drift (Stubbins et al., 2011). Napierian absorption coefficients ($a_g(\lambda)$; m^{-1}) were calculated using the following equation (Hu et al., 2002b): $a_g(\lambda) = \frac{A(\lambda)\ \ln 10}{L}$, where L (m) is the pathlength. $a_g(\lambda)$ values were normalized to microfiber mass (mg) in each cell ($a_g(\lambda)_N$, m^{-1} (mg

microfiber)$^{-1}$) so that the differences in the initial masses of microfibers among cells can be accounted for. Dissolved organic carbon concentrations ([*DOC*], mg L^{-1} C) in the filtrates were determined by high temperature catalytic oxidation method using a Shimadzu TOC-V CPN Total Organic Carbon Analyzer with autosampler (Stubbins et al., 2012), at Skidaway Institute of Oceanography within a week of collection. [*DOC*] was also normalized to microfiber mass (mg) in each cell ($[DOC]_N$, mg L^{-1} C (mg microfiber)$^{-1}$).

The rate of change in microfiber mass with irradiation time was calculated using linear regression (lm in R, RCoreTeam, 2021). The rates of change in CDOM and DOC between two adjacent time points were calculated by dividing the difference in the parameter values by the time difference (h).

All labware was first rinsed with copious amount of Milli-Q water, and soaked overnight in 10 % HCl solution, then rinsed again with an excess of Milli-Q water. Glassware and GF/F filters were baked at 450 °C for at least 5 h. Quartz cells used in photochemistry experiments were cleaned following the same procedure but not baked. The cartridge filter used to filter seawater was rinsed with 20 L of Milli-Q water before use. All acid solutions were made using Fisher Chemical Certified ACS Plus Safe-Cote® HCl and Milli-Q water.

Results

No statistically significant change in microfiber mass with irradiation time was observed for experiment 1 (P = 0.3. Figure 4.1), likely due to the difficulty in collecting all microfibers from the cells and the filtration set. The large loss in microfiber mass in the dark control at the last irradiation time point supported this hypothesis. The large error in measuring loss of microfiber mass at each time point likely obscured any change occurring over time. Microfiber

masses were not measured for the other experiments due to this lack of precision in measuring losses.

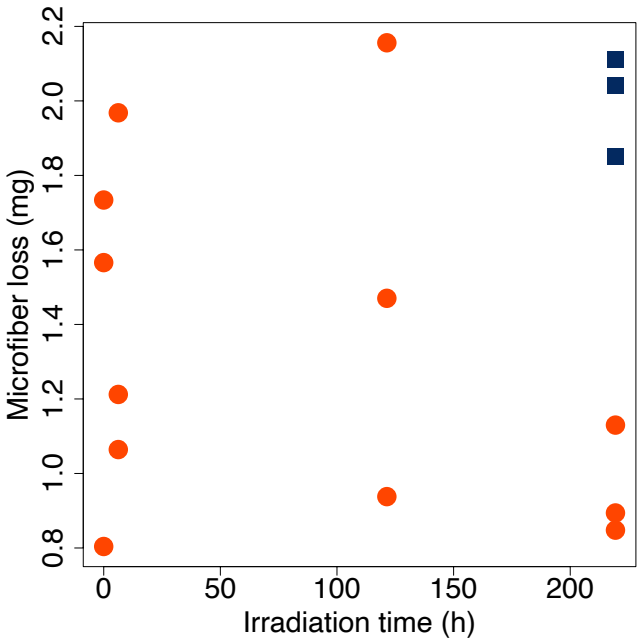

Figure 4.1. Loss of microfiber mass (mg) over irradiation time (h) for photoirradiation experiment 1, microfibers in Milli-Q water. Orange red circles-irradiated samples, blue squares-dark control.

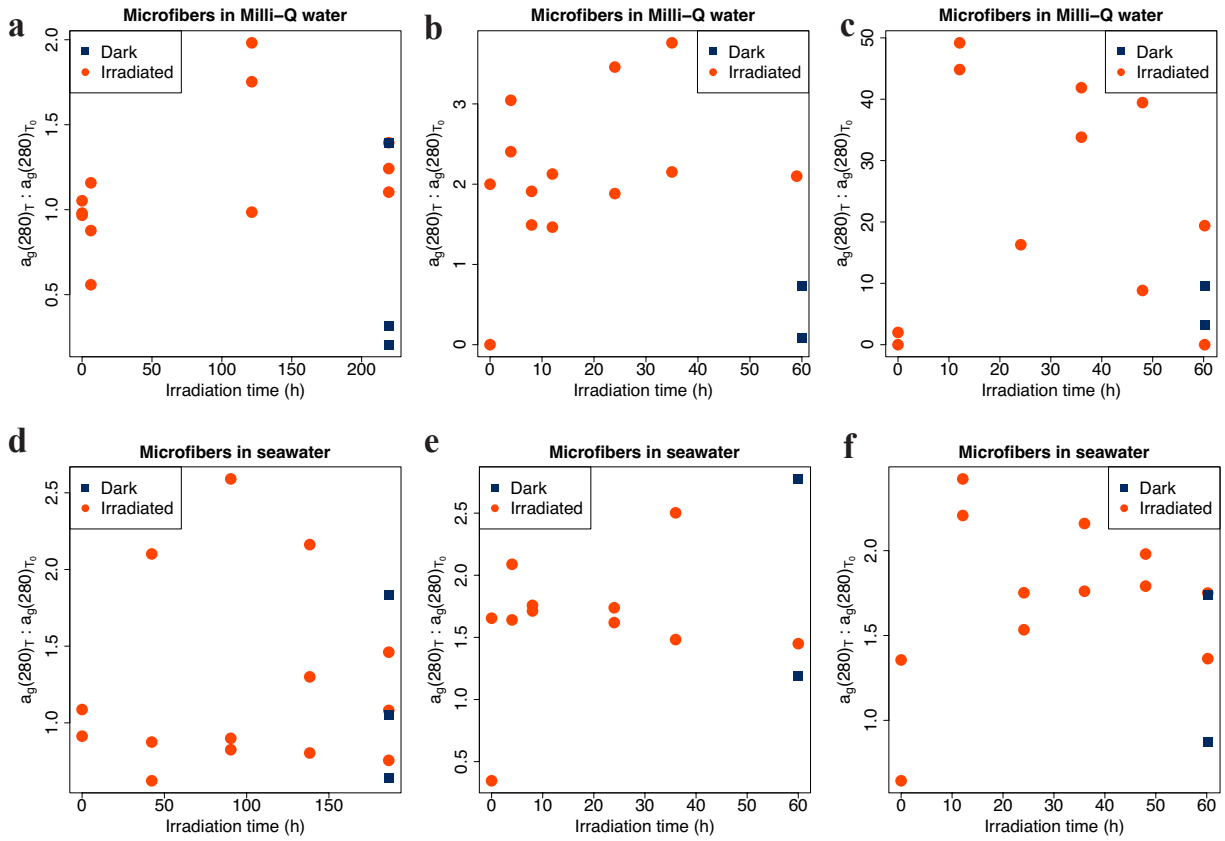

Figure 4.2. Chromophoric dissolved organic matter absorption coefficients at 280 nm, normalized to initial microfiber mass ($a_g(280)_N$, m^{-1} (mg microfiber)$^{-1}$), versus irradiation time (h) in photoirradiation experiments: (a, b, c) microfibers in Milli-Q ultrapure water, (d, e, f) microfibers in open ocean seawater from the Atlantic subtropical gyre. (a) experiment 1, (d) experiment 2, (b) and (e) experiment 3, and (c) and (f) experiment 4. Expressed as ratios of $a_g(280)_N$ at any irradiation point (T) to $a_g(280)_N$ at time zero (T_0). Note the different irradiation time among experiments. Experiment 1 and 2 used the same type of microfibers (from red polyester yarn) while experiment 3 and 4 used a different type of microfibers (from white polyester fabric).

There was no statistically significant change in normalized absorption at 280 nm, 300 nm, 325 nm, and 350 nm in the filtrate with irradiation time in any experiment (linear regressions, $P > 0.05$), however, there may be changes in normalized absorption values between time points (Figures 4.2, 4.3 and Supplemental figures S4.1, S4.2, and S4.3).

Over the week-long experiments (experiment 1 and 2, Figure 4.2a, b and 4.3a), the rates of change in $a_g(280)_N$ ($a_g(\lambda)_N$ at 280 nm) of the filtrate with irradiation time were low, in the 10^{-3} m^{-1} (mg microfiber)$^{-1}$ h^{-1} range for microfibers in Milli-Q water and in seawater. $a_g(280)_N$ in the Milli-Q water samples may have increased from 6.25 h to 121.38 h first, and then decreased.

In the shorter experiments 3 and 4 (Figure 4.2b, c, e, f and 4.3b, c), $a_g(280)_N$ increased from time 0 to the first time point in both water types and remained high after (in experiment 3) or decreased over time (in experiment 4). The rates of change in $a_g(280)_N$ were in the 10^{-2} m^{-1} (mg microfiber)$^{-1}$ h^{-1} range for both water types from 0-4 h in experiment 3, and 0-12.1 h in experiment 4 (Figure 4.3b, c). The rates of change then decreased in magnitude, and in some cases the signs were reversed, indicating fluctuations in CDOM absorption over time.

There were no net changes in normalized absorption at 280 nm, 300 nm, 325 nm, and 350 nm in any experiment (t tests between T_0 samples and irradiated samples of last time point, $P > 0.05$, Figure 4.2 and Supplemental Figures S4.1, S4.2, and S4.3). The normalized absorption at 280 nm, 300 nm, 325 nm, and 350 nm in dark control samples at the last time point were also not statistically different from those in T_0 samples (t tests, $P > 0.05$, Figure 4.2 and Supplemental Figures S4.1, S4.2, and S4.3).

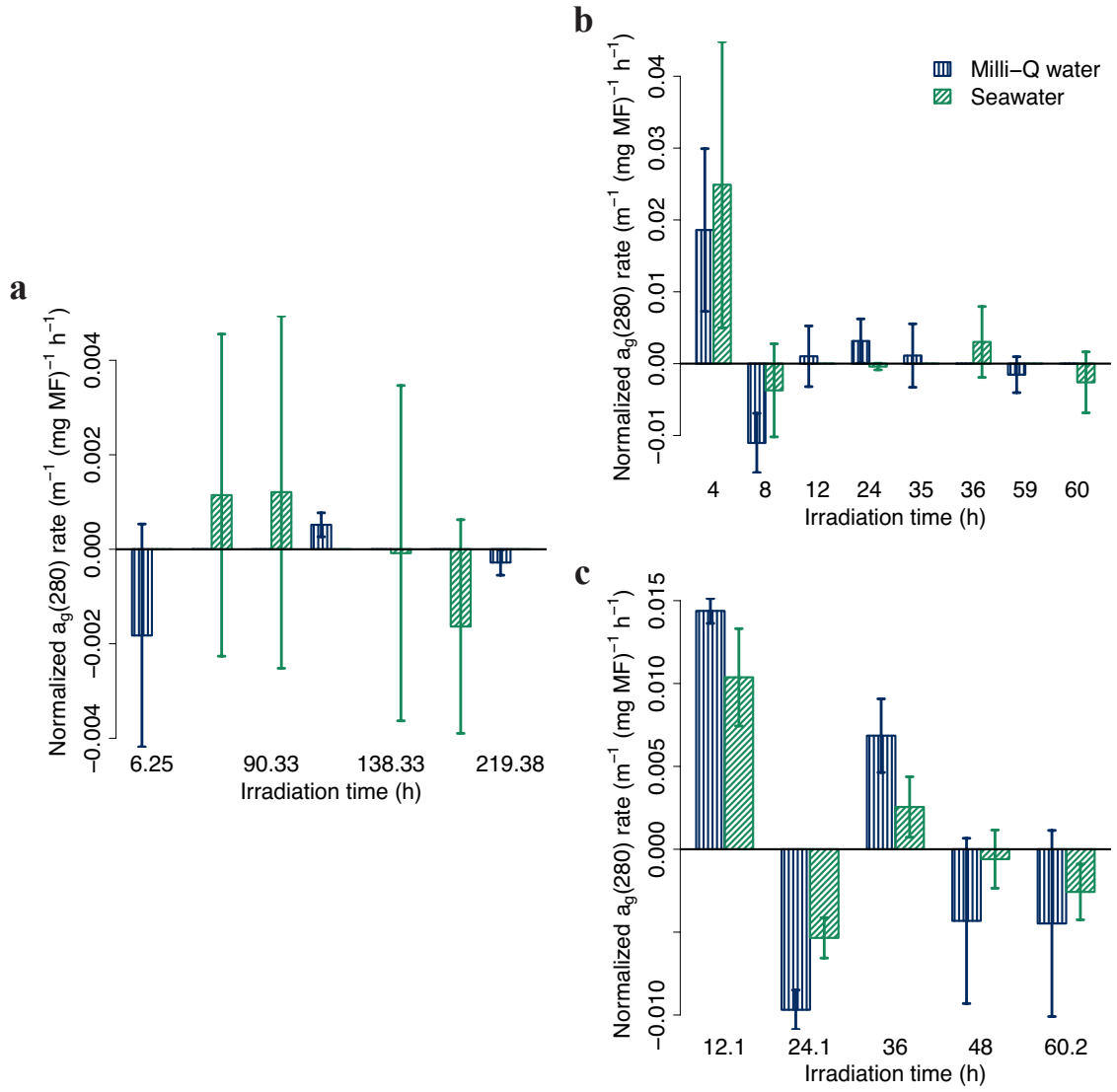

Figure 4.3. Rates of change (m^{-1} (mg microfiber)$^{-1}$ h^{-1}) for absorption coefficients at 280 nm (a_g(280)) with irradiation time in photoirradiation experiments. a_g(280) (m^{-1}) were normalized to initial microfiber mass (mg). Microfibers were irradiated either in Milli-Q ultrapure water or seawater from the Atlantic subtropical gyre. (a) experiment 1 and 2, (b) experiment 3, and (c) experiment 4. Note the different irradiation time among experiments. Experiment 1 and 2 used the same type of microfibers (from red polyester yarn) while experiment 3 and 4 used a different type of microfibers (from white polyester fabric). Error bars are ±1 standard error from triplicates.

Normalized DOC concentrations ($[DOC]_N$) increased with time in the Milli-Q water samples in experiment 3 (linear regression, $P = 0.03$). There was no statistically significant change in $[DOC]_N$ with irradiation time in the rest of the experiments (linear regressions, $P > 0.05$), however, there may be changes in $[DOC]_N$ values between time points (Figures 4.4 and 4.5).

The rates of change in $[DOC]_N$ were in the 0-10 μg L^{-1} C (mg microfiber)$^{-1}$ h^{-1} range (Figure 4.5). For the week-long experiments using red microfibers, $[DOC]_N$ may have increased before 6.25 h and subsequently decreased in the Milli-Q water samples (Figure 4.4a and 4.5a). In seawater samples, $[DOC]_N$ remained stable until 138.33 h, then decreased (Figure 4.4d and 4.5a). Although the samples in Milli-Q water in the shorter experiments didn't show initial rates of increase in $[DOC]_N$ as large as that in the first time period of experiment 1, there was a trend of increase followed by a decrease in $[DOC]_N$ in experiment 3, and maybe fluctuations in experiment 4 (Figure 4.4b, c and 4.5b, c). The highest rate of increase occurred at 35 and 36 h in Milli-Q water samples in experiment 3 and 4, respectively. $[DOC]_N$ fluctuated in the seawater samples of the shorter experiments over time (Figure 4.4e, f and 4.5b, c).

Normalized DOC concentrations were higher in irradiated samples of the last time point than in T_0 samples in experiment 1 (microfibers in Milli-Q water; t tests between T_0 samples and irradiated samples of last time point, $P = 0.01$), but there were no net changes in $[DOC]_N$ in the rest of the experiments ($P > 0.05$, Figure 4.4). $[DOC]_N$ in dark control samples at the last time point were also not statistically different from those in T0 samples (t tests, $P > 0.05$, Figure 4.4).

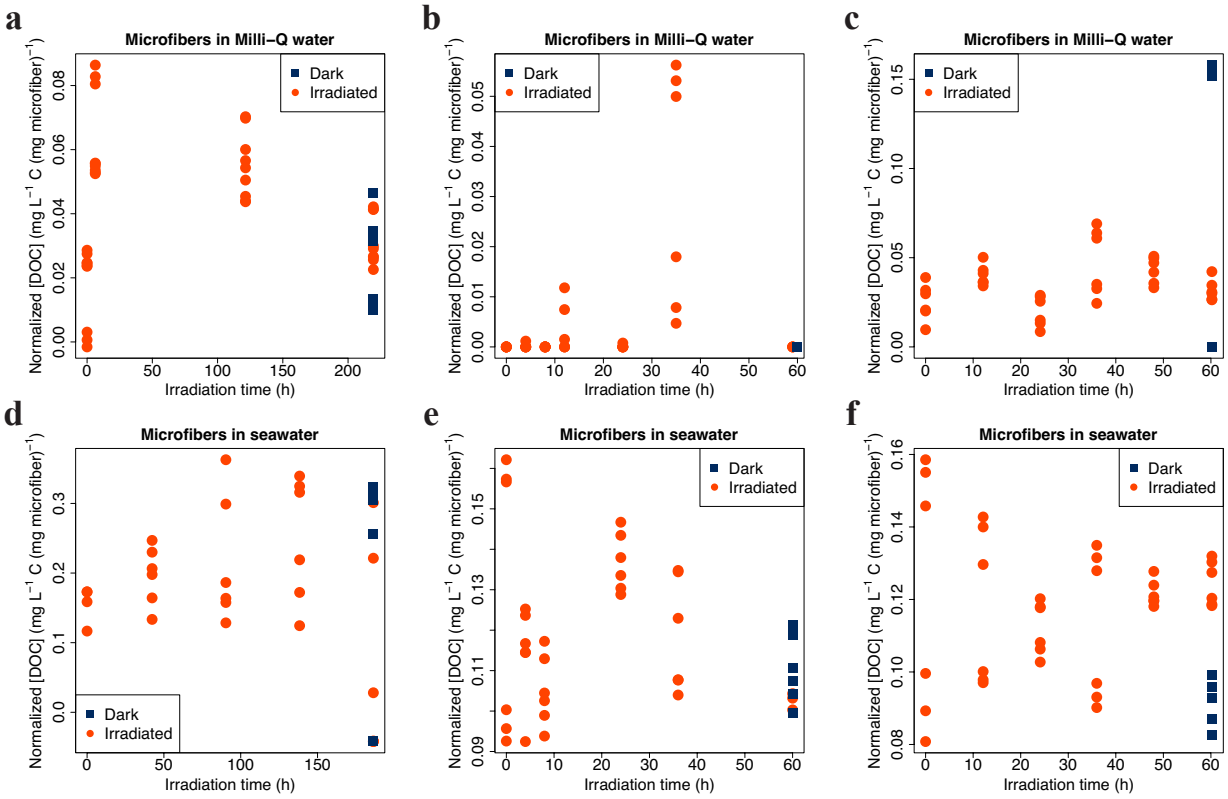

Figure 4.4. Dissolved organic carbon (DOC) concentrations ($[DOC]_N$), normalized to initial microfiber mass (mg L^{-1} C (mg microfiber)$^{-1}$), versus irradiation time (h) in photoirradiation experiments: (a, b, c) microfibers in Milli-Q ultrapure water, (d, e, f) microfibers in open ocean seawater from the Atlantic subtropical gyre. (a) experiment 1, (d) experiment 2, (b) and (e) experiment 3, and (c) and (f) experiment 4. Note the different irradiation time among experiments. Experiment 1 and 2 used the same type of microfibers (from red polyester yarn) while experiment 3 and 4 used a different type of microfibers (from white polyester fabric).

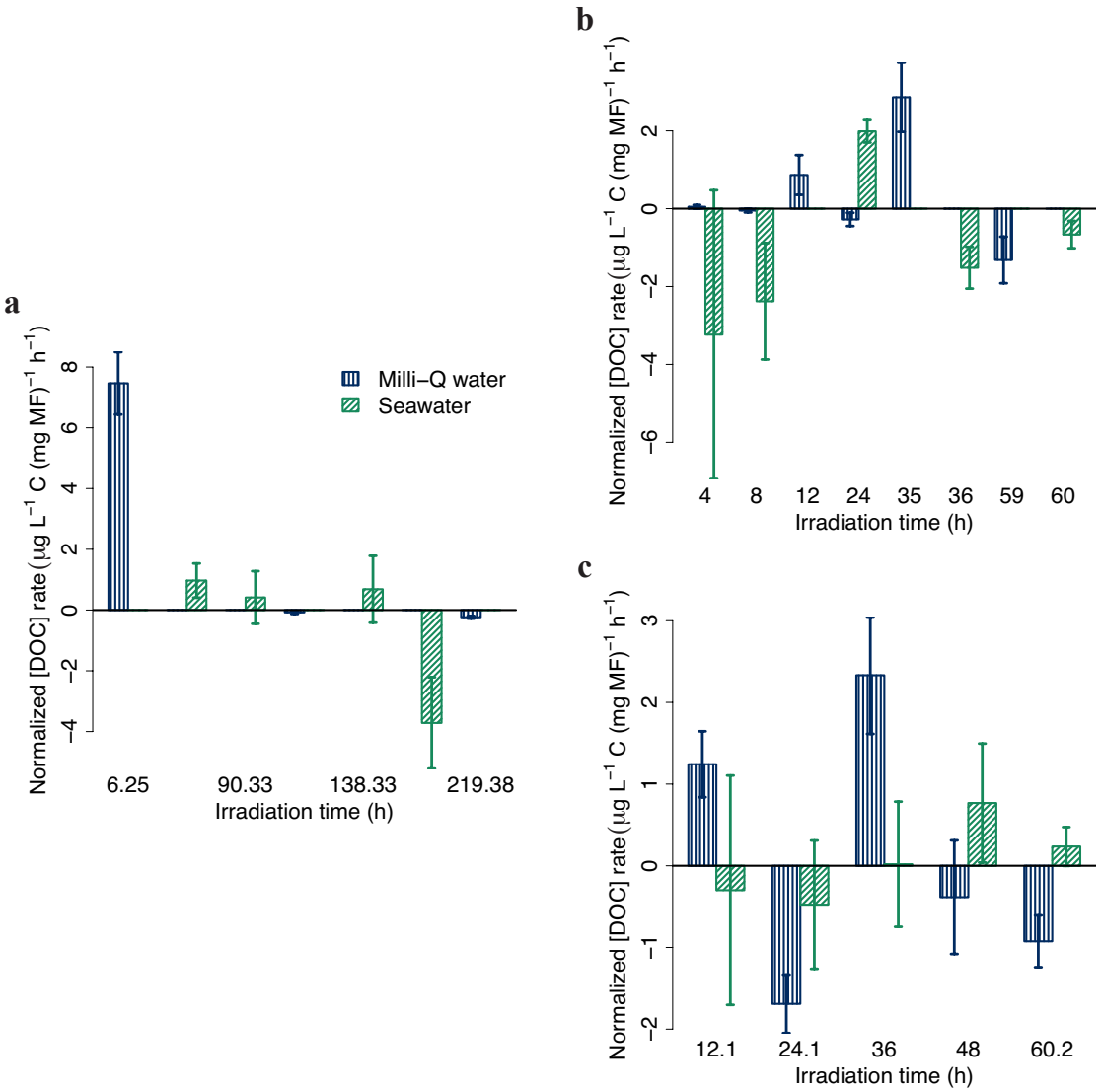

Figure 4.5. Rates of change for dissolved organic carbon (DOC) concentrations with irradiation time (h) in photoirradiation experiments (µg L^{-1} C (mg microfiber)$^{-1}$ h^{-1}). DOC concentrations (µg L^{-1} C) were normalized to initial microfiber mass (mg). Microfibers were irradiated either in Milli-Q ultrapure water or open ocean seawater from the Atlantic subtropical gyre. (a) experiment 1 and 2, (b) experiment 3, and (c) experiment 4. Note the different irradiation time among experiments. Experiment 1 and 2 used the same type of microfibers (from red polyester yarn) while experiment 3 and 4 used a different type of microfibers (from white polyester fabric). Error bars are ±1 standard error from triplicates.

Discussion

Our results suggest that it is possible that CDOM/DOC can be produced from the photodegradation of microfibers and be subsequently photodegraded, but the net change in CDOM/DOC is not straightforward (Figure 4.2, 4.3, 4.4, and 4.5). It is highly likely that a number of organic compounds were produced from the PET polymers in the microfibers, through a range of reactions including photo-hydrolysis and photo-oxidation (Fagerburg and Clauberg, 2003). Such compounds could include PET monomer ethylene terephthalate, terephthalic acid, carboxylic acids, and dicarboxylic acids (Fagerburg and Clauberg, 2003; Gewert et al., 2018; Gewert et al., 2015; Sait et al., 2021). Microplastics could also fragment during photodegradation (Gewert et al., 2015; Lambert and Wagner, 2016; Sait et al., 2021; Zhu et al., 2020b). Very small microplastic pieces or nanoplastics resulting from fragmentation may be able to pass the 0.7 μm filter we used in our study and be reported as DOC, unless they were lost as CO_2. These can all contribute to any increase in DOC concentrations with irradiation time.

An abundance of aromatic carboxylic acids could form during photodegradation of PET, as PET is an aromatic polyester and contains benzene rings in its backbone (Fagerburg and Clauberg, 2003; Gewert et al., 2015). These aromatic compounds could contribute significantly to the absorption of ultraviolet (UV) light, and lead to the potential observed increase in CDOM absorption.

Aromatic compounds could be highly photo-labile (Stubbins and Dittmar, 2015; Stubbins et al., 2010b), therefore, it is not surprising that the produced CDOM could also be photo-labile and be photodegraded following formation. The production and degradation of CDOM could happen simultaneously and create a steady state, which might explain the lack of statistical

significance in CDOM absorption change with time. In addition, photodegradation of microplastic can produce an abundance of reactive oxygen species and other radicals (Fagerburg and Clauberg, 2003; Zhu et al., 2020a), which could trigger a suite of photochemical processes and transformations, and lead to the photo-oxidation of the newly released and/or native DOC/CDOM (Mopper and Kieber, 2000a; Mopper et al., 2015).

Even though microfiber losses weren't significant in this study due to the difficulty of precise measurements, the production and subsequent degradation of CDOM/DOC reflected carbon taken away from the microfibers and represented losses in microfiber mass. The highest initial DOC photoproduction rate was 1.99 ± 0.29 μg L^{-1} C (mg microfiber)$^{-1}$ h^{-1} in seawater (Figure 4.5). This is equivalent to 0.0573 ± 0.0089 μg C (mg microfiber)$^{-1}$ h^{-1} since the mean volume of the cell was 28.8 ± 1.6 for the cells used in obtaining this rate. The mass of the microfibers added to these cells were 9.99 ± 0.04 mg and the time difference between the two time points were 16 h (this rate occurred between 8 h and 24 h of irradiation). The mass of carbon produced via DOC photoproduction is thus 9.15 ± 1.43 μg C (amount of carbon produced per microfiber mass per unit time × microfiber mass × irradiation time). Percent carbon by mass (66.7 %) in the PET polymer is estimated from the chemical formula of a generic PET in Gewert et al. (2015). Based on this percentage and the microfiber mass in the cell, the photoproduced DOC accounts for only 0.137 ± 0.021 % of the microfibers irradiated in terms of carbon mass. This is a very small portion of carbon compared to the initial mass of microfibers added to the cells.

Using the above calculated carbon percentage of photoproduced DOC and estimated sea surface microplastic mass, we can estimate an amount of DOC production from microfiber photodegradation in the ocean. One study by Enders et al. (2015) found 6 % of the microplastics

they captured in the surface Atlantic Ocean were polyester. Using this estimation, assuming only 6 % of the 2.7×10^{11} g microplastics floating at the sea surface (Eriksen et al., 2014) are polyester microfibers, about $(2.22 \pm 0.35) \times 10^{9}$ g DOC can be produced from polyester microfiber photochemistry. This is a small amount of DOC compared to the $(21.4 \pm 5.3) \times 10^{15}$ g C y^{-1} epipelagic production of biolabile DOC in the ocean. There are a few assumptions in this estimation that need to be addressed. First, this estimation is based on DOC photoproduction rates obtained from post-consumer plastic textile, essentially virgin plastics, however, microplastics found in the ocean tend to be aged through physical abrasion and photodegradation (Barnes et al., 2009). The aging of plastics could lead to increase in photodegradability (Gewert et al., 2015; Stubbins et al., 2021). Second, the calculation assumes that the microfibers stay in the sunlight region of the surface ocean, however, since polyester is denser than water, polyester microfibers can sink out of the sunlit surface ocean and subsequently cease to produce DOC photochemically. Third, the % carbon is a rough estimate based on a model chemical formula, but real-world plastics frequently have impurities and additives that could change the carbon ratio (Barnes et al., 2009).

Our results of possible DOC production from microfiber photodegradation were consistent with Zhu et al. (2020b), even though different microplastic types were used. However, there was no net accumulation of CDOM or DOC except for an increase in $[DOC]_N$ in Milli-Q water samples in experiment 1 (Figures 4.2 and 4.4). The Zhu et al. (2020b) study was longer than ours. The longest experiment we carried out was 9.1 days, which was equivalent to 12.7 July days under natural sunlight in Bermuda, whereas the Zhu et al. (2020b) study conducted 54-day and 68-day photoirradiation, which was equivalent to 54 and 68 solar days in the subtropical ocean gyre. Therefore, the microfibers in our study were exposed to photoirradiation for shorter

time. The DOC photoproduction was also very low at the beginning of the experiment (< 10 days) in Zhu et al. (2020b). It is possible that we captured the early stages of DOC/CDOM photoproduction and subsequent photodegradation that are less apparent in a 54-day or 68-day experiment. Photo-induced autoxidation can occur in PET, and as reactions proceeds, carboxylic acid end groups formed during the cleavage of PET ester bonds can further promote photooxidation (Gewert et al., 2015). More fragmentation of microfibers could also occur over time, expose more surface area, making the inside plastic material available for degradation, and further speed up microplastic photodegradation (Fahem and Yousif, 2017). Photoproducts that are vulnerable to photodegradation, such as olefins, aldehydes and ketones, can form from termination of the radical reactions (Gewert et al., 2015). Whether DOC accumulates could be influenced by the relatively proportion of the formation of these photoproducts and their simultaneous/subsequent degradation.

Nonetheless, short-term fluctuations in CDOM/DOC observed in our study can still be significant if biology were considered. DOC can serve as food for microbes nearby who can take advantage of the release immediately (Amon and Benner, 1996; Kroer, 1993; R. and E., 2017), as well as provide protection from reactive oxygen radicals (Del Vecchio and Blough, 2002); CDOM can offer a short-term protection from UV light at 280 - 400 nm (Arrigo and Brown, 1996). Any benefit provided to the microbial communities can in turn affect CDOM and DOC processing of the immediate environment and lead to more changes in organic carbon cycling downstream (Boldrini et al., 2021; Galgani et al., 2018).

Although neither was significant, the changes in $a_g(280)_N$ and $[DOC]_N$ generally tracked each other for both types of water (Figure 4.2 and 4.4). As CDOM is the light absorbing portion of DOC and thus presumably the dominant photoreactant, CDOM absorption changes likely

reflects the overall DOC changes during photoproduction and subsequent photodegradation (Coble, 2007; Mopper and Kieber, 2000a; Nelson and Siegel, 2013). Any differences between the rates of $a_g(280)_N$ and $[DOC]_N$ photoproduction and subsequent photodegradation may be attributed to the difference between CDOM and DOC. It is possible that a portion of DOC was produced from microfiber photodegradation but does not absorb light. In addition, DOC components that don't absorb light can still participate in photochemistry through indirect secondary photoreactions and photodegrade (Coble, 2007; Mopper et al., 2015).

The chemical environment of seawater might have affected the CDOM/DOC production and degradation in ways different from Milli-Q water. The rates and changes in CDOM and DOC were mostly different between samples in Milli-Q and in seawater. Seawater under solar radiation produces a variety of oxidants, such as reactive oxygen species (Heller and Croot, 2010), and these reactive species may affect microfiber photodegradation. Furthermore, we used Milli-Q water in this study because we wanted to provide baseline results in aquatic environments, but microplastic photodegradation in freshwater samples from a river or lake likely differs from that in Milli-Q water. For example, the presence of clay minerals such as kaolinite promotes the photodegradation of PET, because kaolinite facilitates production of hydroxyl radical, which in turn can promote microplastic degradation (Ding et al., 2022).

The photons absorbed by the sample were impossible to quantify in this study because absorbance of the samples with microfibers was not measured. In addition, in each cell, some microfibers floated on top, others sank to the bottom, and some very small particles may be suspended in between. Light scattering is a major concern in the cells, and the light path, light penetration and absorption might be different between duplicate cells as a result. There were also a number of small bubbles that formed in each cell. Tiny microfiber particles tend to surround

these air bubbles and form rings of concentrated particles around the bubbles. The cells were shaken and left standing for a few hours after being filled, in an attempt to reduce air bubbles. Sometimes the small bubbles coalesced to a large bubble, and then the large bubble was released by opening the cap and the cell topped off with water. However, significant amounts of small bubbles remained in almost all cells. The air bubbles could also affect the light availability for photochemistry in the cells.

The access of the microfibers to sunlight may be called into question because many of our microfibers sank to the bottom of the cells. It is worth noting that the microfibers were allowed to settle in our experiments without interference; whereas in the natural environment, a number of factors, such as capture in the sea surfaced microlayer (Song et al., 2015; Song et al., 2014), and water mixing/turbulence (Browne et al., 2010), could keep the microplastics in the surface with constant exposure to sunlight. Thompson et al. (2004) found microplastics among archived plankton samples, and they were similar types of polymers to those found in sediments. The majority of these microplastics were fibrous in morphology. The authors suggested that polymer density was not a major control of distribution.

In conclusion, it is possible that DOC and CDOM were released during microfiber photodegradation, and the DOC and CDOM produced are photolabile and can be simultaneously photodegraded. These produced DOC and CDOM can still have biological and carbon cycling impacts if microbes were there to take advantage of the production, but it is likely that there's a competition between biology and photochemistry for the produced DOC and CDOM. Marine microbes may be in better position to take advantage of the produced DOC and CDOM, as there could be short-term net productions in seawater.

Acknowledgement

This work was supported by United States National Science Foundation Chemical Oceanography grant #1635618 and the 2019 Georgia Sea Grant's Graduate Traineeship Program. The authors would like to thank Dorothea Sanders at University of Georgia Marine Extension and Georgia Sea Grant for her work on microplastic survey at the Georgia coast, Abby McCormick at Skidaway Institute of Oceanography for helping in microplastic identification using Raman microscopy. The authors would also like to thank the scientists of Bermuda Atlantic Time-series Study and the crew of the R/V Atlantic Explorer for assisting sampling of seawater.

REFERENCES

Amon, R.M.W. and Benner, R., 1996. Bacterial utilization of different size classes of dissolved organic matter. Limnology and Oceanography, 41(1): 41-51.

Andrady, A.L., 2015. Persistence of Plastic Litter in the Oceans. In: M. Bergmann, L. Gutow and M. Klages (Editors), Marine Anthropogenic Litter. Springer-Verlag Berlin, Berlin, pp. 57-72.

Arrigo, K.R. and Brown, C.W., 1996. Impact of chromophoric dissolved organic matter on UV inhibition of primary productivity in the sea. Marine Ecology Progress Series, 140(1-3): 207-216.

Arthur, C., Baker, J.E. and Bamford, H.A., 2009. Proceedings of the International Research Workshop on the Occurrence, Effects, and Fate of Microplastic Marine Debris, September 9-11, 2008, University of Washington Tacoma, Tacoma, WA, USA.

Ashton, K., Holmes, L. and Turner, A., 2010. Association of metals with plastic production pellets in the marine environment. Marine Pollution Bulletin, 60(11): 2050-2055.

Aves, A.R. et al., 2022. First evidence of microplastics in Antarctic snow. The Cryosphere, 16(6): 2127-2145.

Barnes, D.K.A., Galgani, F., Thompson, R.C. and Barlaz, M., 2009. Accumulation and fragmentation of plastic debris in global environments. Philosophical Transactions of the Royal Society B-Biological Sciences, 364(1526): 1985-1998.

Betts, K., 2008. Why small plastic particles may pose a big problem in the oceans. Environmental Science & Technology, 42(24): 8995-8995.

Bohdan, K., 2022. Estimating global marine surface microplastic abundance: systematic literature review. Science of the Total Environment, 832: 8.

Boldrini, A., Galgani, L., Consumi, M. and Loiselle, S.A., 2021. Microplastics Contamination versus Inorganic Particles: Effects on the Dynamics of Marine Dissolved Organic Matter. Environments, 8(3): 14.

Bonanno, G. and Orlando-Bonaca, M., 2018. Ten inconvenient questions about plastics in the sea. Environmental Science & Policy, 85: 146-154.

Brandes, J.A. and Sanders, D., 2019. Microplastic pollution: how bad is it and what can we do to solve it? Futurum, 3: 4-7.

Brennecke, D., Duarte, B., Paiva, F., Cacador, I. and Canning-Clode, J., 2016. Microplastics as vector for heavy metal contamination from the marine environment. Estuarine Coastal and Shelf Science, 178: 189-195.

Browne, M.A. et al., 2011. Accumulation of Microplastic on Shorelines Woldwide: Sources and Sinks. Environmental Science & Technology, 45(21): 9175-9179.

Browne, M.A., Galloway, T.S. and Thompson, R.C., 2010. Spatial Patterns of Plastic Debris along Estuarine Shorelines. Environmental Science & Technology, 44(9): 3404-3409.

Coble, P.G., 2007. Marine optical biogeochemistry: The chemistry of ocean color. Chemical Reviews, 107(2): 402-418.

Cole, M., Lindeque, P., Fileman, E., Halsband, C. and Galloway, T.S., 2015. The Impact of Polystyrene Microplastics on Feeding, Function and Fecundity in the Marine Copepod Calanus helgolandicus. Environmental Science & Technology, 49(2): 1130-1137.

Cole, M., Lindeque, P., Halsband, C. and Galloway, T.S., 2011. Microplastics as contaminants in the marine environment: A review. Marine Pollution Bulletin, 62(12): 2588-2597.

Dauvergne, P., 2018. Why is the global governance of plastic failing the oceans? Global Environmental Change-Human and Policy Dimensions, 51: 22-31.

Del Vecchio, R. and Blough, N.V., 2002. Photobleaching of chromophoric dissolved organic matter in natural waters: kinetics and modeling. Marine Chemistry, 78(4): 231-253.

Ding, L. et al., 2022. The photodegradation processes and mechanisms of polyvinyl chloride and polyethylene terephthalate microplastic in aquatic environments: Important role of clay minerals. Water Research, 208: 9.

Enders, K., Lenz, R., Stedmon, C.A. and Nielsen, T.G., 2015. Abundance, size and polymer composition of marine microplastics >= 10 mu m in the Atlantic Ocean and their modelled vertical distribution. Marine Pollution Bulletin, 100(1): 70-81.

Eriksen, M. et al., 2014. Plastic Pollution in the World's Oceans: More than 5 Trillion Plastic Pieces Weighing over 250,000 Tons Afloat at Sea. Plos One, 9(12): 15.

Fagerburg, D.R. and Clauberg, H., 2003. 18 Photodegradation of Poly(Ethylene Terephthalate) and Poly(Ethylene/1,4- Cyclohexylenedimethylene Terephthalate). In: J. Scheirs and T.E.

Long (Editors), Modern Polyesters: Chemistry and Technology of Polyesters and Copolyesters. Wiley Series in Polymer Science. John Wiley & Sons.

Fahem, R. and Yousif, E., 2017. Photo-Irradiation of Polymer Films: Review. Journal of Thin Films Research, 1(1): 17-23.

Galgani, L., Engel, A., Rossi, C., Donati, A. and Loiselle, S.A., 2018. Polystyrene microplastics increase microbial release of marine Chromophoric Dissolved Organic Matter in microcosm experiments. Scientific Reports, 8(1): 14635.

Galgani, L. and Loiselle, S.A., 2019. Plastic Accumulation in the Sea Surface Microlayer: An Experiment-Based Perspective for Future Studies. Geosciences, 9(2).

Gewert, B., Plassmann, M., Sandblom, O. and MacLeod, M., 2018. Identification of Chain Scission Products Released to Water by Plastic Exposed to Ultraviolet Light. Environmental Science & Technology Letters, 5(5): 272-276.

Gewert, B., Plassmann, M.M. and MacLeod, M., 2015. Pathways for degradation of plastic polymers floating in the marine environment. Environmental Science-Processes & Impacts, 17(9): 1513-1521.

Geyer, R., Jambeck, J.R. and Law, K.L., 2017. Production, use, and fate of all plastics ever made. Science Advances, 3(7).

Hakkarainen, M. and Albertsson, A.C., 2004. Environmental degradation of polyethylene. Long-Term Properties of Polyolefins, 169: 177-199.

Hartline, N.L. et al., 2016. Microfiber Masses Recovered from Conventional Machine Washing of New or Aged Garments. Environmental Science & Technology, 50(21): 11532-11538.

Heller, M.I. and Croot, P.L., 2010. Kinetics of superoxide reactions with dissolved organic matter in tropical Atlantic surface waters near Cape Verde (TENATSO). Journal of Geophysical Research-Oceans, 115: 13.

Hu, C.M., Muller-Karger, F.E. and Zepp, R.G., 2002. Absorbance, absorption coefficient, and apparent quantum yield: A comment on common ambiguity in the use of these optical concepts. Limnology and Oceanography, 47(4): 1261-1267.

Huang, W. et al., 2021. Microplastics and associated contaminants in the aquatic environment: A review on their ecotoxicological effects, trophic transfer, and potential impacts to human health. Journal of Hazardous Materials, 405: 124187.

Karbalaei, S., Hanachi, P., Walker, T.R. and Cole, M., 2018. Occurrence, sources, human health impacts and mitigation of microplastic pollution. Environmental Science and Pollution Research, 25(36): 36046-36063.

Kroer, N., 1993. Bacterial-growth efficiency on natural dissolved organic matter. Limnology and Oceanography, 38(6): 1282-1290.

Lambert, S. and Wagner, M., 2016. Characterisation of nanoplastics during the degradation of polystyrene. Chemosphere, 145: 265-268.

Le Guen, C. et al., 2020. Microplastic study reveals the presence of natural and synthetic fibres in the diet of King Penguins (Aptenodytes patagonicus) foraging from South Georgia. Environment International, 134: 9.

Lee, S. and Kim, S., 2021. Study on Photodegradable Water-Soluble Compounds of Expanded Polystyrene. Mass Spectrometry Letters, 12(3): 118-124.

Lithner, D., Damberg, J., Dave, G. and Larsson, A., 2009. Leachates from plastic consumer products - Screening for toxicity with Daphnia magna. Chemosphere, 74(9): 1195-1200.

Lithner, D., Larsson, A. and Dave, G., 2011. Environmental and health hazard ranking and assessment of plastic polymers based on chemical composition. Science of the Total Environment, 409(18): 3309-3324.

Mishra, S., Rath, C.C. and Das, A.P., 2019. Marine microfiber pollution: A review on present status and future challenges. Marine Pollution Bulletin, 140: 188-197.

Mopper, K. and Kieber, D.J., 2000. Marine photochemistry and its impact on carbon cycling. In: S. De Mora, S. Demers and M. Vernet (Editors), The Effects of UV Radiation in the Marine Environment. Cambridge University Press, Cambridge, UNITED KINGDOM.

Mopper, K., Kieber, D.J. and Stubbins, A., 2015. Marine Photochemistry of Organic Matter: Processes and Impacts. In: D.A. Hansell and C.A. Carlson (Editors), Biogeochemistry of Marine Dissolved Organic Matter, 2nd Edition. Academic Press Ltd-Elsevier Science Ltd, London, pp. 389-450.

Nelson, N.B. and Siegel, D.A., 2013. The Global Distribution and Dynamics of Chromophoric Dissolved Organic Matter. In: C.A. Carlson and S.J. Giovannoni (Editors), Annual Review of Marine Science, Vol 5. Annual Review of Marine Science. Annual Reviews, Palo Alto, pp. 447-476.

Ng, K.L. and Obbard, J.P., 2006. Prevalence of microplastics in Singapore's coastal marine environment. Marine Pollution Bulletin, 52(7): 761-767.

Powers, L.C., Brandes, J.A., Stubbins, A. and Miller, W.L., 2017. MoDIE: Moderate dissolved inorganic carbon ((DIC)-C-13) isotope enrichment for improved evaluation of DIC photochemical production in natural waters. Marine Chemistry, 194: 1-9.

R., F. and E., Y., 2017. Photo-Irradiation of Polymer Films: Review. Journal of Thin Films Research, 1(1): 17-23.

Ranby, B. and Lucki, J., 1980. New aspects of photodegradation and photooxidation of polystyrene. Pure and Applied Chemistry, 52(2): 295-303.

Ravandi, S.A.H. and Valizadeh, M., 2011. Properties of fibers and fabrics that contribute to human comfort. In: G. Song (Editor), Improving Comfort in Clothing. Woodhead Publishing Series in Textiles. Woodhead Publ Ltd, Cambridge, pp. 61-78.

RCoreTeam, 2021. R: A language and environment for statistical computing. The R Foundation for Statistical Computing, Vienna, Austria.

Rehse, S., Kloas, W. and Zarfl, C., 2016. Short-term exposure with high concentrations of pristine microplastic particles leads to immobilisation of Daphnia magna. Chemosphere, 153: 91-99.

Rios, L.M., Moore, C. and Jones, P.R., 2007. Persistent organic pollutants carried by Synthetic polymers in the ocean environment. Marine Pollution Bulletin, 54(8): 1230-1237.

Romera-Castillo, C., Pinto, M., Langer, T.M., Alvarez-Salgado, X.A. and Herndl, G.J., 2018. Dissolved organic carbon leaching from plastics stimulates microbial activity in the ocean. Nature Communications, 9: 7.

Ross, P.S. et al., 2021. Pervasive distribution of polyester fibres in the Arctic Ocean is driven by Atlantic inputs. Nature Communications, 12(1): 9.

Sait, S.T.L. et al., 2021. Microplastic fibres from synthetic textiles: Environmental degradation and additive chemical content. Environmental Pollution, 268: 10.

Sanders, D. and Brandes, J., 2020. Helping the Public Understand the Microplastics Issue: Integrating Citizen Science Techniques and Hands-On Education Experiences with Ongoing Microplastics Research. . Current: The Journal of Marine Education, 34(3): 1-8.

Schrank, I. et al., 2019. Effects of microplastic particles and leaching additive on the life history and morphology of Daphnia magna. Environmental Pollution, 255: 113233.

Song, Y.K., Hong, S.H., Jang, M., Han, G.M. and Shim, W.J., 2015. Occurrence and Distribution of Microplastics in the Sea Surface Microlayer in Jinhae Bay, South Korea. Archives of Environmental Contamination and Toxicology, 69(3): 279-287.

Song, Y.K. et al., 2014. Large Accumulation of Micro-sized Synthetic Polymer Particles in the Sea Surface Microlayer. Environmental Science & Technology, 48(16): 9014-9021.

Stubbins, A. and Dittmar, T., 2015. Illuminating the deep: Molecular signatures of photochemical alteration of dissolved organic matter from North Atlantic Deep Water. Marine Chemistry, 177: 318-324.

Stubbins, A., Law, C.S., Uher, G. and Upstill-Goddard, R.C., 2011. Carbon monoxide apparent quantum yields and photoproduction in the Tyne estuary. Biogeosciences, 8(3): 703-713.

Stubbins, A., Law, K.L., Munoz, S.E., Bianchi, T.S. and Zhu, L.X., 2021. Plastics in the Earth system. Science, 373(6550): 51-55.

Stubbins, A., Niggemann, J. and Dittmar, T., 2012. Photo-lability of deep ocean dissolved black carbon. Biogeosciences, 9(5): 1661-1670.

Stubbins, A. et al., 2010. Illuminated darkness: Molecular signatures of Congo River dissolved organic matter and its photochemical alteration as revealed by ultrahigh precision mass spectrometry. Limnology and Oceanography, 55(4): 1467-1477.

Talsness, C.E., Andrade, A.J.M., Kuriyama, S.N., Taylor, J.A. and vom Saal, F.S., 2009. Components of plastic: experimental studies in animals and relevance for human health. Philosophical Transactions of the Royal Society B-Biological Sciences, 364(1526): 2079-2096.

Talvitie, J., Mikola, A., Setala, O., Heinonen, M. and Koistinen, A., 2017. How well is microlitter purified from wastewater? A detailed study on the stepwise removal of microlitter in a tertiary level wastewater treatment plant. Water Research, 109: 164-172.

Thompson, R.C., Moore, C.J., vom Saal, F.S. and Swan, S.H., 2009. Plastics, the environment and human health: current consensus and future trends. Philosophical Transactions of the Royal Society B-Biological Sciences, 364(1526): 2153-2166.

Thompson, R.C. et al., 2004. Lost at sea: Where is all the plastic? Science, 304(5672): 838-838.

van Sebille, E. et al., 2015. A global inventory of small floating plastic debris. Environmental Research Letters, 10(12): 11.

Wang, Z.Q. et al., 2021. Research progresses of microplastic pollution in freshwater systems. Science of the Total Environment, 795: 11.

Wayman, C. and Niemann, H., 2021. The fate of plastic in the ocean environment - a minireview. Environmental Science-Processes & Impacts, 23(2): 16.

Zhu, K. et al., 2020a. Long-term phototransformation of microplastics under simulated sunlight irradiation in aquatic environments: Roles of reactive oxygen species. Water Research, 173: 115564.

Zhu, L.X., Zhao, S.Y., Bittar, T.B., Stubbins, M. and Li, D.J., 2020b. Photochemical dissolution of buoyant microplastics to dissolved organic carbon: Rates and microbial impacts. Journal of Hazardous Materials, 383: 10.

CHAPTER 5

CONCLUSIONS AND FUTURE DIRECTIONS

Photodegradation can be a sink of marine DOM, however, teasing out its relative importance remains difficult. The work in this dissertation examined the photodegradation rates and efficiencies of a range of DOM samples and attempted to find an alternative approach to estimate difficult-to-measure properties, such as DIC photoproduction.

In Chapter 2, we presented work comparing the rates of CDOM photobleaching, DOM photodegradation, and DIC photoproduction among humic substances amended, humic and nutrients amended and unamended samples, in order to understand the role photodegradation could play in remedying the browning effect in surface water caused by increased terrestrial DOM input. The measurement of optical properties was quick and easy, the MoDIE method produced excellent results in measuring DIC photoproduction for this site, and we determined that photoirradiation could rapidly degrade added allochthonous CDOM and DOM in the laboratory; however, the story is more complicated *in situ* in the mesocosms. Photodegradation can be an important sink based on laboratory a_g fading rates and DIC photoproduction, however, the relative importance of photodegradation remained difficult to determine. It was especially surprising that nutrient additions did not lead to any major differences in the optical properties and compounding the browning effect. Future studies to better constrain the importance of photodegradation to remove added humic substances should include DIC quantum yield experiments with *in situ* light measurements to better estimate *in situ* DIC photoproduction rates and infer DOM photodegradation rates.

For sites that do not have easily measurable DIC photoproduction, such as marine sites that have high DIC background and low DIC photoproduction, we attempted to approach the problem using DOM extraction and amendment/enrichment (Chapter 3). The experiments need to be repeated using amendment of different extract concentrations, and for a variety of locations (inshore to offshore), but the results suggested that this extract-amendment method can be effective. DOM extraction and enrichment could effectively concentrate CDOM and DOM in the samples, which in turn can increase the amount of photoproduced DIC in the sample, to a level more easily measurable by the MoDIE method. But DOM extraction and enrichment does not significantly change the CDOM fading rate or DIC photoproduction efficiencies.

We applied this extraction and amendment method to some blue ocean water samples ($a_g(325) < 0.25$ m^{-1}) from the North Atlantic Subtropical Gyre (NASG) (Table 5.1). Following the protocols in Chapter 3, we extracted DOM from the original seawater using SPE with PPL resin. The SPE-DOM was then added to a blue water matrix from the same site. The DIC photoproduction rates (P_{DIC}, μmol mol^{-1}) in the amended samples were then measured and extrapolated using either the [*DOC*] or $a_g(325)$ values. Specifically, a set of concentration factors were calculated by dividing the [*DOC*] or $a_g(325)$ values in the amended samples by those in the original blue water. The P_{DIC} values in the amended samples were then divided by these concentration factors to estimate the rates in the original blue water. We compared these extrapolated rates to those of Gulf Stream from Powers et al. (2017b). The Gulf Stream sample had initial $a_g(325)$ of 0.299 m^{-1} and P_{DIC} of 247 μmol (mol)$^{-1}$ for the first time point. If we assume a constant ratio of $a_g(325)$ to P_{DIC} and use this Gulf Stream sample as a reference point, then we should have 177 μmol (mol)$^{-1}$ and 59.9 μmol (mol)$^{-1}$ DIC photoproduction for the two NASG samples (calculate a ratio of $a_g(325)$ between the Gulf Stream sample and our sample,

and then use this ratio to extrapolate the Gulf Stream P_{DIC}). The much lower number we obtained from the amendment experiment provided us with more questions than answers: 1. Does SPE NOT extract a representative pool of DOM that is capable of DIC photoproduction in the open ocean? 2. Are DIC photoproduction rates inherently lower in blue ocean water? 3. Is color extrapolation not applicable to the open ocean?

Table 5.1. DIC photoproduction extrapolated (Extrapolated P_{DIC}, μmol mol^{-1}) from the rates in solid-phase-extract-amended North Atlantic Subtropical Gyre (NASG) water. P_{DIC}: DIC photoproduction in solid-phase-extract-amended NASG water. Concentration factors were calculated by dividing the [*DOC*] and $a_g(325)$ values in the amended samples by those in the original blue water.

Expt. No.	P_{DIC} (μmol (mol photon)$^{-1}$)	Amended samples		Original blue water		Concentration factors		Extrapolated P_{DIC} (μmol mol^{-1})	
		[*DOC*] (mg L^{-1})	$a_g(325)$ (m^{-1})	[*DOC*] (mg L^{-1})	$a_g(325)$ (m^{-1})	By DOC	By $a_g(325)$	By DOC	By $a_g(325)$
1	113	678 ± 19	2.31	65.1 ± 4.3	0.178	10	13	10.85	8.71
2	253	2143 ± 18	7.38	60.1 ± 1.2	0.060	36	123	7.08	2.06

It remains difficult to directly measure DIC photoproduction in the open ocean and thus answering these three questions will not be easy. The MoDIE method can measure DIC photoproduction in coastal sites well, however, we have failed to apply the method to directly measure rates in unamended blue ocean water. During photoirradiation experiments, a drift in δ ^{13}C signal occurs even in the dark control samples, thus producing a fake signal of DIC photoproduction (Equation 3 in Chapter 3). We have taken many measures to try to prevent this

from happening but were without success. Direct measurement of DIC photoproduction in blue water will remain challenging, and we must keep improving our analytical abilities.

There might have been photochemical production and simultaneous degradation of CDOM and DOM in our microfiber photoirradiation experiment, however, the trends were unclear and variable (Chapter 4). The non-significant results of our microfiber photoirradiation in terms of CDOM or DOM production may have been due to the difficulty in working with microfibers in our existing irradiation system. The cells were not best suited for accommodating particulate samples, and there was no uniform distribution of the microfibers to ensure that the microfibers will receive equal quantity of light. Large flat quartz flasks may be better suited for this purpose.

It is interesting that our results from the Baltic Sea humic substance amendment experiments suggested that color change, or CDOM fading, may not be a good predictor of DOM photodegradation, particularly for DIC photoproduction. Traditionally, it is assumed that CDOM fading is proportional to DOM photodegradation, as CDOM is the light absorbing portion of DOM and thus presumably the dominant photoreactant (Coble, 2007; Mopper and Kieber, 2000a; Nelson and Siegel, 2013). This assumption is also supported by increased carbon monoxide photoproduction in higher CDOM samples (Hong et al., 2014; Stubbins et al., 2011; Xie et al., 2009; Zhang et al., 2006). However, this assumption may not hold for DIC photoproduction. In Chapter 2, added humic substances reduced the CDOM fading rates, but did not affect DIC photoproduction significantly. Photons absorbed in the samples may lead to other photochemical reactions in CDOM/DOM but not complete remineralization, and DOM source could have a large impact on DIC photoproduction rates.

Results in Chapter 3 again provided support that color does not tell the whole story. Rates in EDRO- and SPE-amended samples could overestimate or approximate well the DIC photoproduction rates in unamended samples when the rates were scaled by color/CDOM (Figure 3.5a, b), but both methods significantly underestimated the DIC photoproduction rates when the rates were scaled by [*DOC*] (Figure 3.5c, d). The relationship between CDOM fading and DIC photoproduction need to be investigated further, using water samples from a range of site with differing CDOM and DOM properties.

REFERENCES

Aarnos, H., Ylostalo, P. and Vähätalo, A.V., 2012. Seasonal phototransformation of dissolved organic matter to ammonium, dissolved inorganic carbon, and labile substrates supporting bacterial biomass across the Baltic Sea. Journal of Geophysical Research-Biogeosciences, 117: 14.

Aitkenhead, J.A. and McDowell, W.H., 2000. Soil C : N ratio as a predictor of annual riverine DOC flux at local and global scales. Global Biogeochemical Cycles, 14(1): 127-138.

Amon, R.M.W. and Benner, R., 1996. Bacterial utilization of different size classes of dissolved organic matter. Limnology and Oceanography, 41(1): 41-51.

Anderson, S. et al., 2001. Indicators of UV exposure in corals and their relevance to global climate change and coral bleaching. Human and Ecological Risk Assessment, 7(5): 1271-1282.

Andersson, A. et al., 2013. Can Humic Water Discharge Counteract Eutrophication in Coastal Waters? PLOS ONE, 8(4): e61293.

Andrady, A.L., 2015. Persistence of Plastic Litter in the Oceans. In: M. Bergmann, L. Gutow and M. Klages (Editors), Marine Anthropogenic Litter. Springer-Verlag Berlin, Berlin, pp. 57-72.

Arellano, A.R., Bianchi, T.S., Hutchings, J.A., Shields, M.R. and Cui, X.Q., 2018. Differential effects of solid-phase extraction resins on the measurement of dissolved lignin-phenols and organic matter composition in natural waters. Limnology and Oceanography-Methods, 16(1): 22-34.

Arrieta, J.M. et al., 2015. Dilution limits dissolved organic carbon utilization in the deep ocean. Science, 348(6232): 331-333.

Arrigo, K.R. and Brown, C.W., 1996. Impact of chromophoric dissolved organic matter on UV inhibition of primary productivity in the sea. Marine Ecology Progress Series, 140(1-3): 207-216.

Arthur, C., Baker, J.E. and Bamford, H.A., 2009. Proceedings of the International Research Workshop on the Occurrence, Effects, and Fate of Microplastic Marine Debris, September 9-11, 2008, University of Washington Tacoma, Tacoma, WA, USA.

Ashton, K., Holmes, L. and Turner, A., 2010. Association of metals with plastic production pellets in the marine environment. Marine Pollution Bulletin, 60(11): 2050-2055.

Asmala, E., Autio, R., Kaartokallio, H., Stedmon, C.A. and Thomas, D.N., 2014a. Processing of humic-rich riverine dissolved organic matter by estuarine bacteria: effects of predegradation and inorganic nutrients. Aquatic Sciences, 76(3): 451-463.

Asmala, E., Bowers, D.G., Autio, R., Kaartokallio, H. and Thomas, D.N., 2014b. Qualitative changes of riverine dissolved organic matter at low salinities due to flocculation. Journal of Geophysical Research-Biogeosciences, 119(10): 1919-1933.

Aves, A.R. et al., 2022. First evidence of microplastics in Antarctic snow. The Cryosphere, 16(6): 2127-2145.

Barnes, D.K.A., Galgani, F., Thompson, R.C. and Barlaz, M., 2009. Accumulation and fragmentation of plastic debris in global environments. Philosophical Transactions of the Royal Society B-Biological Sciences, 364(1526): 1985-1998.

Bauer, J.E. and Bianchi, T.S., 2011. Dissolved Organic Carbon Cycling and Transformation. In: E. Wolanski and D. McLusky (Editors), Treatise on Estuarine and Coastal Science, Vol 5: Biogeochemistry. Elsevier Academic Press Inc, San Diego, pp. 7-67.

Bélanger, S. et al., 2006. Photomineralization of terrigenous dissolved organic matter in Arctic coastal waters from 1979 to 2003: Interannual variability and implications of climate change. Global Biogeochemical Cycles, 20(4): 13.

Benner, R. and Kaiser, K., 2011. Biological and photochemical transformations of amino acids and lignin phenols in riverine dissolved organic matter. Biogeochemistry, 102(1-3): 209-222.

Bertilsson, S. and Tranvik, L.J., 1998. Photochemically produced carboxylic acids as substrates for freshwater bacterioplankton. Limnology and Oceanography, 43(5): 885-895.

Betts, K., 2008. Why small plastic particles may pose a big problem in the oceans. Environmental Science & Technology, 42(24): 8995-8995.

Bittar, T.B. et al., 2016. Seasonal dynamics of dissolved, particulate and microbial components of a tidal saltmarsh-dominated estuary under contrasting levels of freshwater discharge. Estuarine Coastal and Shelf Science, 182: 72-85.

Bittar, T.B., Vieira, A.A.H., Stubbins, A. and Mopper, K., 2015. Competition between photochemical and biological degradation of dissolved organic matter from the cyanobacteria Microcystis aeruginosa. Limnology and Oceanography, 60(4): 1172-1194.

Blough, N.V. and Del Vecchio, R., 2002. Chapter 10 - Chromophoric DOM in the Coastal Environment. In: D.A. Hansell and C.A. Carlson (Editors), Biogeochemistry of Marine Dissolved Organic Matter. Academic Press, San Diego, pp. 509-546.

Blough, N.V. and Zepp, R.G., 1995. Reactive Oxygen Species in Natural Waters. In: C.S. Foote, J.S. Valentine, A. Greenberg and J.F. Liebman (Editors), Active Oxygen in Chemistry. Springer Netherlands, Dordrecht, pp. 280-333.

Bohdan, K., 2022. Estimating global marine surface microplastic abundance: systematic literature review. Science of the Total Environment, 832: 8.

Boldrini, A., Galgani, L., Consumi, M. and Loiselle, S.A., 2021. Microplastics Contamination versus Inorganic Particles: Effects on the Dynamics of Marine Dissolved Organic Matter. Environments, 8(3): 14.

Bonanno, G. and Orlando-Bonaca, M., 2018. Ten inconvenient questions about plastics in the sea. Environmental Science & Policy, 85: 146-154.

Brandes, J.A., 2009. Rapid and precise delta C-13 measurement of dissolved inorganic carbon in natural waters using liquid chromatography coupled to an isotope-ratio mass spectrometer. Limnology and Oceanography-Methods, 7: 730-739.

Brandes, J.A. and Sanders, D., 2019. Microplastic pollution: how bad is it and what can we do to solve it? Futurum, 3: 4-7.

Brennecke, D., Duarte, B., Paiva, F., Cacador, I. and Canning-Clode, J., 2016. Microplastics as vector for heavy metal contamination from the marine environment. Estuarine Coastal and Shelf Science, 178: 189-195.

Brothers, S. et al., 2014. A feedback loop links brownification and anoxia in a temperate, shallow lake. Limnology and Oceanography, 59(4): 1388-1398.

Browne, M.A. et al., 2011. Accumulation of Microplastic on Shorelines Woldwide: Sources and Sinks. Environmental Science & Technology, 45(21): 9175-9179.

Browne, M.A., Galloway, T.S. and Thompson, R.C., 2010. Spatial Patterns of Plastic Debris along Estuarine Shorelines. Environmental Science & Technology, 44(9): 3404-3409.

Budac, D. and Wan, P., 1992. PHOTODECARBOXYLATION - MECHANISM AND SYNTHETIC UTILITY. Journal of Photochemistry and Photobiology a-Chemistry, 67(2): 135-166.

Carlson, C.A. and Hansell, D.A., 2015. Chapter 3 - DOM Sources, Sinks, Reactivity, and Budgets. Biogeochemistry of Marine Dissolved Organic Matter: 65-126.

Carstensen, J. et al., 2020. Factors regulating the coastal nutrient filter in the Baltic Sea. Ambio, 49(6): 1194-1210.

Cauwet, G., 1999. Determination of dissolved organic carbon and nitrogen by high temperature combustion. In: K. Grasshoff, K. Kremling and M. Ehrhardt (Editors), Methods of Seawater Analysis. Wiley-VCH, Weinheim, pp. 407-420.

Cawley, K.M., Hakala, J.A. and Chin, Y.-P., 2009. Evaluating the triplet state photoreactivity of dissolved organic matter isolated by chromatography and ultrafiltration using an alkylphenol probe molecule. Limnology and Oceanography: Methods, 7(6): 391-398.

Chambers, L.R. et al., 2016. Enhanced Dissolved Organic Matter Recovery from Saltwater Samples with Electrodialysis. Aquatic Geochemistry, 22(5-6): 555-572.

Chen, M., Kim, S., Park, J.E., Jung, H.J. and Hur, J., 2016. Structural and compositional changes of dissolved organic matter upon solid-phase extraction tracked by multiple analytical tools. Analytical and Bioanalytical Chemistry, 408(23): 6249-6258.

Cherrier, J. and Bauer, J.E., 2004. Bacterial utilization of transient plankton-derived dissolved organic carbon and nitrogen inputs in surface ocean waters. Aquatic Microbial Ecology, 35(3): 229-241.

Chupakova, A.A., Chupakov, A.V., Neverova, N.V., Shirokova, L.S. and Pokrovsky, O.S., 2018. Photodegradation of river dissolved organic matter and trace metals in the largest European Arctic estuary. Science of the Total Environment, 622: 1343-1352.

Clark, C.D. et al., 2004. CDOM distribution and CO(2) production on the southwest Florida shelf. Marine Chemistry, 89(1-4): 145-167.

Coble, P.G., 2007. Marine optical biogeochemistry: The chemistry of ocean color. Chemical Reviews, 107(2): 402-418.

Cole, M., Lindeque, P., Fileman, E., Halsband, C. and Galloway, T.S., 2015. The Impact of Polystyrene Microplastics on Feeding, Function and Fecundity in the Marine Copepod Calanus helgolandicus. Environmental Science & Technology, 49(2): 1130-1137.

Cole, M., Lindeque, P., Halsband, C. and Galloway, T.S., 2011. Microplastics as contaminants in the marine environment: A review. Marine Pollution Bulletin, 62(12): 2588-2597.

Dalzell, B.J., Minor, E.C. and Mopper, K.M., 2009. Photodegradation of estuarine dissolved organic matter: a multi-method assessment of DOM transformation. Organic Geochemistry, 40(2): 243-257.

Dauvergne, P., 2018. Why is the global governance of plastic failing the oceans? Global Environmental Change-Human and Policy Dimensions, 51: 22-31.

de Wit, H.A. et al., 2016. Current Browning of Surface Waters Will Be Further Promoted by Wetter Climate. Environmental Science & Technology Letters, 3(12): 430-435.

Deininger, A. and Frigstad, H., 2019. Reevaluating the Role of Organic Matter Sources for Coastal Eutrophication, Oligotrophication, and Ecosystem Health. Frontiers in Marine Science, 6: 11.

Del Vecchio, R. and Blough, N.V., 2002. Photobleaching of chromophoric dissolved organic matter in natural waters: kinetics and modeling. Marine Chemistry, 78(4): 231-253.

Deutsch, B., Alling, V., Humborg, C., Korth, F. and Morth, C.M., 2012. Tracing inputs of terrestrial high molecular weight dissolved organic matter within the Baltic Sea ecosystem. Biogeosciences, 9(11): 4465-4475.

Ding, L. et al., 2022. The photodegradation processes and mechanisms of polyvinyl chloride and polyethylene terephthalate microplastic in aquatic environments: Important role of clay minerals. Water Research, 208: 9.

Dittmar, T., Koch, B., Hertkorn, N. and Kattner, G., 2008. A simple and efficient method for the solid-phase extraction of dissolved organic matter (SPE-DOM) from seawater. Limnology and Oceanography-Methods, 6: 230-235.

Enders, K., Lenz, R., Stedmon, C.A. and Nielsen, T.G., 2015. Abundance, size and polymer composition of marine microplastics >= 10 mu m in the Atlantic Ocean and their modelled vertical distribution. Marine Pollution Bulletin, 100(1): 70-81.

Eriksen, M. et al., 2014. Plastic Pollution in the World's Oceans: More than 5 Trillion Plastic Pieces Weighing over 250,000 Tons Afloat at Sea. Plos One, 9(12): 15.

Fagerburg, D.R. and Clauberg, H., 2003. 18 Photodegradation of Poly(Ethylene Terephthalate) and Poly(Ethylene/1,4- Cyclohexylenedimethylene Terephthalate). In: J. Scheirs and T.E. Long (Editors), Modern Polyesters: Chemistry and Technology of Polyesters and Copolyesters. Wiley Series in Polymer Science. John Wiley & Sons.

Fahem, R. and Yousif, E., 2017. Photo-Irradiation of Polymer Films: Review. Journal of Thin Films Research, 1(1): 17-23.

Farjalla, V.F., Amado, A.M., Suhett, A.L. and Meirelles-Pereira, F., 2009. DOC removal paradigms in highly humic aquatic ecosystems. Environmental Science and Pollution Research, 16(5): 531-538.

Feuchtmayr, H. et al., 2019. Effects of brownification and warming on algal blooms, metabolism and higher trophic levels in productive shallow lake mesocosms. Science of the Total Environment, 678: 227-238.

Fichot, C.G. and Benner, R., 2014. The fate of terrigenous dissolved organic carbon in a river-influenced ocean margin. Global Biogeochemical Cycles, 28(3): 300-318.

Fichot, C.G. and Miller, W.L., 2010. An approach to quantify depth-resolved marine photochemical fluxes using remote sensing: Application to carbon monoxide (CO) photoproduction. Remote Sensing of Environment, 114(7): 1363-1377.

Franke, D., Hamilton, M.W. and Ziegler, S.E., 2012. Variation in the photochemical lability of dissolved organic matter in a large boreal watershed. Aquatic Sciences, 74(4): 751-768.

Galgani, L., Engel, A., Rossi, C., Donati, A. and Loiselle, S.A., 2018. Polystyrene microplastics increase microbial release of marine Chromophoric Dissolved Organic Matter in microcosm experiments. Scientific Reports, 8(1): 14635.

Galgani, L. and Loiselle, S.A., 2019. Plastic Accumulation in the Sea Surface Microlayer: An Experiment-Based Perspective for Future Studies. Geosciences, 9(2).

Gewert, B., Plassmann, M., Sandblom, O. and MacLeod, M., 2018. Identification of Chain Scission Products Released to Water by Plastic Exposed to Ultraviolet Light. Environmental Science & Technology Letters, 5(5): 272-276.

Gewert, B., Plassmann, M.M. and MacLeod, M., 2015. Pathways for degradation of plastic polymers floating in the marine environment. Environmental Science-Processes & Impacts, 17(9): 1513-1521.

Geyer, R., Jambeck, J.R. and Law, K.L., 2017. Production, use, and fate of all plastics ever made. Science Advances, 3(7).

Gonsior, M. et al., 2014. Photochemical production of polyols arising from significant photo-transformation of dissolved organic matter in the oligotrophic surface ocean. Marine Chemistry, 163: 10-18.

Green, N.W. et al., 2014. An intercomparison of three methods for the large-scale isolation of oceanic dissolved organic matter. Marine Chemistry, 161: 14-19.

Hakkarainen, M. and Albertsson, A.C., 2004. Environmental degradation of polyethylene. Long-Term Properties of Polyolefins, 169: 177-199.

Hansell, D.A., 2002. DOC in the global ocean carbon cycle. In: D.A. Hansell and C.A. Carlson (Editors), Biogeochemistry of marine dissolved organic matter. Academic Press, pp. 685-716.

Hansell, D.A. and Carlson, C.A., 1998. Deep-ocean gradients in the concentration of dissolved organic carbon. Nature, 395(6699): 263-266.

Hansell, D.A., Carlson, C.A., Repeta, D.J. and Schlitzer, R., 2009a. DISSOLVED ORGANIC MATTER IN THE OCEAN A CONTROVERSY STIMULATES NEW INSIGHTS. Oceanography, 22(4): 202-211.

Hansell, D.A., Carlson, C.A., Repeta, D.J. and Schlitzer, R., 2009b. Dissolved organic matter in the ocean: a controversy stimulates new insights. Oceanography, 22(4): 202-211.

Hartline, N.L. et al., 2016. Microfiber Masses Recovered from Conventional Machine Washing of New or Aged Garments. Environmental Science & Technology, 50(21): 11532-11538.

Hedges, J.I., 1992. GLOBAL BIOGEOCHEMICAL CYCLES - PROGRESS AND PROBLEMS. Marine Chemistry, 39(1-3): 67-93.

Hedges, J.I., 2002. Why dissolved organics matter? . In: D.A. Hansell and C.A. Carlson (Editors), Biogeochemistry of marine dissolved organic matter. Academic Press, pp. 1-34.

Heller, M.I. and Croot, P.L., 2010. Kinetics of superoxide reactions with dissolved organic matter in tropical Atlantic surface waters near Cape Verde (TENATSO). Journal of Geophysical Research-Oceans, 115: 13.

Helms, J.R. et al., 2014. Loss of optical and molecular indicators of terrigenous dissolved organic matter during long-term photobleaching. Aquatic Sciences, 76(3): 353-373.

Helms, J.R. et al., 2015. Spectroscopic characterization of oceanic dissolved organic matter isolated by reverse osmosis coupled with electrodialysis. Marine Chemistry, 177: 278-287.

Helms, J.R. et al., 2013. Photochemical bleaching of oceanic dissolved organic matter and its effect on absorption spectral slope and fluorescence. Marine Chemistry, 155: 81-91.

Helms, J.R. et al., 2008. Absorption spectral slopes and slope ratios as indicators of molecular weight, source, and photobleaching of chromophoric dissolved organic matter. Limnology and Oceanography, 53(3): 955-969.

Hertkorn, N., Harir, M., Koch, B.P., Michalke, B. and Schmitt-Kopplin, P., 2013. High-field NMR spectroscopy and FTICR mass spectrometry: powerful discovery tools for the molecular level characterization of marine dissolved organic matter. Biogeosciences, 10(3): 1583-1624.

Hong, J., Xie, H.X., Guo, L.D. and Song, G.S., 2014. Carbon Monoxide Photoproduction: Implications for Photoreactivity of Arctic Permafrost-Derived Soil Dissolved Organic Matter. Environmental Science & Technology, 48(16): 9113-9121.

Hu, C., Muller-Karger, F.E. and Zepp, R.G., 2002a. Absorbance, absorption coefficient, and apparent quantum yield: A comment on common ambiguity in the use of these optical concepts. Limnology and Oceanography, 47(4): 1261-1267.

Hu, C.M., Muller-Karger, F.E. and Zepp, R.G., 2002b. Absorbance, absorption coefficient, and apparent quantum yield: A comment on common ambiguity in the use of these optical concepts. Limnology and Oceanography, 47(4): 1261-1267.

Huang, W. et al., 2021. Microplastics and associated contaminants in the aquatic environment: A review on their ecotoxicological effects, trophic transfer, and potential impacts to human health. Journal of Hazardous Materials, 405: 124187.

Johannessen, S.C. and Miller, W.L., 2001. Quantum yield for the photochemical production of dissolved inorganic carbon in seawater. Marine Chemistry, 76(4): 271-283.

Johannessen, S.C., Pena, M.A. and Quenneville, M.L., 2007. Photochemical production of carbon dioxide during a coastal phytoplankton bloom. Estuarine Coastal and Shelf Science, 73(1-2): 236-242.

Jones, R.I., 1992. THE INFLUENCE OF HUMIC SUBSTANCES ON LACUSTRINE PLANKTONIC FOOD-CHAINS. Hydrobiologia, 229: 73-91.

Karbalaei, S., Hanachi, P., Walker, T.R. and Cole, M., 2018. Occurrence, sources, human health impacts and mitigation of microplastic pollution. Environmental Science and Pollution Research, 25(36): 36046-36063.

Karlsson, J. et al., 2009. Light limitation of nutrient-poor lake ecosystems. Nature, 460(7254): 506-U80.

Koehler, B., Landelius, T., Weyhenmeyer, G.A., Machida, N. and Tranvik, L.J., 2014. Sunlight-induced carbon dioxide emissions from inland waters. Global Biogeochemical Cycles, 28(7): 696-711.

Koistinen, J., Sjöblom, M. and Spilling, K., 2020. Determining Inorganic and Organic Carbon. In: K. Spilling (Editor), Biofuels from Algae: Methods and Protocols. Springer New York, New York, NY, pp. 63-70.

Koprivnjak, J.F., Perdue, E.M. and Pfromm, P.H., 2006. Coupling reverse osmosis with electrodialysis to isolate natural organic matter from fresh waters. Water Research, 40(18): 3385-3392.

Koprivnjak, J.F. et al., 2009. Chemical and spectroscopic characterization of marine dissolved organic matter isolated using coupled reverse osmosis-electrodialysis. Geochimica Et Cosmochimica Acta, 73(14): 4215-4231.

Kowalczuk, P., Olszewski, J., Darecki, M. and Kaczmarek, S., 2005. Empirical relationships between coloured dissolved organic matter (CDOM) absorption and apparent optical properties in Baltic Sea waters. International Journal of Remote Sensing, 26(2): 345-370.

Kritzberg, E.S. et al., 2014. Warming and browning of lakes: consequences for pelagic carbon metabolism and sediment delivery. Freshwater Biology, 59(2): 325-336.

Kroer, N., 1993. Bacterial-growth efficiency on natural dissolved organic matter. Limnology and Oceanography, 38(6): 1282-1290.

Krogh, A., 1934. Conditions of Life in the Ocean. Ecological Monographs, 4(4): 421-429.

Kullenberg, G., 1981. Chapter 3 Physical Oceanography. In: A. Voipio (Editor), Elsevier Oceanography Series. Elsevier, pp. 135-181.

Lalonde, K., Vähätalo, A.V. and Gelinas, Y., 2014. Revisiting the disappearance of terrestrial dissolved organic matter in the ocean: a delta C-13 study. Biogeosciences, 11(13): 3707-3719.

Lambert, S. and Wagner, M., 2016. Characterisation of nanoplastics during the degradation of polystyrene. Chemosphere, 145: 265-268.

Lauerwald, R., Hartmann, J., Ludwig, W. and Moosdorf, N., 2012. Assessing the nonconservative fluvial fluxes of dissolved organic carbon in North America. Journal of Geophysical Research-Biogeosciences, 117: 19.

Le Guen, C. et al., 2020. Microplastic study reveals the presence of natural and synthetic fibres in the diet of King Penguins (Aptenodytes patagonicus) foraging from South Georgia. Environment International, 134: 9.

Lee, S. and Kim, S., 2021. Study on Photodegradable Water-Soluble Compounds of Expanded Polystyrene. Mass Spectrometry Letters, 12(3): 118-124.

Lithner, D., Damberg, J., Dave, G. and Larsson, A., 2009. Leachates from plastic consumer products - Screening for toxicity with Daphnia magna. Chemosphere, 74(9): 1195-1200.

Lithner, D., Larsson, A. and Dave, G., 2011. Environmental and health hazard ranking and assessment of plastic polymers based on chemical composition. Science of the Total Environment, 409(18): 3309-3324.

Lu, C.J. et al., 2016. Sources and Transformations of Dissolved Lignin Phenols and Chromophoric Dissolved Organic Matter in Otsuchi Bay, Japan. Frontiers in Marine Science, 3.

Massicotte, P., Asmala, E., Stedmon, C. and Markager, S., 2017. Global distribution of dissolved organic matter along the aquatic continuum: Across rivers, lakes and oceans. Science of the Total Environment, 609: 180-191.

Mayorga, E. et al., 2010. Global Nutrient Export from WaterSheds 2 (NEWS 2): Model development and implementation. Environmental Modelling & Software, 25(7): 837-853.

Miller, W.L. and Moran, M.A., 1997. Interaction of photochemical and microbial processes in the degradation of refractory dissolved organic matter from a coastal marine environment. Limnology and Oceanography, 42(6): 1317-1324.

Miller, W.L., Moran, M.A., Sheldon, W.M., Zepp, R.G. and Opsahl, S., 2002. Determination of apparent quantum yield spectra for the formation of biologically labile photoproducts. Limnology and Oceanography, 47(2): 343-352.

Miller, W.L. and Zepp, R.G., 1995. Photochemical production of dissolved inorganic carbon from terrestrial organic matter: significance to the oceanic organic carbon cycle Geophysical Research Letters, 22(4): 417-420.

Minor, E.C., Dalzell, B.L., Stubbins, A. and Mopper, K., 2007. Evaluating the photoalteration of estuarine dissolved organic matter using direct temperature-resolved mass spectrometry and UV-visible spectroscopy. Aquatic Sciences, 69(4): 440-455.

Minor, E.C., Pothen, J., Dalzell, B.J., Abdulla, H. and Mopper, K., 2006. Effects of salinity changes on the photodegradation and ultraviolet-visible absorbance of terrestrial dissolved organic matter. Limnology and Oceanography, 51(5): 2181-2186.

Mishra, S., Rath, C.C. and Das, A.P., 2019. Marine microfiber pollution: A review on present status and future challenges. Marine Pollution Bulletin, 140: 188-197.

Monteith, D.T. et al., 2007. Dissolved organic carbon trends resulting from changes in atmospheric deposition chemistry. Nature, 450(7169): 537-U9.

Moody, C.S. and Worrall, F., 2017. Modeling rates of DOC degradation using DOM composition and hydroclimatic variables. Journal of Geophysical Research: Biogeosciences, 122(5): 1175-1191.

Mopper, K. and Kieber, D.J., 2000a. Marine photochemistry and its impact on carbon cycling. In: S. De Mora, S. Demers and M. Vernet (Editors), The Effects of UV Radiation in the Marine Environment. Cambridge University Press, Cambridge, UNITED KINGDOM.

Mopper, K. and Kieber, D.J., 2000b. Marine photochemistry and its impact on carbon cycling. In: M. Vernet, S. Demers and S. De Mora (Editors), The Effects of UV Radiation in the Marine Environment. Cambridge Environmental Chemistry Series. Cambridge University Press, Cambridge, pp. 101-129.

Mopper, K. and Kieber, D.J., 2002a. Chapter 9 - Photochemistry and the Cycling of Carbon, Sulfur, Nitrogen and Phosphorus. In: D.A. Hansell and C.A. Carlson (Editors), Biogeochemistry of Marine Dissolved Organic Matter. Academic Press, San Diego, pp. 455-507.

Mopper, K. and Kieber, D.J., 2002b. Chapter 9 - Photochemistry and the Cycling of Carbon, Sulfur, Nitrogen and Phosphorus. Biogeochemistry of Marine Dissolved Organic Matter: 455-507.

Mopper, K., Kieber, D.J. and Stubbins, A., 2015. Marine Photochemistry of Organic Matter: Processes and Impacts. In: D.A. Hansell and C.A. Carlson (Editors), Biogeochemistry of Marine Dissolved Organic Matter, 2nd Edition. Academic Press Ltd-Elsevier Science Ltd, London, pp. 389-450.

Mopper, K., Stubbins, A., Ritchie, J.D., Bialk, H.M. and Hatcher, P.G., 2007. Advanced instrumental approaches for characterization of marine dissolved organic matter: Extraction techniques, mass spectrometry, and nuclear magnetic resonance spectroscopy. Chemical Reviews, 107(2): 419-442.

Mopper, K. et al., 1991. Photochemical degradation of dissolved organic carbon and its impact on the oceanic carbon cycle. Nature, 353(6339): 60-62.

Moran, M.A., Sheldon, W.M. and Sheldon, J.E., 1999. Biodegradation of riverine dissolved organic carbon in five estuaries of the southeastern United States. Estuaries, 22(1): 55-64.

Moran, M.A., Sheldon, W.M. and Zepp, R.G., 2000. Carbon loss and optical property changes during long-term photochemical and biological degradation of estuarine dissolved organic matter. Limnology and Oceanography, 45(6): 1254-1264.

Nelson, N.B., Carlson, C.A. and Steinberg, D.K., 2004. Production of chromophoric dissolved organic matter by Sargasso Sea microbes. Marine Chemistry, 89(1): 273-287.

Nelson, N.B. and Siegel, D.A., 2013. The Global Distribution and Dynamics of Chromophoric Dissolved Organic Matter. In: C.A. Carlson and S.J. Giovannoni (Editors), Annual Review of Marine Science, Vol 5. Annual Review of Marine Science. Annual Reviews, Palo Alto, pp. 447-476.

Ng, K.L. and Obbard, J.P., 2006. Prevalence of microplastics in Singapore's coastal marine environment. Marine Pollution Bulletin, 52(7): 761-767.

O'Sullivan, D.W., Neale, P.J., Coffin, R.B., Boyd, T.J. and Osburn, S.L., 2005. Photochemical production of hydrogen peroxide and methylhydroperoxide in coastal waters. Marine Chemistry, 97(1-2): 14-33.

Obernosterer, I. and Benner, R., 2004. Competition between biological and photochemical processes in the mineralization of dissolved organic carbon. Limnology and Oceanography, 49(1): 117-124.

Opsahl, S.P. and Zepp, R.G., 2001. Photochemically-induced alteration of stable carbon isotope ratios (delta C-13) in terrigenous dissolved organic carbon. Geophysical Research Letters, 28(12): 2417-2420.

Osburn, C.L. and Bianchi, T.S., 2016. Editorial: Linking Optical and Chemical Properties of Dissolved Organic Matter in Natural Waters. Frontiers in Marine Science, 3: 3.

Osburn, C.L., Retamal, L. and Vincent, W.F., 2009. Photoreactivity of chromophoric dissolved organic matter transported by the Mackenzie River to the Beaufort Sea. Marine Chemistry, 115(1-2): 10-20.

Pinsonneault, A.J. et al., 2020. Dissolved organic carbon sorption dynamics in tidal marsh soils. Limnology and Oceanography: 12.

Powers, L.C., Brandes, J.A., Miller, W.L. and Stubbins, A., 2017a. Using liquid chromatography-isotope ratio mass spectrometry to measure the delta C-13 of dissolved inorganic carbon photochemically produced from dissolved organic carbon. Limnology and Oceanography-Methods, 15(1): 103-115.

Powers, L.C., Brandes, J.A., Stubbins, A. and Miller, W.L., 2017b. MoDIE: Moderate dissolved inorganic carbon ((DIC)-C-13) isotope enrichment for improved evaluation of DIC photochemical production in natural waters. Marine Chemistry, 194: 1-9.

Powers, L.C. and Miller, W.L., 2015a. Hydrogen peroxide and superoxide photoproduction in diverse marine waters: A simple proxy for estimating direct CO2 photochemical fluxes. Geophysical Research Letters, 42(18): 7696-7704.

Powers, L.C. and Miller, W.L., 2015b. Photochemical production of CO and CO2 in the Northern Gulf of Mexico: Estimates and challenges for quantifying the impact of photochemistry on carbon cycles. Marine Chemistry, 171: 21-35.

Qian, J.G., Mopper, K. and Kieber, D.J., 2001. Photochemical production of the hydroxyl radical in Antarctic waters. Deep-Sea Research Part I-Oceanographic Research Papers, 48(3): 741-759.

R., F. and E., Y., 2017. Photo-Irradiation of Polymer Films: Review. Journal of Thin Films Research, 1(1): 17-23.

Ranby, B. and Lucki, J., 1980. New aspects of photodegradation and photooxidation of polystyrene. Pure and Applied Chemistry, 52(2): 295-303.

Ravandi, S.A.H. and Valizadeh, M., 2011. Properties of fibers and fabrics that contribute to human comfort. In: G. Song (Editor), Improving Comfort in Clothing. Woodhead Publishing Series in Textiles. Woodhead Publ Ltd, Cambridge, pp. 61-78.

RCoreTeam, 2021. R: A language and environment for statistical computing. The R Foundation for Statistical Computing, Vienna, Austria.

Reader, H.E. and Miller, W.L., 2012. Variability of carbon monoxide and carbon dioxide apparent quantum yield spectra in three coastal estuaries of the South Atlantic Bight. Biogeosciences, 9(11): 4279-4294.

Rehse, S., Kloas, W. and Zarfl, C., 2016. Short-term exposure with high concentrations of pristine microplastic particles leads to immobilisation of Daphnia magna. Chemosphere, 153: 91-99.

Repeta, D.J., 2015. Chemical characterization and cycling of dissolved organic matter. In: D.A. Hansell and C.A. Carlson (Editors), Biogeochemistry of marine dissolved organic matter. Academic Press.

Ridgwell, A. and Arndt, S., 2015. Why dissolved organics matter: DOC in ancient oceans and past climate change. In: D.A. Hansell and C.A. Carlson (Editors), Biogeochemistry of marine dissolved organic matter. Academic Press.

Rios, L.M., Moore, C. and Jones, P.R., 2007. Persistent organic pollutants carried by Synthetic polymers in the ocean environment. Marine Pollution Bulletin, 54(8): 1230-1237.

Ritz, C. and Streibig, J.C., 2008. Nonlinear Regression with R. Use R! Springer, 144 pp.

Rolff, C. and Elmgren, R., 2000. Use of riverine organic matter in plankton food webs of the Baltic Sea. Marine Ecology Progress Series, 197: 81-101.

Romera-Castillo, C., Pinto, M., Langer, T.M., Alvarez-Salgado, X.A. and Herndl, G.J., 2018. Dissolved organic carbon leaching from plastics stimulates microbial activity in the ocean. Nature Communications, 9: 7.

Ross, P.S. et al., 2021. Pervasive distribution of polyester fibres in the Arctic Ocean is driven by Atlantic inputs. Nature Communications, 12(1): 9.

Ruggaber, A., Dlugi, R. and Nakajima, T., 1994. MODELING RADIATION QUANTITIES AND PHOTOLYSIS FREQUENCIES IN THE TROPOSPHERE. Journal of Atmospheric Chemistry, 18(2): 171-210.

Sait, S.T.L. et al., 2021. Microplastic fibres from synthetic textiles: Environmental degradation and additive chemical content. Environmental Pollution, 268: 10.

Sanders, D. and Brandes, J., 2020. Helping the Public Understand the Microplastics Issue: Integrating Citizen Science Techniques and Hands-On Education Experiences with Ongoing Microplastics Research. . Current: The Journal of Marine Education, 34(3): 1-8.

Sankar, M.S. et al., 2019. Effect of photo-biodegradation and biodegradation on the biogeochemical cycling of dissolved organic matter across diverse surface water bodies. Journal of Environmental Sciences, 77: 130-147.

Santonja, M., Minguez, L., Gessner, M.O. and Sperfeld, E., 2017. Predator-prey interactions in a changing world: humic stress disrupts predator threat evasion in copepods. Oecologia, 183(3): 887-898.

Santos, L., Santos, E.B.H., Dias, J.M., Cunha, A. and Almeida, A., 2014. Photochemical and microbial alterations of DOM spectroscopic properties in the estuarine system Ria de Aveiro. Photochemical & Photobiological Sciences, 13(8): 1146-1159.

Scharnweber, K. et al., 2021. Comprehensive analysis of chemical and biological problems associated with browning agents used in aquatic studies. bioRxiv: 2021.02.26.433092.

Schrank, I. et al., 2019. Effects of microplastic particles and leaching additive on the life history and morphology of Daphnia magna. Environmental Pollution, 255: 113233.

Seidel, M. et al., 2017. Composition and Transformation of Dissolved Organic Matter in the Baltic Sea. Frontiers in Earth Science, 5(31).

Sholkovitz, E.R., 1976. FLOCCULATION OF DISSOLVED ORGANIC AND INORGANIC MATTER DURING MIXING OF RIVER WATER AND SEAWATER. Geochimica Et Cosmochimica Acta, 40(7): 831-845.

Siegel, D.A., Maritorena, S., Nelson, N.B., Behrenfeld, M.J. and McClain, C.R., 2005. Colored dissolved organic matter and its influence on the satellite-based characterization of the ocean biosphere. Geophysical Research Letters, 32(20): 4.

Siegel, D.A., Maritorena, S., Nelson, N.B., Hansell, D.A. and Lorenzi-Kayser, M., 2002. Global distribution and dynamics of colored dissolved and detrital organic materials. Journal of Geophysical Research-Oceans, 107(C12).

Song, Y.K., Hong, S.H., Jang, M., Han, G.M. and Shim, W.J., 2015. Occurrence and Distribution of Microplastics in the Sea Surface Microlayer in Jinhae Bay, South Korea. Archives of Environmental Contamination and Toxicology, 69(3): 279-287.

Song, Y.K. et al., 2014. Large Accumulation of Micro-sized Synthetic Polymer Particles in the Sea Surface Microlayer. Environmental Science & Technology, 48(16): 9014-9021.

Stedmon, C.A. and Nelson, N.B., 2015. Chapter 10: The Optical Properties of DOM in the Ocean. Biogeochemistry of Marine Dissolved Organic Matter: 481-508.

Stubbins, A. and Dittmar, T., 2012. Low volume quantification of dissolved organic carbon and dissolved nitrogen. Limnology and Oceanography-Methods, 10: 347-352.

Stubbins, A. and Dittmar, T., 2015. Illuminating the deep: Molecular signatures of photochemical alteration of dissolved organic matter from North Atlantic Deep Water. Marine Chemistry, 177: 318-324.

Stubbins, A., Law, C.S., Uher, G. and Upstill-Goddard, R.C., 2011. Carbon monoxide apparent quantum yields and photoproduction in the Tyne estuary. Biogeosciences, 8(3): 703-713.

Stubbins, A., Law, K.L., Munoz, S.E., Bianchi, T.S. and Zhu, L.X., 2021. Plastics in the Earth system. Science, 373(6550): 51-55.

Stubbins, A., Niggemann, J. and Dittmar, T., 2012. Photo-lability of deep ocean dissolved black carbon. Biogeosciences, 9(5): 1661-1670.

Stubbins, A. et al., 2010a. Illuminated darkness: Molecular signatures of Congo River dissolved organic matter and its photochemical alteration as revealed by ultrahigh precision mass spectrometry. Limnology and Oceanography, 55(4): 1467-1477.

Stubbins, A. et al., 2010b. Illuminated darkness: Molecular signatures of Congo River dissolved organic matter and its photochemical alteration as revealed by ultrahigh precision mass spectrometry. Limnology and Oceanography, 55(4): 1467-1477.

Stubbins, A. et al., 2006. Open-ocean carbon monoxide photoproduction. Deep-Sea Research Part Ii-Topical Studies in Oceanography, 53(14-16): 1695-1705.

Talsness, C.E., Andrade, A.J.M., Kuriyama, S.N., Taylor, J.A. and vom Saal, F.S., 2009. Components of plastic: experimental studies in animals and relevance for human health. Philosophical Transactions of the Royal Society B-Biological Sciences, 364(1526): 2079-2096.

Talvitie, J., Mikola, A., Setala, O., Heinonen, M. and Koistinen, A., 2017. How well is microlitter purified from wastewater? A detailed study on the stepwise removal of microlitter in a tertiary level wastewater treatment plant. Water Research, 109: 164-172.

Tfaily, M.M., Hodgkins, S., Podgorski, D.C., Chanton, J.P. and Cooper, W.T., 2012. Comparison of dialysis and solid-phase extraction for isolation and concentration of dissolved organic matter prior to Fourier transform ion cyclotron resonance mass spectrometry. Analytical and Bioanalytical Chemistry, 404(2): 447-457.

Thomas, H., Pempkowiak, J., Wulff, F. and Nagel, K., 2010. The Baltic Sea. In: K.-K. Liu, L. Atkinson, R.Q. ones and L. Talaue-McManus (Editors), Carbon and Nutrient Fluxes in Continental Margins: a Global Synthesis. Springer, pp. 1-741.

Thompson, R.C., Moore, C.J., vom Saal, F.S. and Swan, S.H., 2009. Plastics, the environment and human health: current consensus and future trends. Philosophical Transactions of the Royal Society B-Biological Sciences, 364(1526): 2153-2166.

Thompson, R.C. et al., 2004. Lost at sea: Where is all the plastic? Science, 304(5672): 838-838.

Tranvik, L.J. et al., 2009. Lakes and reservoirs as regulators of carbon cycling and climate. Limnology and Oceanography, 54(6): 2298-2314.

Urrutia-Cordero, P. et al., 2017. Phytoplankton diversity loss along a gradient of future warming and brownification in freshwater mesocosms. Freshwater Biology, 62(11): 1869-1878.

Vähätalo, A.V. and Wetzel, R.G., 2008. Long-term photochemical and microbial decomposition of wetland-derived dissolved organic matter with alteration of C-13 : C-12 mass ratio. Limnology and Oceanography, 53(4): 1387-1392.

van Sebille, E. et al., 2015. A global inventory of small floating plastic debris. Environmental Research Letters, 10(12): 11.

Vasconcelos, F.R., Diehl, S., Rodriguez, P., Karlsson, J. and Bystrom, P., 2018. Effects of Terrestrial Organic Matter on Aquatic Primary Production as Mediated by Pelagic-Benthic Resource Fluxes. Ecosystems, 21(6): 1255-1268.

Vetter, T.A., Perdue, E.M., Ingall, E., Koprivnjak, J.F. and Pfromm, P.H., 2007. Combining reverse osmosis and electrodialysis for more complete recovery of dissolved organic matter from seawater. Separation and Purification Technology, 56(3): 383-387.

Vione, D., 2016. Photochemical Reactions in Sunlit Surface Waters. In: G. Bergamini and S. Silvi (Editors), Applied Photochemistry-When Light Meets Molecules, pp. 343-376.

Wagner, S. et al., 2020. Soothsaying DOM: A Current Perspective on the Future of Oceanic Dissolved Organic Carbon. Frontiers in Marine Science, 7: 17.

Wang, Z.Q. et al., 2021. Research progresses of microplastic pollution in freshwater systems. Science of the Total Environment, 795: 11.

Wayman, C. and Niemann, H., 2021. The fate of plastic in the ocean environment - a minireview. Environmental Science-Processes & Impacts, 23(2): 16.

Weishaar, J.L. et al., 2003. Evaluation of specific ultraviolet absorbance as an indicator of the chemical composition and reactivity of dissolved organic carbon. Environmental Science & Technology, 37(20): 4702-4708.

White, E.M., Kieber, D.J. and Mopper, K., 2008. Determination of photochemically produced carbon dioxide in seawater. Limnology and Oceanography-Methods, 6: 441-453.

White, E.M., Kieber, D.J., Sherrard, J., Miller, W.L. and Mopper, K., 2010. Carbon dioxide and carbon monoxide photoproduction quantum yields in the Delaware Estuary. Marine Chemistry, 118(1-2): 11-21.

Williams, P.M. and Druffel, E.R.M., 1987. Radiocarbon in dissolved organic matter in the central North Pacific Ocean. Nature, 330(6145): 246-248.

Wünsch, U.J. et al., 2018. Quantifying the impact of solid-phase extraction on chromophoric dissolved organic matter composition. Marine Chemistry, 207: 33-41.

Xie, H., Belanger, S., Demers, S., Vincent, W.F. and Papakyriakou, T.N., 2009. Photobiogeochemical cycling of carbon monoxide in the southeastern Beaufort Sea in spring and autumn. Limnology and Oceanography, 54(1): 234-249.

Xie, H.X., Zafiriou, O.C., Cai, W.J., Zepp, R.G. and Wang, Y.C., 2004. Photooxidation and its effects on the carboxyl content of dissolved organic matter in two coastal rivers in the Southeastern United States. Environmental Science & Technology, 38(15): 4113-4119.

Yang, L., Zhang, J. and Yang, G.P., 2021. Mixing behavior, biological and photolytic degradation of dissolved organic matter in the East China Sea and the Yellow Sea. Science of the Total Environment, 762: 19.

Young, C.L. and Ingall, E.D., 2010. Marine Dissolved Organic Phosphorus Composition: Insights from Samples Recovered Using Combined Electrodialysis/Reverse Osmosis. Aquatic Geochemistry, 16(4): 563-574.

Zafiriou, O.C., Andrews, S.S. and Wang, W., 2003. Concordant estimates of oceanic carbon monoxide source and sink processes in the Pacific yield a balanced global "blue-water" CO budget. Global Biogeochemical Cycles, 17(1).

Zepp, R.G., Erickson, D.J., Paul, N.D. and Sulzberger, B., 2011. Effects of solar UV radiation and climate change on biogeochemical cycling: interactions and feedbacks. Photochemical & Photobiological Sciences, 10(2): 261-279.

Zhang, Y., Xie, H. and Chen, G., 2006. Factors affecting the efficiency of carbon monoxide photoproduction in the St. Lawrence estuarine system (Canada). Environmental Science & Technology, 40(24): 7771-7777.

Zhu, K. et al., 2020a. Long-term phototransformation of microplastics under simulated sunlight irradiation in aquatic environments: Roles of reactive oxygen species. Water Research, 173: 115564.

Zhu, L.X., Zhao, S.Y., Bittar, T.B., Stubbins, M. and Li, D.J., 2020b. Photochemical dissolution of buoyant microplastics to dissolved organic carbon: Rates and microbial impacts. Journal of Hazardous Materials, 383: 10.

Ziolkowski, L.A. and Miller, W.L., 2007. Variability of the apparent quantum efficiency of CO photoproduction in the Gulf of Maine and Northwest Atlantic. Marine Chemistry, 105(3-4): 258-270.

APPENDIX A. SUPPLEMENTAL FIGURES FOR CHAPTER 2

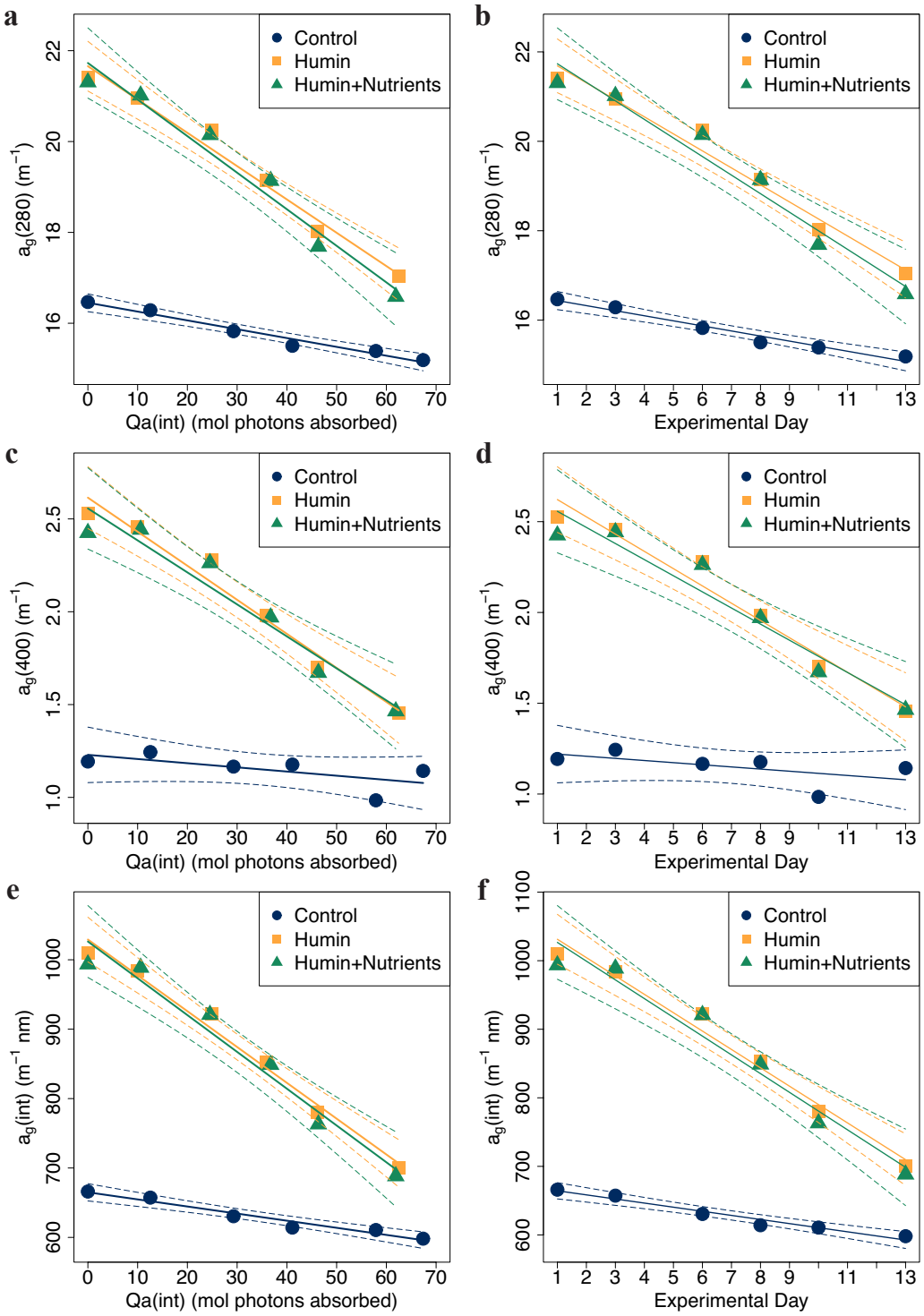

Figure S2.1. Chromophoric dissolved organic matter absorption coefficient a), c), e) versus photon doses (Q_a(int), mol photons absorbed), and b), d), f) versus time (day), for JOMEX amendment experiment samples that reflect the *in situ* conditions, a) b) at 280 nm, a_g(280), m^{-1}; c) d) at 400 nm, a_g(400), m^{-1}; e) f) integrated from 280 nm to 400 nm a_g(int), m^{-1} nm. Samples were taken right after the initial amendment (day 1), and around the same time in subsequent days. Solid lines with corresponding colors are linear regression lines for each group, and dashed lines are 95 % confidence bands for the slopes of the regression lines.

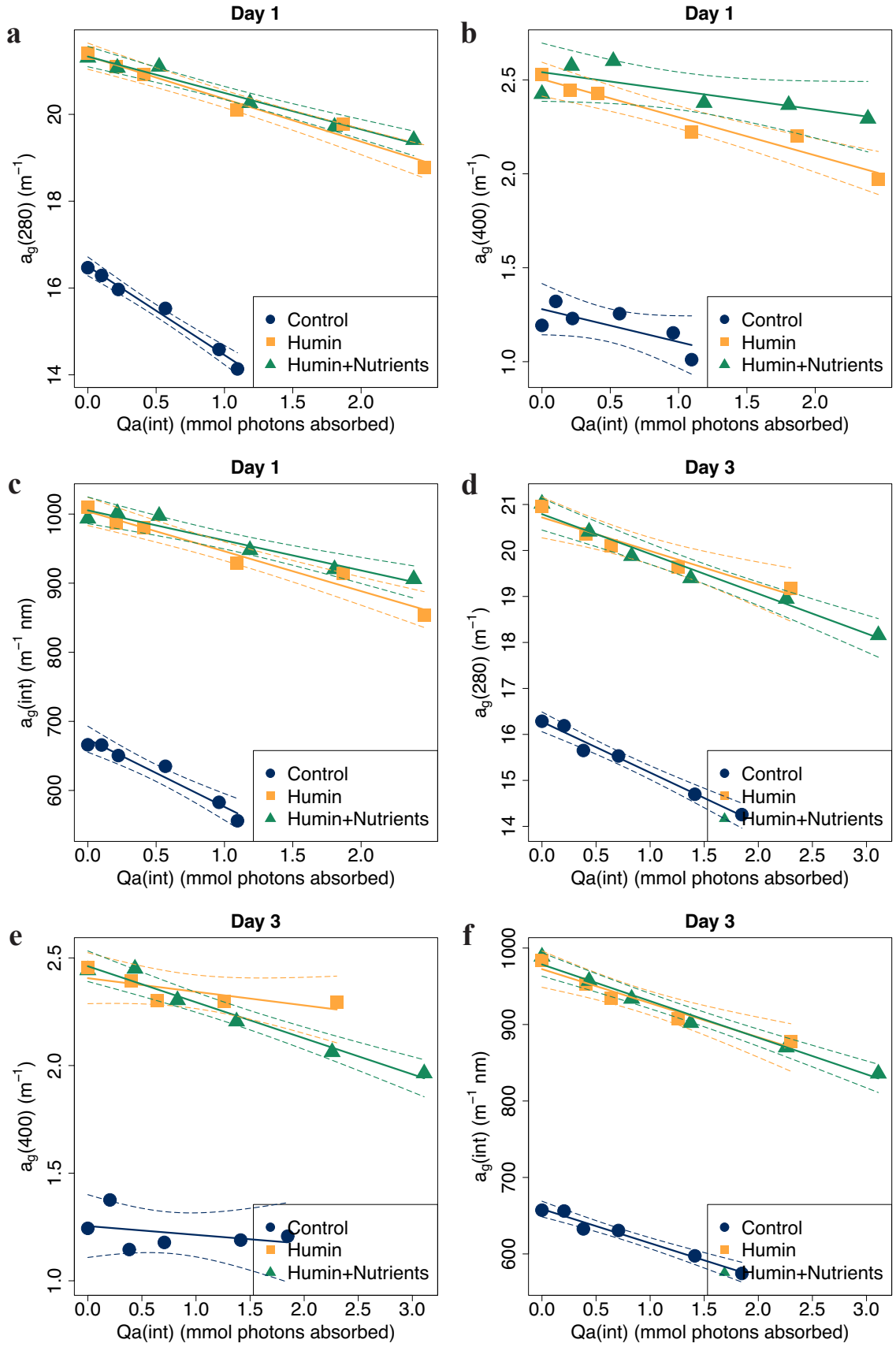
a
Day 1
$a_g(280)$ (m^{-1})
Qa(int) (mmol photons absorbed)
b
Day 1
$a_g(400)$ (m^{-1})
Qa(int) (mmol photons absorbed)
c
Day 1
$a_g(int)$ (m^{-1} nm)
Qa(int) (mmol photons absorbed)
d
Day 3
$a_g(280)$ (m^{-1})
Qa(int) (mmol photons absorbed)
e
Day 3
$a_g(400)$ (m^{-1})
Qa(int) (mmol photons absorbed)
f
Day 3
$a_g(int)$ (m^{-1} nm)
Qa(int) (mmol photons absorbed)
Control
Humin
Humin+Nutrients

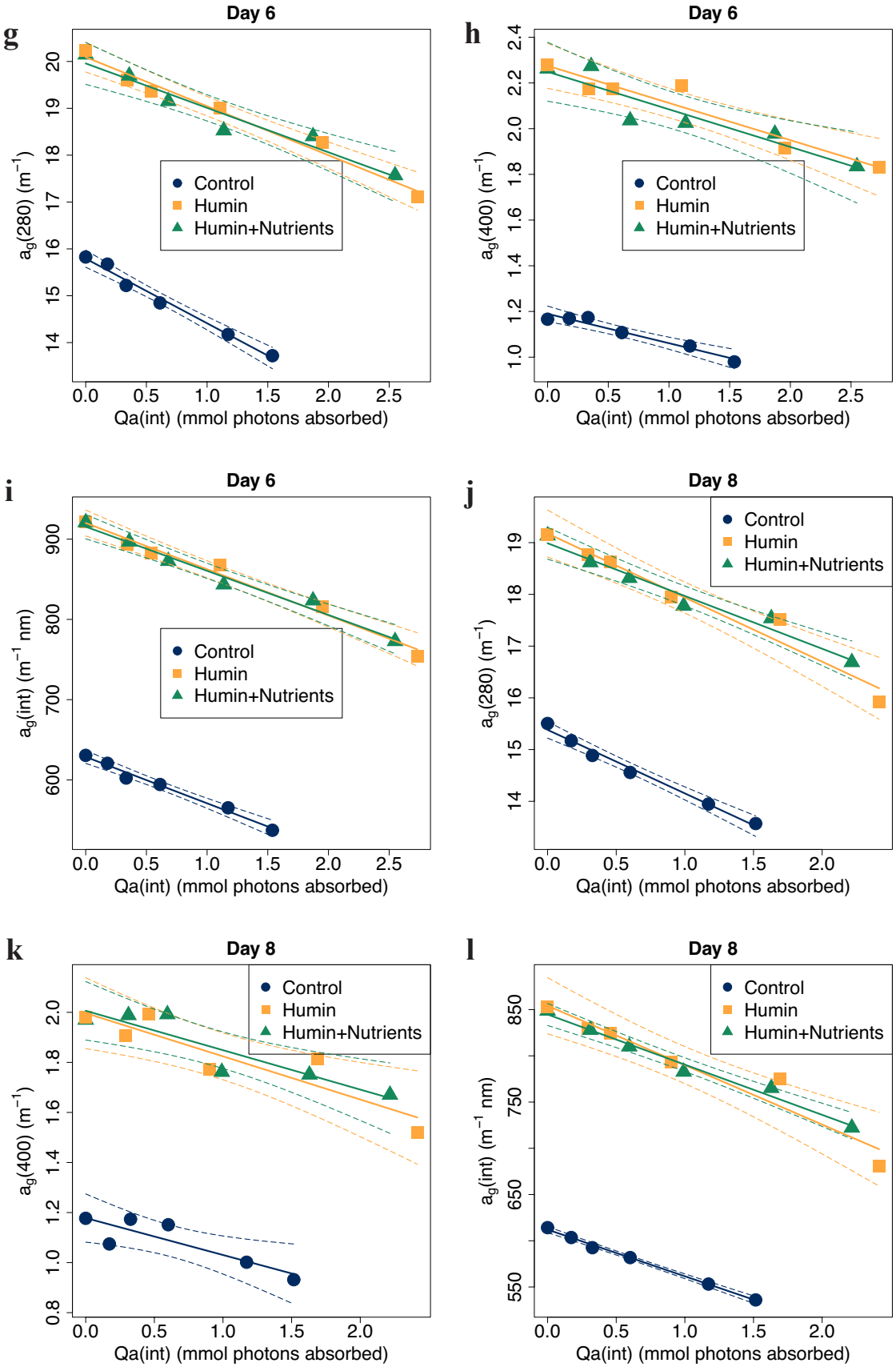
g
Day 6
Control
Humin
Humin+Nutrients
$a_g(280)$ (m^{-1})
Qa(int) (mmol photons absorbed)
h
Day 6
$a_g(400)$ (m^{-1})
i
Day 6
a_g(int) (m^{-1} nm)
j
Day 8
k
Day 8
l
Day 8

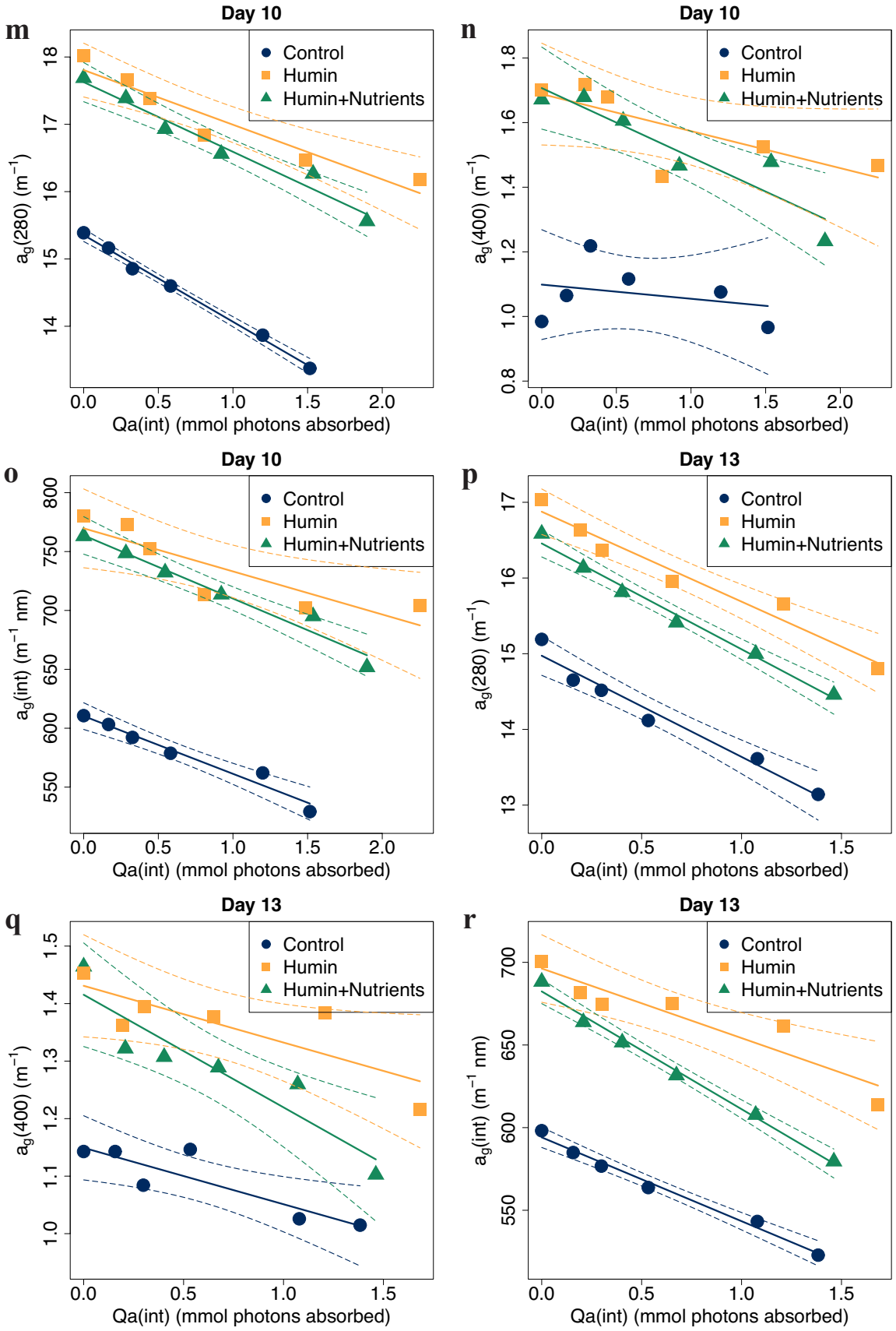
m
Day 10
Control
Humin
Humin+Nutrients
$a_g(280)$ (m^{-1})
Qa(int) (mmol photons absorbed)
n
Day 10
$a_g(400)$ (m^{-1})
o
Day 10
a_g(int) (m^{-1} nm)
p
Day 13
$a_g(280)$ (m^{-1})
q
Day 13
$a_g(400)$ (m^{-1})
r
Day 13
a_g(int) (m^{-1} nm)

Figure S2.2. Chromophoric dissolved organic matter absorption coefficients at a) d) g) j) m) p) 280 nm ($a_g(280)$, m^{-1}), b) e) h) k) n) q) 400 nm ($a_g(400)$, m^{-1}), and c) f) i) l) o) r) integrated over 280-400 nm ($a_g(int)$, m^{-1} nm) versus photon dose ($Q_a(int)$, mmol photons absorbed) for laboratory irradiation experiments conducted on a) b) c) day 1, d) e) f) day 3, g) h) i) day 6, j) k) l) day 8, m) n) o) day 10, and p) q) r) day 13 mesocosm samples of the JOMEX experiment (day 1 was the day of initial amendment). Samples were taken right after the initial amendment, and around the same time in subsequent days. Solid lines with corresponding colors are linear regression lines for each group, and dashed lines are 95 % confidence bands for the slopes of the regression lines.

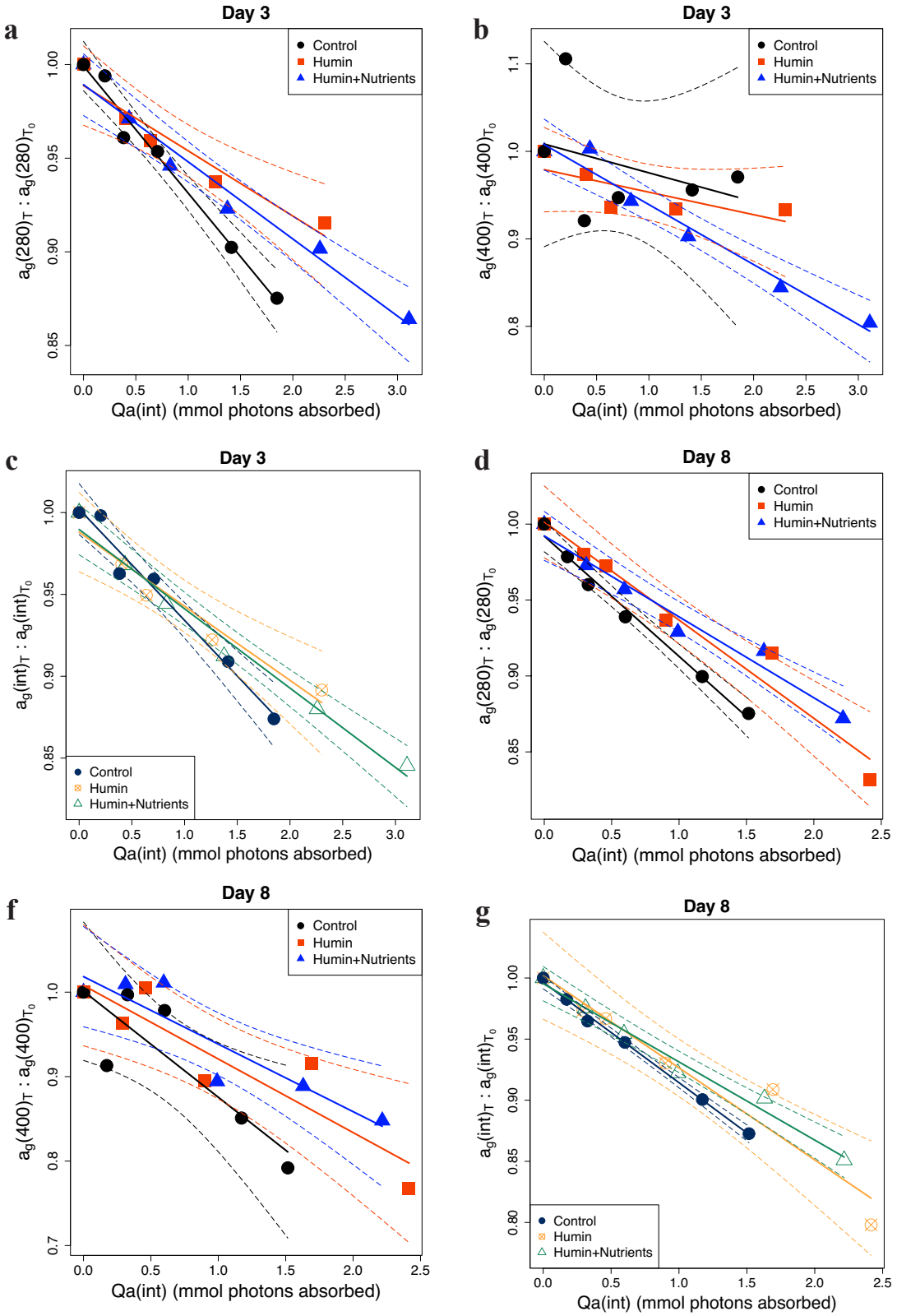
a
Day 3
Control
Humin
Humin+Nutrients
$a_g(280)_T : a_g(280)_{T_0}$
Qa(int) (mmol photons absorbed)
b
Day 3
$a_g(400)_T : a_g(400)_{T_0}$
c
Day 3
$a_g(int)_T : a_g(int)_{T_0}$
d
Day 8
$a_g(280)_T : a_g(280)_{T_0}$
f
Day 8
$a_g(400)_T : a_g(400)_{T_0}$
g
Day 8
$a_g(int)_T : a_g(int)_{T_0}$

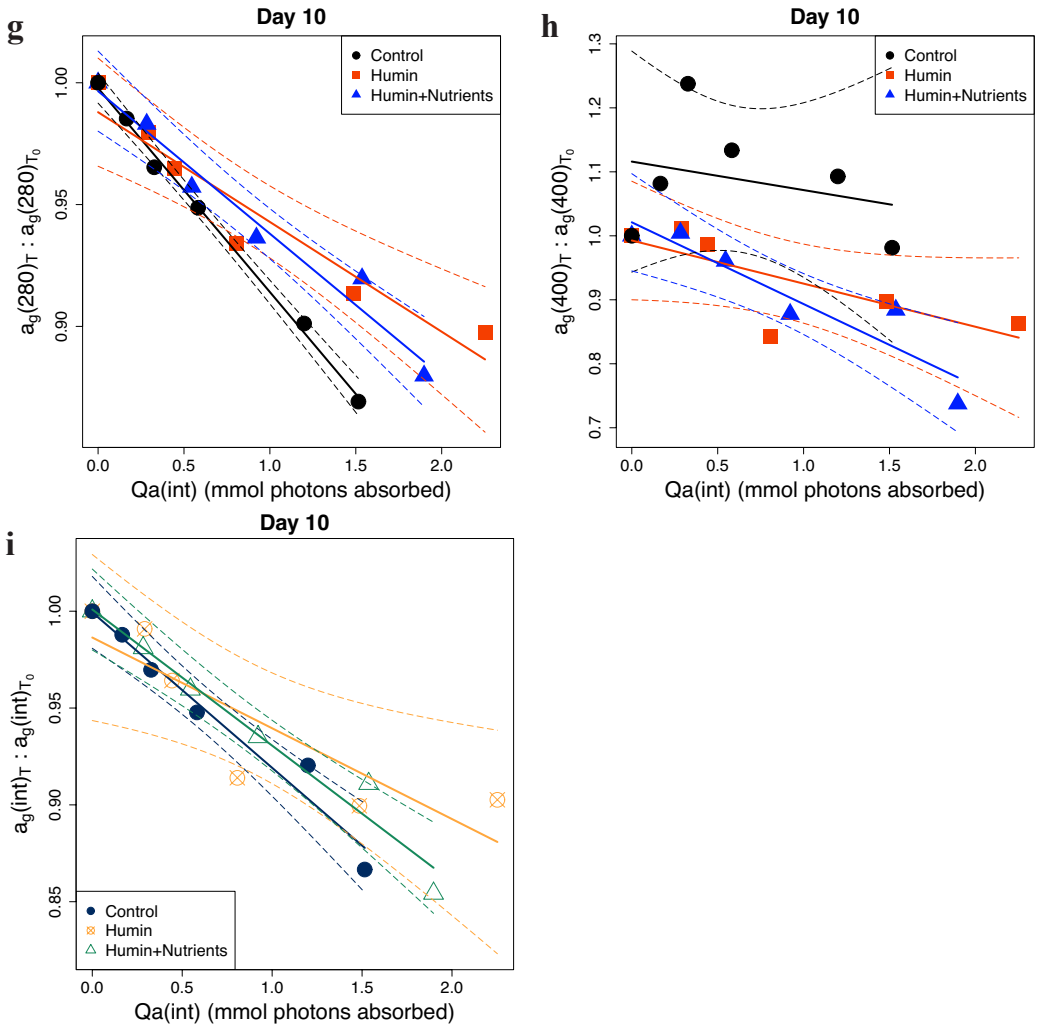

Figure S2.3. Ratios of chromophoric dissolved organic matter absorption coefficients at a) d) g) 280 nm ($a_g(280)_T : a_g(280)_{T0}$), b) e) h) 400 nm ($a_g(400)_T : a_g(400)_{T0}$), and c) f) i) integrated over 280-400 nm ($a_g(int)_T : a_g(int)_{T0}$) versus photon dose (mmol photons absorbed) for laboratory irradiation experiments conducted on a) b) c) day 3, d) e) f) day 8, and g) h) i) day 10 mesocosm samples of the JOMEX experiment (day 1 was the day of initial amendment). Samples were taken right after the initial amendment, and around the same time in subsequent days. Ratios were calculated by dividing the corresponding a_g ratio at time T by that at time T_0. Solid lines with corresponding colors are linear regression lines for each group, and dashed lines are 95 % confidence bands for the slopes of the regression lines.

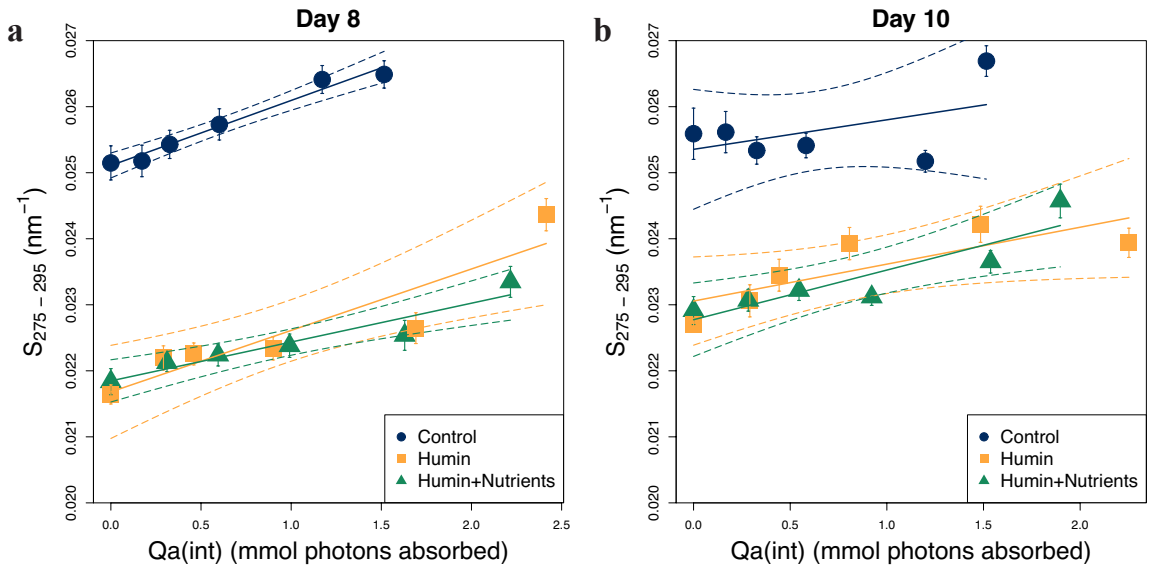

Figure S2.4. Chromophoric dissolved organic matter absorption spectral slope $S_{275\text{-}295}$ (nm^{-1}) versus photon dose (Q_a(int), mmol photons absorbed) for individual laboratory experiments, using a) experimental day 8, and b) day 10, samples of the JOMEX amendment experiment. Samples were taken right after the initial amendment (day 1), and around the same time in subsequent days. Solid lines with corresponding colors are linear regression lines for each group, and dashed lines are 95 % confidence bands for the slopes of the regression lines. Error bars were ±1 standard error for $S_{275\text{-}295}$ (linear regression slopes of natural-log-transformed absorbance versus wavelength at 275-295 nm).

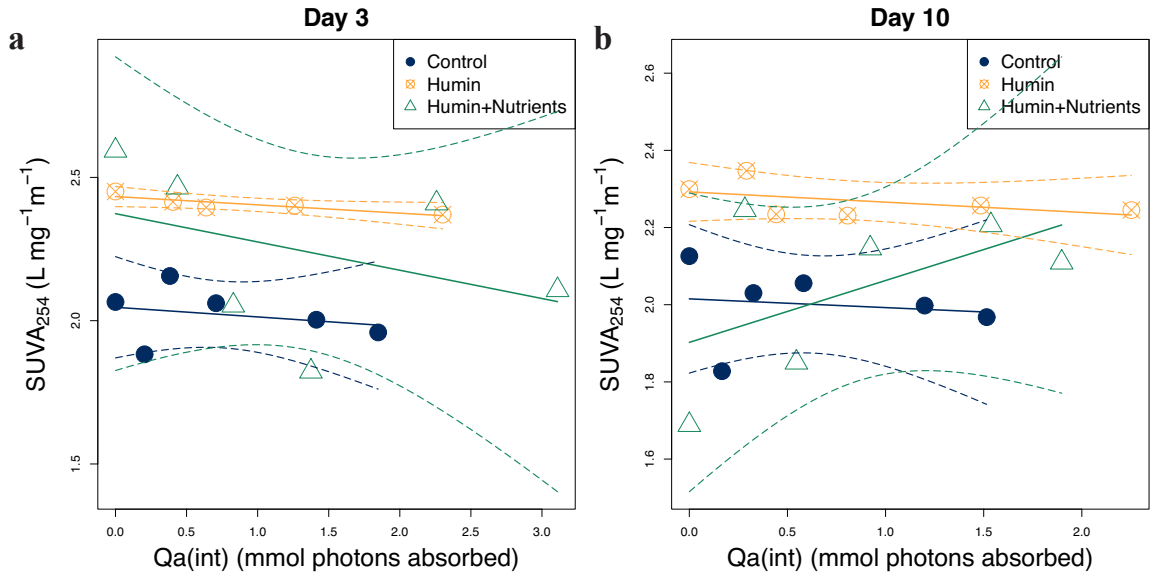

Figure S2.5. Specific ultraviolet absorbance $SUVA_{254}$ (L mg^{-1} m^{-1}) versus photon doses (Q_a(int), mmol photons absorbed) for laboratory irradiation experiments using a) day 3, and b) day 10 samples of the JOMEX amendment experiment. Day 1 was the day of initial amendment. Samples were taken right after the initial amendment, and around the same time in subsequent days. Solid lines with corresponding colors are linear regression lines for each group, and dashed lines are 95 % confidence bands for the slopes of the regression lines.

APPENDIX B. SUPPLEMENTAL FIGURES FOR CHAPTER 4

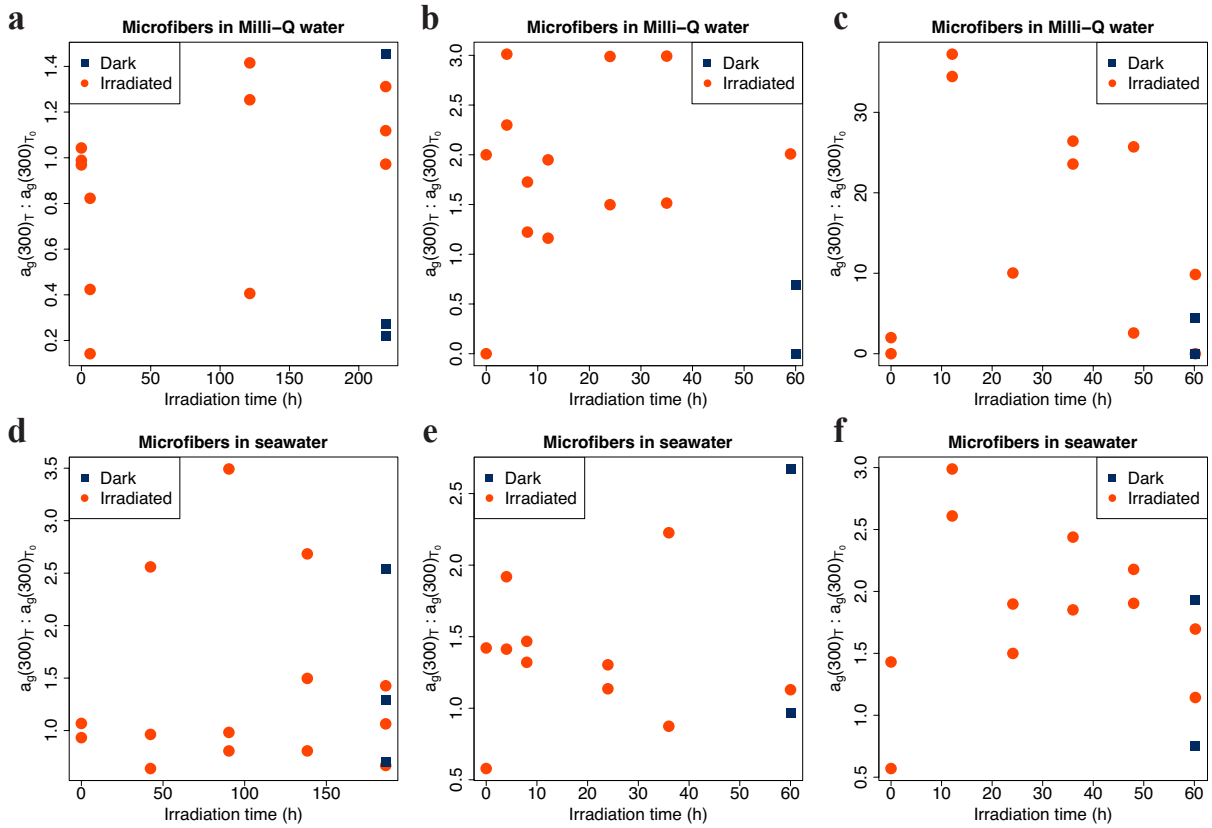

Figure S4.1. Chromophoric dissolved organic matter absorption coefficients at 300 nm ($a_g(300)$), normalized to initial microfiber mass (m^{-1} (mg microfiber)$^{-1}$), versus irradiation time (h) in photoirradiation experiments: (a, b, c) microfibers in Milli-Q ultrapure water, (d, e, f) microfibers in open ocean seawater from the Atlantic subtropical gyre. (a) experiment 1, (d) experiment 2, (b) and (e) experiment 3, and (c) and (f) experiment 4. Expressed as ratios of normalized $a_g(300)$ at any irradiation point (T) to normalized $a_g(300)$) at time zero (T_0). Note the different irradiation time among experiments. Experiment 1 and 2 used the same type of microfibers (from red polyester yarn) while experiment 3 and 4 used a different type of microfibers (from white polyester fabric).

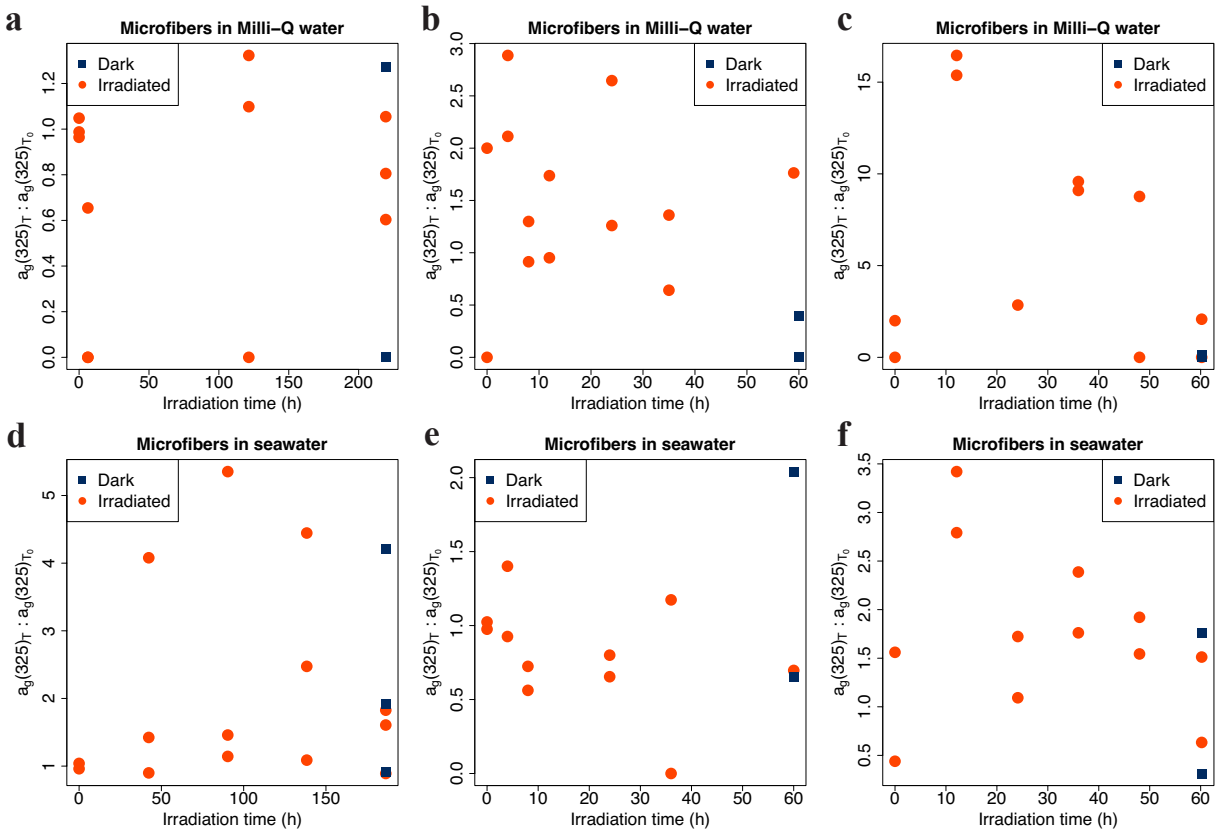

Figure S4.2. Chromophoric dissolved organic matter absorption coefficients at 325 nm ($a_g(325)$), normalized to initial microfiber mass (m^{-1} (mg microfiber)$^{-1}$), versus irradiation time (h) in photoirradiation experiments: (a, b, c) microfibers in Milli-Q ultrapure water, (d, e, f) microfibers in open ocean seawater from the Atlantic subtropical gyre. (a) experiment 1, (d) experiment 2, (b) and (e) experiment 3, and (c) and (f) experiment 4. Expressed as ratios of normalized $a_g(325)$ at any irradiation point (T) to normalized $a_g(325)$) at time zero (T_0). Note the different irradiation time among experiments. Experiment 1 and 2 used the same type of microfibers (from red polyester yarn) while experiment 3 and 4 used a different type of microfibers (from white polyester fabric).

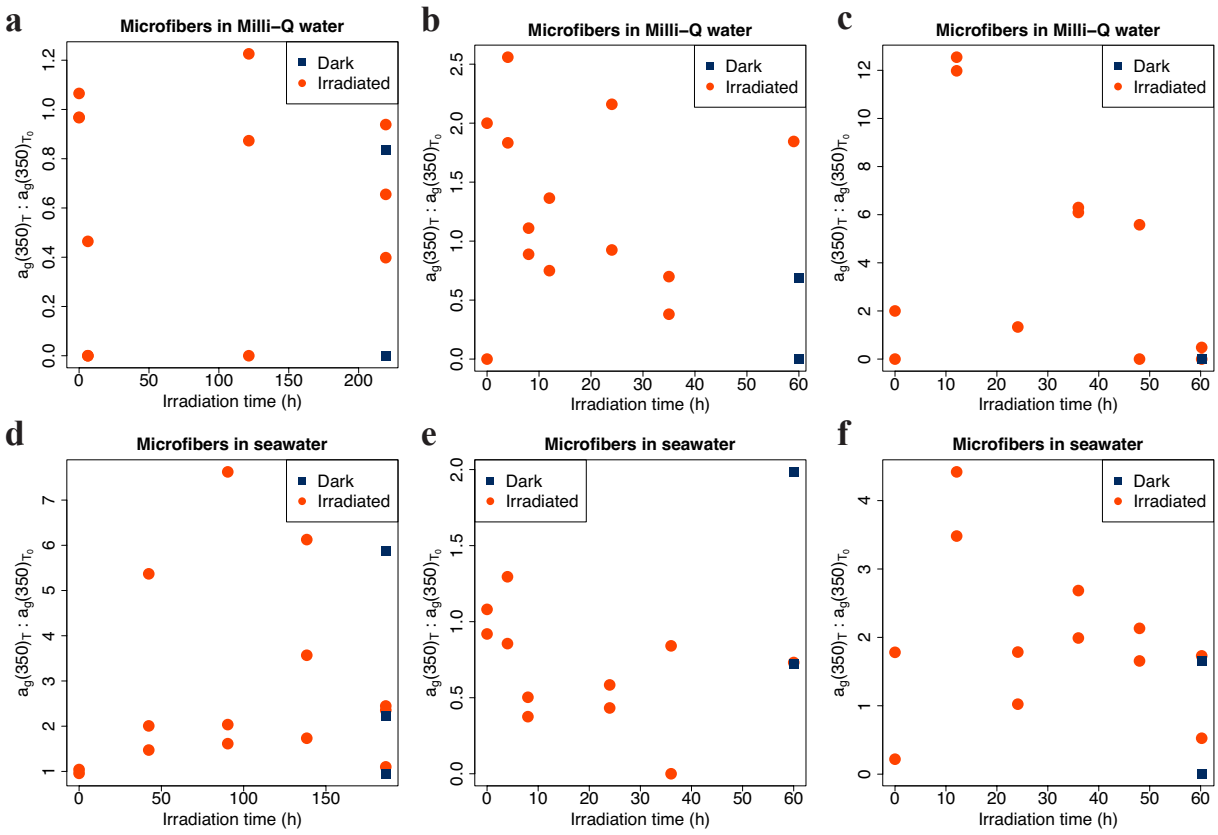

Figure S4.3. Chromophoric dissolved organic matter absorption coefficients at 350 nm ($a_g(350)$), normalized to initial microfiber mass (m^{-1} (mg microfiber)$^{-1}$), versus irradiation time (h) in photoirradiation experiments: (a, b, c) microfibers in Milli-Q ultrapure water, (d, e, f) microfibers in open ocean seawater from the Atlantic subtropical gyre. (a) experiment 1, (d) experiment 2, (b) and (e) experiment 3, and (c) and (f) experiment 4. Expressed as ratios of normalized $a_g(350)$ at any irradiation point (T) to normalized $a_g(350)$) at time zero (T_0). Note the different irradiation time among experiments. Experiment 1 and 2 used the same type of microfibers (from red polyester yarn) while experiment 3 and 4 used a different type of microfibers (from white polyester fabric).